LEVEL

AD A109054

THE
GEORGE
WASHINGTON
UNIVERSITY

STUDENTS FACULTY STUDY R
ESEARCH DEVELOPMENT FUT
URE CAREER CREATIVITY CC
MMUNITY LEADERSHIP TECH
NOLOGY FRONTIE   SIGN
ENGINEERING APP   ENC
GEORGE WASHIN   NI\

SCHOOL OF ENGINEERING
AND APPLIED SCIENCE

81 12 29 042

REPORT DOCUMENTATION PAGE	READ INSTRUCTIONS BEFORE COMPLETING FORM

1. REPORT NUMBER	2. GOVT ACCESSION NO.	3. RECIPIENT'S CATALOG NUMBER
AFOSR-TR- 81-0856	AD-A109057	

4. TITLE (and Subtitle)	5. TYPE OF REPORT & PERIOD COVERED
FRACTURE AND FATIGUE CHARACTERIZATION OF AIR-CRAFT STRUCTURAL MATERIALS UNDER BIAXIAL LOADING	FINAL 1 OCT 76 - MAY 80
	6. PERFORMING ORG. REPORT NUMBER

7. AUTHOR(s)	8. CONTRACT OR GRANT NUMBER(s)
D L JONES J EFTIS	AFOSR-76-3099

9. PERFORMING ORGANIZATION NAME AND ADDRESS	10. PROGRAM ELEMENT, PROJECT, TASK AREA & WORK UNIT NUMBERS
GEORGE WASHINGTON UNIV DEPT OF CIVIL, MECHANICAL & ENVIRONMENTAL ENG WASHINGTON, DC 20052	61102F 2307/B2

11. CONTROLLING OFFICE NAME AND ADDRESS	12. REPORT DATE
AIR FORCE OFFICE OF SCIENTIFIC RESEARCH/NA BOLLING AIR FORCE BASE, DC 20332	DEC 81
	13. NUMBER OF PAGES
	187

14. MONITORING AGENCY NAME & ADDRESS(if different from Controlling Office)	15. SECURITY CLASS. (of this report)
	UNCLASSIFIED
	15a. DECLASSIFICATION/DOWNGRADING SCHEDULE

16. DISTRIBUTION STATEMENT (of this Report)

Approved for public release; distribution unlimited.

17. DISTRIBUTION STATEMENT (of the abstract entered in Block 20, if different from Report)

18. SUPPLEMENTARY NOTES

19. KEY WORDS (Continue on reverse side if necessary and identify by block number)

BIAXIAL
FRACTURE
FATIGUE
FRACTURE MECHANICS
FRACTURE TOUGHNESS

20. ABSTRACT (Continue on reverse side if necessary and identify by block number)

A research program, comprising both analytical and experimental tasks, has been pursued with the objective of examining the influence of biaxial applied loads on the mechanical behavior of bodies containing cracks. Under the analytical part of this program, a general fracture mechanics analysis was performed to examine the influence of biaxial applied loads on the mechanical state of the body. The geometries examined were the single crack and two coplanar cracks with an arbitrary orientation and the cracked shear panel. It was found that

DD FORM 1473 1 JAN 73   EDITION OF 1 NOV 65 IS OBSOLETE

the biaxial loads influenced all aspects of the mechanical state of the body, with the exception of the stress intensity factor for a crack oriented parallel to the biaxial load. The extent and nature of the biaxial effect on the crack-tip stress field, stress intensity factor, angly of initial crack extension, crack-tip displacements, elastic strain energy, fracture load and fatigue crack growth rates are all presented in this report. The experimental part of this program involved developing a biaxial test facility and performing a considerable number of photoelastic fracture toughness, and fatigue crack growth rate experiments. Confirmation of the analytical predictions was obtained for the biaxial effects on the crack-tip stress field, the angle of initial crack extension, the fracture load, and the fatigue crack growth rates. The biaxial loads were seen to influence all of these parameters in varying degrees, and a considerable amount of experimental data is included in the report.

FRACTURE AND FATIGUE CHARACTERIZATION OF AIRCRAFT

STRUCTURAL MATERIALS UNDER BIAXIAL LOADING

Final Scientific Report
October 1, 1976 - May 30, 1980

D. L. Jones and J. Eftis

Submitted To

Air Force Office of Scientific Research
Building 410
Bolling Air Force Base
Washington, D.C. 20032

School of Engineering and Applied Science
The George Washington University
Washington, D.C. 20052

ABSTRACT

A research program, comprising both analytical and experimental tasks, has been pursued with the objective of examining the influence of biaxial applied loads on the mechanical behavior of bodies containing cracks.

Under the analytical part of this program, a general fracture mechanics analysis was performed to examine the influence of biaxial applied loads on the mechanical state of the body. The geometries examined were the single crack and two coplanar cracks with an arbitrary orientation and the cracked shear panel. It was found that the biaxial loads influenced all aspects of the mechanical state of the body, with the exception of the stress intensity factor for a crack oriented parallel to the biaxial load. The extent and nature of the biaxial effect on the crack-tip stress field, stress intensity factor, angle of initial crack extension, crack-tip displacements, elastic strain energy, fracture load and fatigue crack growth rates are all presented in this report.

The experimental part of this program involved developing a biaxial test facility and performing a considerable number of photoelastic, fracture toughness, and fatigue crack growth rate experiments. Confirmation of the analytical predictions was obtained for the biaxial effects on the crack-tip stress field, the angle of initial crack extension, the fracture load, and the fatigue crack growth rates. The biaxial loads were seen to influence all of these parameters in varying degrees, and a considerable amount of experimental data is included in the report.

TABLE OF CONTENTS

iii

LIST OF SYMBOLS

(x,y), (r,θ)	= rectangular and polar coordinates respectively.
z	= $x+iy$, complex variable.
t_{jk}, e_{jk}	= components of the stress and strain tensors, respectively.
T_k, u_k, b_k	= components of the surface traction, displacement and body force vectors, respectively.
t_{xx}, t_{yy}, t_{xy}	= rectangular stress components.
u_x, u_y	= rectangular displacement components.
a	= half crack length.
$\ell = (b-a)$	= crack dimension.
υ	= elastic strain energy density (per unit volume).
U	= elastic strain energy of body (per unit thickness).
W	= work of forces applied to the body.
P, V	= potential energies.
Γ	= surface energy.
R	= bound region of the x-y plane.
$\overline{R}$	= load ratio.
C_k	= closed boundary curves of R.
Φ, Ω, ϕ, ω	= sectionally holomorphic functions of the complex variable z.
$F(\phi,p)$, $E(\phi,p)$	= elliptic integrals of the first and second kinds, respectively.
$F(p)$, $E(p)$	= complete elliptic integrals of the first and second kinds.
$\lambda(p)$	= $E(p)/F(p)$.
K_1, K_2	= elastic stress intensity factors.

LIST OF SYMBOLS (con't)

K_c, K_{1c} = plane stress, plane strain fracture toughness, respectively.

ΔK_1 = range of stress intensity factor.

Δk_0 = fatigue crack propagation threshold.

da/dN = rate of fatigue crack propagation.

N = number of load cycles.

E = Young's elastic modulus.

k = applied load biaxiality ratio, $t_{xx}(\infty)/t_{yy}(\infty)$.

σ = normal stress applied at the outer boundary surface.

τ = shear stress applied at the outer boundary surface.

τ_m = maximum shear stress.

σ_c = fracture stress.

θ_0 = angle of initial crack extension.

α = angle of crack inclination.

μ = elastic shear modulus.

ν = Poisson's ratio.

γ = surface energy density (per unit area).

κ = $(3-\nu)/(1+\nu)$ for plane stress, $(3-4\nu)$ for plane strain.

LIST OF ILLUSTRATIONS

LIST OF ILLUSTRATIONS (con't)

FIGURE

LIST OF ILLUSTRATIONS (con't)

LIST OF ILLUSTRATIONS (con't)

FIGURE

LIST OF ILLUSTRATIONS (con't)

FIGURE

FIGURE

LIST OF TABLES

SECTION 1

INTRODUCTION

Ever since the seminal research of Griffith into the
nature of the fracture of solids in early 1920, the opinion
of many associated with the materials science and fracture
mechanics communities has been that loads applied parallel to
an existing crack (in addition to the tensile load perpendi-
cular to it) have no effect on fracture behavior. This idea
was first advanced by Griffith himself in postulating his
well known criterion for the onset of crack instability [12,
13]. The mathematical or analytical justification for such
an assertion can be shown to be lacking however, and has been
a source of controversy over the years [48].

Apparent corroboration of this idea of the unimportance
of loads applied parallel to a crack (in a biaxial load situ-
ation) appeared to come some thirty-five years later, when
Irwin introduced the crack-tip elastic stress intensity fac-
tor approach to fracture mechanics [49,50]. Irwin's deriva-
tion of the singular one-term series approximations for the
elastic stress in the neighborhood of the crack-tip, utilized
Westergaard's form for the solution of the problem of a biax-
ially loaded plane infinite sheet with a central horizontal
crack [51]. Westergaard's solution, however, incorrectly
omitted a term containing the horizontal load parameter, (i.e.,
the second term of the right side of Eq. (2.11) of this report).
Consequently, in Irwin's subsequent series representations of

the stress field near the crack-tip, no manifestation of the presence of the horizontal load could possibly appear. However, Irwin seemed to understand the significance or importance of loads parallel to the crack, because he added a constant but unspecified term, σ_{0x}, to his expression for the x-direction stress component near the crack-tip, [50]. It is now understood that this term corresponds to the second, non-singular, term of Eq. $(2.24)_1$ of this report.

Thus two analytical errors, with the latter one accidently having the effect of masking the presence of the earlier one, led to a general misunderstanding of the significance of the biaxial load effect. This situation still persists. Now that fragments of contradictory experimental data have begun to appear, during the last five to ten years, the need to clarify this question is apparent.

This research effort addresses itself to this problem, that is, to the question of the presence, or lack of presence, of the effect of load biaxiality on fracture or on fracture related behavior. It attempts to examine the problem systematically and in detail, utilizing specially designed experiments where possible to check on the validity of the analytical findings. The experiments were performed on materials that are used extensively in aircraft structures.

PART I

ANALYSIS

When a cracked body is subjected to forces that act parallel to the plane of the crack (in addition to the tensile forces applied perpendicular to it), any influence that the parallel loads may have on the fracture behavior of the body should, if present, manifest itself in several different ways. Moreover, if the biaxial load effect exists and is significant, it must obviously affect the mechanical state of that region of the body in close proximity to the crack tip. Investigation of the problem should therefore direct initial emphasis on illuminating the possible relation of load biaxiality on those aspects of fracture that can be observed experimentally. These would include crack-tip shear isochromatics, which may be seen photoelastically, the angle of initial crack extension, which may be observed directly, as can the rate at which fatigue crack growth takes place under cyclic normal loads at varying states of load biaxiality. The critical value of the normal tensile load, that is, the fracture load, can also be measured at different levels of load biaxiality, which suggests that the analysis should concern itself with this facet of the problem as well.

The infinite sheet geometry was chosen for the theoretical part of the investigation because exact solutions for several cracked-body geometries are known, thereby permitting derivation of specific results that give explicit demonstration

of the effects of the load applied parallel to the plane of
the crack. Although experiments must be performed on test
specimens that have finite dimensions, analysis based upon
infinite body geometry can be useful, nevertheless, because
it can serve as a prototype that provides, at the very least,
valuable information of an insightful and qualitative nature.

SECTION 2

STRESS AND DISPLACEMENT IN THE VICINITY OF THE CRACK TIP

In the linear theory of isotropic elastic solids in which body forces are neglected, the plane problem of statics is reduced to a boundary value problem for the biharmonic stress function. The same problem can also be formulated equivalently in terms of a pair of analytic functions, Φ and Ω, of the complex variable $z = x + iy = re^{i\theta}$, which uniquely specify the plane stress and displacement components by means of the following relations [1]:

$$t_{xx} + t_{yy} = 2[\Phi(z) + \overline{\Phi(z)}]$$

$$t_{yy} - t_{xx} + 2it_{xy} = 2[(\bar{z}-z)\frac{d\Phi}{dz} + \bar{\Omega}(z) - \Phi(z)] \qquad (2.1)$$

$$2\mu[u_x + iu_y] = \kappa\phi(z) - \omega(\bar{z}) - (z-\bar{z})\overline{\Phi(z)} \quad ,$$

where the overbar designates complex conjugation and

$$\phi(z) = \int \Phi(z)dz, \qquad \omega(z) = \int \Omega(z)dz \quad . \qquad (2.2)$$

When for a given boundary value problem, that is, for a given applied load and cracked body geometry, the functions Φ and Ω are determined, then the stress and displacements, and all other mechanical quantities expressed in terms of them, are determinable from Eqs. (2.1) and (2.2).

2.1 SINGLE CRACK

The plane components of the stress tensor referred to the pair of coordinate systems shown in Fig. 1 are related by expressions

$$t_{yy} - t_{xx} + 2it_{xy} = e^{2i\beta}(t'_{yy} - t'_{xx} + 2it'_{xy})$$

$$= e^{-2i\alpha}(t'_{xx} - t'_{yy} - 2it'_{xy}) \qquad (2.3)$$

and

$$t_{yy} + t_{xx} = t'_{yy} + t'_{xx} . \qquad (2.4)$$

The boundary condition along the exterior boundary of the plane infinite body having an inclined interior crack geometry (cf. Fig. 1) is specified to be

$$t'_{yy}(\infty) = \sigma , \qquad t'_{xx}(\infty) = k\sigma , \qquad t'_{xy}(\infty) = 0 , \qquad (2.5)$$

which can be expressed relative to the $(x-y)$ coordinate system by means of Eqs. (2.3) and (2.4) as

$$t_{yy}(\infty) = \frac{\sigma}{2}(1+k) - \frac{\sigma}{2}(1-k)\cos 2\alpha$$

$$t_{xx}(\infty) = \frac{\sigma}{2}(1+k) + \frac{\sigma}{2}(1-k)\cos 2\alpha \qquad (2.6)$$

$$t_{xy}(\infty) = \frac{\sigma}{2}(1-k)\sin 2\alpha .$$

Along the interior (crack) boundary

$$t_{yy}(x,0) = t_{xy}(x,0) = 0 , \qquad |x|<|a|. \qquad (2.7)$$

The solution to the boundary value problem posed by Eqs. (2.5)-(2.7) has the form [2]

$$\left.\begin{array}{c} \phi(z) \\ \\ \Omega(z) \end{array}\right\} = \frac{1}{2} \frac{(2A+B)z}{(z^2-a^2)^{\frac{1}{2}}} \mp \frac{1}{2}B \qquad (2.8)$$

where

$$\frac{1}{2}(2A+B) = \frac{\sigma}{4}\left[(1-e^{2i\alpha}) + k(1+e^{2i\alpha})\right]$$

$$\frac{1}{2}B = -\frac{\sigma}{4}(1-k)e^{2i\alpha} . \qquad (2.9)$$

From Eqs. (2.2), (2.8) and (2.9), it follows that

$$
\left.\begin{array}{c} \phi(z) \\ \\ \omega(z) \end{array}\right\} = \frac{\sigma}{4}\left\{\left[(1-e^{2i\alpha})+k(1+e^{2i\alpha})\right](z^2-a^2)^{\frac{1}{2}} \pm (1-k)e^{2i\alpha}z\right\} . \quad (2.10)
$$

When the crack has a horizontal orientation, $\alpha=\pi/2$, the above expressions reduce to

$$
\left.\begin{array}{c} \phi(z) \\ \\ \Omega(z) \end{array}\right\} = \frac{\sigma z}{2(z^2-a^2)^{\frac{1}{2}}} \pm \frac{\sigma}{4}(1-k) \quad (2.11)
$$

and

$$
\left.\begin{array}{c} \phi(z) \\ \\ \omega(z) \end{array}\right\} = \frac{\sigma}{2}(z^2-a^2)^{\frac{1}{2}} \pm \frac{\sigma}{4}(1-k)z \quad . \quad (2.12)
$$

Expression of the stress and displacement components in the immediate vicinity of the crack tip is facilitated by the following coordinate transformation (cf. Fig. 2)

$$
z - a = \zeta = re^{i\theta} , \quad (2.13)
$$

relative to which $\Phi(z) \rightarrow \Phi(\zeta)$ may be shown to have the power series representation

$$
\Phi(\zeta) = \frac{\sigma(\pi)^{\frac{1}{2}}}{(2\pi)^{\frac{1}{2}}} \frac{C}{4}\left\{\left(\frac{\zeta}{a}\right)^{-\frac{1}{2}} + \frac{(2)^{\frac{1}{2}}}{C}(1-k)e^{2i\alpha}\left(\frac{\zeta}{a}\right)^0 + \frac{3}{4}\left(\frac{\zeta}{a}\right)^{\frac{1}{2}} - \ldots\ldots\right\}
$$

$$
= \frac{\sigma(\pi a)^{\frac{1}{2}}}{(2\pi\zeta)^{\frac{1}{2}}} \frac{C}{4} + \frac{\sigma}{4}(1-k)e^{2i\alpha} + O\left(\frac{\zeta}{a}\right)^{\frac{1}{2}} , \quad (2.14)
$$

in which

$$
C = (1-e^{2i\alpha}) + k(1+e^{2i\alpha}).
$$

However

-7-

$$\frac{\sigma(\pi a)^{\frac{1}{2}}C}{4} = \frac{1}{2} \frac{\sigma(\pi a)^{\frac{1}{2}}}{2}\left[(1+k)-(1-k)\cos 2\alpha - i(1-k)\sin 2\alpha\right]$$

$$\qquad (2.15)$$

$$= \frac{1}{2}(K_1 - iK_2)$$

where

$$K_1 - iK_2 = \lim_{z \to a}\left[2(2\pi)^{\frac{1}{2}}(z-a)^{\frac{1}{2}}\phi(z)\right] \qquad (2.16)$$

is the complex elastic stress intensity factor [3,4]. The equivalence of expressions (2.15) and (2.16) can be shown by direct calculation of the limit Eq. (2.16) with ϕ as given by Eq. (2.8). Thus

$$\phi(\zeta) = \frac{K_1 - iK_2}{2(2\pi\zeta)^{\frac{1}{2}}} + \frac{\sigma}{4}(1-k)e^{2i\alpha} + O\left(\frac{\zeta}{a}\right)^{\frac{1}{2}} , \qquad (2.17)$$

and for $0<|\zeta/a|=(r/a)\ll 1$, we have the following series approximations for ϕ and Ω taken to order $(r/a)^{\frac{1}{2}}$:

$$\left.\begin{array}{c} 2\phi(\zeta) \\ \\ 2\Omega(\zeta) \end{array}\right\} \cong \frac{K_1 - iK_2}{(2\pi r)^{\frac{1}{2}}} \ e^{-i\left(\frac{\theta}{2}\right)} \pm \frac{\sigma}{2}(1-k)e^{2i\alpha} . \qquad (2.18)$$

Similarly, a series expansion for $\phi(\zeta)$ has the form

$$\phi(\zeta) = \frac{\sigma a(2)^{\frac{1}{2}}C}{4}\left[\left(\frac{\zeta}{a}\right)^{\frac{1}{2}} + \frac{(1-k)e^{2i\alpha}}{(2)^{\frac{1}{2}}C}\left(\frac{\zeta}{a}\right)^1 + \frac{1}{2}\left(\frac{\zeta}{a}\right)^{3/2} - \cdots\cdots\cdots\right]$$

$$= (K_1 - iK_2)\left(\frac{\zeta}{2\pi}\right)^{\frac{1}{2}} + \frac{\sigma a}{4}(1-k)\left(1+\frac{\zeta}{a}\right)e^{2i\alpha} + O\left(\frac{\zeta}{a}\right)^{3/2} , \qquad (2.19)$$

which can be approximated by

$$\left.\begin{array}{c} \phi(\zeta) \\ \\ \omega(\zeta) \end{array}\right\} \cong (K_1 - iK_2)\left(\frac{r}{2\pi}\right)^{\frac{1}{2}} e^{i\left(\frac{\theta}{2}\right)} \pm \frac{\sigma a}{4}(1-k)\left(\frac{a+re^{i\theta}}{a}\right)e^{2i\alpha} , \qquad (2.20)$$

when $0<|\zeta/a| = (r/a)\ll 1$.

The stress and displacement components near the crack tip are thus obtainable from Eqs. (2.1), (2.18) and (2.20), where in Eq. (2.1) z and $\bar{z}$ are replaced by ζ and $\bar{\zeta}$, with the results

$$t_{xx} \cong \frac{K_1}{(2\pi r)^{\frac{1}{2}}} \cos\frac{\theta}{2}\left(1-\sin\frac{\theta}{2}\sin\frac{3\theta}{2}\right) - \frac{K_2}{(2\pi r)^{\frac{1}{2}}} \sin\frac{\theta}{2}\left(2+\cos\frac{\theta}{2}\cos\frac{3\theta}{2}\right)$$

$$+ \ \sigma(1-k)\cos 2\alpha$$

$$t_{yy} \cong \frac{K_1}{(2\pi r)^{\frac{1}{2}}} \cos\frac{\theta}{2}\left(1+\sin\frac{\theta}{2}\sin\frac{3\theta}{2}\right) + \frac{K_2}{(2\pi r)^{\frac{1}{2}}}\sin\frac{\theta}{2}\cos\frac{\theta}{2}\cos\frac{3\theta}{2} \quad (2.21)$$

$$t_{xy} \cong \frac{K_1}{(2\pi r)^{\frac{1}{2}}} \sin\frac{\theta}{2}\cos\frac{\theta}{2}\cos\frac{3\theta}{2} + \frac{K_2}{(2\pi r)^{\frac{1}{2}}} \cos\frac{\theta}{2}\left(1-\sin\frac{\theta}{2}\sin\frac{3\theta}{2}\right)$$

and

$$u_x \cong \frac{K_1}{\mu}\left(\frac{r}{2\pi}\right)^{\frac{1}{2}} \cos\frac{\theta}{2}\left[\frac{1}{2}(\kappa-1)+\sin^2\frac{\theta}{2}\right] + \frac{K_2}{\mu}\left(\frac{r}{2\pi}\right)^{\frac{1}{2}} \sin\frac{\theta}{2}\left[\frac{1}{2}(\kappa+1)+\cos^2\frac{\theta}{2}\right]$$

$$+\frac{(1-k)\sigma}{8\mu}\left\{r[\cos(\theta+2\alpha)+\kappa\cos(\theta-2\alpha)-2\sin\theta\sin 2\alpha]+(\kappa+1)a\ \cos 2\alpha\right\}$$

$$(2.22)$$

$$u_y \cong \frac{K_1}{\mu}\left(\frac{r}{2\pi}\right)^{\frac{1}{2}} \sin\frac{\theta}{2}\left[\frac{1}{2}(\kappa+1)-\cos^2\frac{\theta}{2}\right] + \frac{K_2}{\mu}\left(\frac{r}{2\pi}\right)^{\frac{1}{2}} \cos\frac{\theta}{2}\left[\frac{1}{2}(1-\kappa)+\sin^2\frac{\theta}{2}\right]$$

$$+\frac{(1-k)\sigma}{8\mu}\left\{r[\sin(2\alpha-\theta)+\kappa\sin(2\alpha+\theta)-2\sin\theta\cos 2\alpha]+(\kappa+1)a\ \sin 2\alpha\right\} \ .$$

In the above expressions the elastic stress intensity factor K_1 and K_2 have, from Eq. (2.15), the explicit forms

$$K_1 = \frac{\sigma(\pi a)^{\frac{1}{2}}}{2}\left[(1+k)-(1-k)\cos 2\alpha\right]$$

$$(2.23)$$

$$K_2 = \frac{\sigma(\pi a)^{\frac{1}{2}}}{2}(1-k)\sin 2\alpha \ .$$

-9-

The variation of K_1 and K_2 with the angle of crack inclination, α, and the biaxial load factor, k, are shown in Figures 3 and 4.

For the crack with a horizontal orientation, $\alpha = \pi/2$, Eqs. (2.21)-(2.23) become

$$t_{xx} \cong \frac{K_1}{(2\pi r)^{\frac{1}{2}}} \cos\frac{\theta}{2}\left(1-\sin\frac{\theta}{2}\sin\frac{3\theta}{2}\right) - (1-k)\sigma$$

$$t_{yy} \cong \frac{K_1}{(2\pi r)^{\frac{1}{2}}} \cos\frac{\theta}{2}\left(1+\sin\frac{\theta}{2}\sin\frac{3\theta}{2}\right) \qquad (2.24)$$

$$t_{xy} \cong \frac{K_1}{(2\pi r)^{\frac{1}{2}}} \sin\frac{\theta}{2} \cos\frac{\theta}{2} \cos\frac{3\theta}{2} \quad ,$$

and

$$u_x \cong \frac{K_1}{\mu}\left(\frac{r}{2\pi}\right)^{\frac{1}{2}} \cos\frac{\theta}{2}\left[\frac{1}{2}(\kappa-1)+\sin^2\frac{\theta}{2}\right] - \frac{(1-k)(\kappa+1)\sigma}{8\mu}[r\cos\theta + a]$$

$$(2.25)$$

$$u_y \cong \frac{K_1}{\mu}\left(\frac{r}{2\pi}\right)^{\frac{1}{2}} \sin\frac{\theta}{2}\left[\frac{1}{2}(\kappa+1)-\cos^2\frac{\theta}{2}\right] + \frac{(1-k)(3-\kappa)\sigma}{8\mu} r\sin\theta \quad ,$$

where

$$K_1 = \sigma(\pi a)^{\frac{1}{2}}, \quad K_2 = 0 \quad . \qquad (2.26)$$

From examination of the power series representations given by Eqs. (2.14) and (2.19) for $\Phi(\zeta)$ and $\phi(\zeta)$, respectively, it is observed that the biaxial load factor, k, appears as a coefficient in only the second term of the expansions. Consequently, in order to take proper account of the presence of the horizontal load in the approximate expressions for the elastic crack-tip stress and displacements, a two-term

-10-

approximation of the series expansions for Φ and ϕ must be employed, as shown by Eqs. (2.17) or (2.18) and (2.19) or (2.20). This gives rise to the $\sigma(1-k)\cos 2\alpha$ contribution to Eqs. $(2.21)_1$ and $(2.24)_1$, and to the second lines of the Eqs. (2.22) and (2.25), contributions which do not appear in the usual expression of these equations in the fracture mechanics literature. When the crack is inclined the horizontal load will also effect K_1 and K_2, i.e., will also appear in the coefficient of the first term of the series expansions, while for the horizontal crack orientation K_1 is independent of $k\sigma$ and $K_2 = 0$.

It is also noted that the customary expressions for the displacements (which consist of only the first lines of Eqs. (2.22) and (2.25)) predict zero displacements for the crack ends which, from physical considerations alone, must be incorrect. According to Eq. (2.22)

$$\begin{Bmatrix} u_x \\ u_y \end{Bmatrix}_{r=0} \approx \frac{(1-k)(\kappa+1)\sigma a}{8\mu} \begin{Bmatrix} \cos 2\alpha \\ \sin 2\alpha \end{Bmatrix} , \tag{2.27}$$

whereas for the crack with a horizontal orientation

$$(u_x)_{\substack{r=0 \\ \alpha=\pi/2}} \approx \frac{(1-k)(\kappa+1)\sigma a}{8\mu} , \quad (u_y)_{\substack{r=0 \\ \alpha=\pi/2}} = 0 , \tag{2.28}$$

showing that the crack tips move horizontally out (away from the center) for horizontal tensile loads, $k>1$, and move horizontally in for tensile loads, $0<k<1$, and compressive loads, $k<0$.

-11-

The equations obtained above show explicitly how in situations of biaxial load application along the exterior boundary of the body, the usual approximation for the stress and displacements in the vicinity of the crack tip by means of only the first term of the series expansions of the functions representing them is, in general, <u>inadequate</u>, because it excludes in part, if not entirely*, the presence of the horizontal load $k\sigma$ in its representation of the mechanical state of the crack tip region.

Referred to the polar coordinates at the crack tip (cf. Fig. 2) the plane elastic strain energy density (per unit volume) at any point can be determined by

$$\psi(r,\theta) = \frac{1}{2}\left[t_{xx}\frac{\partial u_x}{\partial x} + t_{yy}\frac{\partial u_y}{\partial y} + t_{xy}\left(\frac{\partial u_x}{\partial y} + \frac{\partial u_y}{\partial x}\right)\right]$$

$$= \frac{1}{2}\left[t_{xx}\left(\frac{\partial u_x}{\partial r}\cos\theta - \frac{\partial u_x}{\partial \theta}\frac{\sin\theta}{r}\right) + t_{yy}\left(\frac{\partial u_y}{\partial r}\sin\theta + \frac{\partial u_y}{\partial \theta}\frac{\cos\theta}{r}\right)\right.$$

$$\left. + t_{xy}\left(\frac{\partial u_x}{\partial r}\sin\theta + \frac{\partial u_x}{\partial \theta}\frac{\cos\theta}{r} + \frac{\partial u_y}{\partial r}\cos\theta - \frac{\partial u_y}{\partial \theta}\frac{\sin\theta}{r}\right)\right]. \quad (2.29)$$

By means of Eqs. (2.21), (2.22) and (2.29) the strain energy density in the immediate vicinity of the crack tip is given by [2,5]

---

* For the horizontally oriented crack the presence of the horizontal load $k\sigma$ appears <u>only</u> through the second term of the series expansions.

$$\psi \cong \frac{K_1^2}{8\mu\pi r} \left[-2\sin^4 \frac{\theta}{2} + (3-\kappa)\sin^2 \frac{\theta}{2} + (\kappa-1) \right]$$

$$+ \frac{K_2^2}{8\mu\pi r} \left[8\sin^7\frac{\theta}{2} - 8\sin^6\frac{\theta}{2} - 10\sin^5\frac{\theta}{2} + 16\sin^4\frac{\theta}{2} + 2\sin^3\frac{\theta}{2} + (\kappa-9)\sin^2\frac{\theta}{2} + 2 \right]$$

$$+ \frac{K_1 K_2}{16\mu\pi r} \left[\cos\frac{\theta}{2}\left\{ -64\sin^9\frac{\theta}{2} + 128\sin^7\frac{\theta}{2} + (8\kappa-25)\sin^5\frac{\theta}{2} - 6(\kappa+5)\sin^3\frac{\theta}{2} + 2(9-\kappa)\sin\frac{\theta}{2} \right\} \right.$$

$$\left. + 128\sin^9\frac{\theta}{2} - 256\sin^7\frac{\theta}{2} + 152\sin^5\frac{\theta}{2} - 24\sin^3\frac{\theta}{2} \right]$$

$$+ \frac{K_1(1-k)\sigma}{4\mu(2\pi r)^{\frac{1}{2}}} \left[\cos\frac{\theta}{2}\left\{ (\kappa-1) - 6\sin^2\frac{\theta}{2} + 8\sin^4\frac{\theta}{2} \right\} \cos 2\alpha \right.$$

$$\left. + 2\sin\frac{\theta}{2}\left\{ 4(\kappa-2)\sin^4\frac{\theta}{2} + (11-5\kappa)\sin^2\frac{\theta}{2} + (\kappa-3) \right\} \sin 2\alpha \right]$$

$$+ \frac{K_2(1-k)\sigma}{4\mu(2\pi r)^{\frac{1}{2}}} \left[\sin\frac{\theta}{2}\left\{ -(\kappa+3) - 8\sin^4\frac{\theta}{2} + 10\sin^2\frac{\theta}{2} \right\} \cos 2\alpha \right.$$

$$\left. + 2\cos\frac{\theta}{2}\left\{ 2(\kappa-3)\sin^4\frac{\theta}{2} + (1-3\kappa)\sin^2\frac{\theta}{2} + (\kappa+1) \right\} \sin 2\alpha \right]$$

$$+ \frac{\sigma^2(1-k)^2}{16\mu} \left[(\kappa+1)\cos^2 2\alpha - \sin 2\theta \sin 4\alpha \right]. \tag{2.30}$$

Were one to calculate ψ from a quadratic representation entirely in terms of the plane stress components, i.e.,

$$\psi = \frac{1}{2E}(t_{xx}^2 + t_{yy}^2) + \frac{1+\nu}{E} t_{xy}^2 - \frac{\nu}{E} t_{xx} t_{yy}$$

and use Eqs. (2.21) with the $\sigma(1-k)\cos 2\alpha$ term omitted, then the resulting expression for ψ would have the form

$$\psi \cong c_1 K_1^2 F_1(\theta) + c_2 K_2^2 F_2(\theta) + c_{12} K_1 K_2 F_{12}(\theta),$$

which is the expression used in Sih's strain energy density theory [6]. A comparison of this approximation with Eq. (2.30) shows that the last three terms of (2.30), which stem from the presence of the non-singular contribution $\sigma(1-k)\cos 2\alpha$ to Eqs. (2.21) and the second line contributions to the displacement equations (2.22), are necessary additional terms which cannot be ignored if proper account is to be taken of the effect of the horizontal load $k\sigma$ on the local (crack tip) elastic strain energy density.

For the horizontal crack Eq. (2.30) reduces to

$$(\psi)_{\alpha/\pi2} \cong \frac{\sigma^2 a}{8\mu r}\left[-2\sin^4\frac{\theta}{2}+(3-\kappa)\sin^2\frac{\theta}{2}+(\kappa-1)\right.$$

$$\left. -(1-k)\left(\frac{2r}{a}\right)^{\frac{1}{2}}\cos\frac{\theta}{2}\left\{(\kappa-1)+8\sin^4\frac{\theta}{2}-6\sin^2\frac{\theta}{2}\right\}\right]$$

$$+\frac{(1-k)^2(\kappa+1)\sigma^2}{8\mu} \qquad (2.31)$$

The local elastic strain energy rate for an arbitrarily small circular region of unit thickness centered at the crack tip with radius r_0, where $0 < r_0/a \ll 1$, is obtained as the derivative with respect to the crack size of the integral

$$\Psi = \int_0^{r_0}\int_{-\pi}^{\pi} \psi(r,\theta)r\,dr\,d\theta ,$$

which, upon utilization of Eqs. (2.30) and (2.23), yields

$$\frac{\partial\Psi}{\partial a} = \frac{\sigma^2\pi r_0}{64\mu}\left[(2\kappa-1)\left\{(1+k)-(1-k)\cos 2\alpha\right\}^2+2(\kappa+2)(1-k)^2\sin^2 2\alpha\right.$$

$$(2.32)$$

$$\left. +\frac{32(1-k)}{45\mu}\left(\frac{r_0}{2a}\right)^{\frac{1}{2}}\left\{3(5\kappa-7)\left[(1+k)-(1-k)\cos 2\alpha\right]\cos 2\alpha+(6\kappa+1)(1-k)\sin^2 2\alpha\right\}\right]$$

-14-

The variation of $(\partial\Psi/\partial a)$ with crack angle and load biaxiality is shown in Fig. 5 for a value of $\nu = 0.30$ and $(r_0/a) = 0.07$. For the horizontal crack Eq. (2.32) simplifies to

$$\left(\frac{\partial\Psi}{\partial a}\right)_{\alpha=\pi/2} = \frac{\sigma^2\pi r_0}{16\mu}\left[(2\kappa-1) - \left(\frac{r_0}{2a}\right)^{\frac{1}{2}}\frac{16(5\kappa-7)(1-k)}{15\pi}\right] . \qquad (2.33)$$

2.2 TWO COLLINEAR CRACKS

For the double collinear crack geometry shown by Fig. 6, the exterior boundary conditions are specified by Eqs. (2.6), whereas along the interior crack boundaries

$$t_{yy}(x,0) = t_{xy}(x,0) = 0, \qquad |a| < |x| < |b| . \qquad (2.34)$$

The solution is given by the sectionally holomorphic functions [7]

$$\left.\begin{array}{c}\phi(z)\\[2mm]\Omega(z)\end{array}\right\} = \frac{A(z^2-B)}{[(z^2-a^2)(z^2-b^2)]^{\frac{1}{2}}} \mp C \qquad (2.35)$$

$$\left.\begin{array}{c}\phi(z)\\[2mm]\omega(z)\end{array}\right\} = A\int\frac{z^2 dz}{[(z^2-a^2)(z^2-b^2)]^{\frac{1}{2}}} - AB\int\frac{dz}{[(z^2-a^2)(z^2-b^2)]^{\frac{1}{2}}} \mp Cz , \qquad (2.36)$$

where

$$A = \frac{\sigma}{4}\left[(1-e^{2i\alpha})+k(1+e^{2i\alpha})\right]$$

$$B = b^2[E(p)/F(p)] = b^2\lambda(p), \quad p^2 = 1-a^2/b^2 \qquad (2.37)$$

$$C = -\frac{1}{4}\sigma(1-k)e^{2i\alpha} .$$

-15-

Note that in the limit as $a \to 0$ the complete elliptic integrals $E(p) \to 1$, $F(p) \to \infty$ and the above expressions reduce to the solution (2.8) and (2.10) for a single crack of length 2b.

In establishing the structure of the functions Φ and Ω near the ends of the cuts, because of the geometrical symmetry, only one cut need be examined, say the one along the positive x-axis. Consider first a circular region R_b enclosing the end of the crack at $z=b$, with radius sufficiently small so as to exclude the point $z=a$, (cf. Fig. 7). Equation (2.35) can be rearranged to the form

$$\left.\begin{array}{c}\Phi(z)\\[2mm]\Omega(z)\end{array}\right\} = \frac{1}{(z-b)^{\frac{1}{2}}}\left[\frac{Az^2}{(z+b)^{\frac{1}{2}}(z^2-a^2)^{\frac{1}{2}}} - \frac{AB}{(z+b)^{\frac{1}{2}}(z^2-a^2)^{\frac{1}{2}}}\right] \div C$$

$$\equiv \frac{f_b(z)}{(z-b)^{\frac{1}{2}}} \div C,$$

where $f_b(z)$, representing the terms appearing within the bracket, is clearly analytic for all points z in R_b. A similar argument can be made for all points of a circular region R_a enclosing the end of the cut at $z=a$, while excluding the point at $z=b$, merely by interchanging b with a in the above expression. Designating the ends of the cut by $z=z_j$, $j=1,2$, so that $z_1=a$ and $z_2=b$, the above arguments can be jointly stated as

$$\left.\begin{array}{c}\Phi(z)\\[2mm]\Omega(z)\end{array}\right| = \frac{f_j(z)}{(z-z_j)^{\frac{1}{2}}} \div C, \qquad j=1,2$$

-16-

where the functions $f_j(z)$ are analytic for all points z of the regions R_j, thus allowing the series representations

$$f_j(z) = \beta_0^j + \beta_1^j(z-z_j) + \beta_2^j(z-z_j)^2 + \ldots\ldots\ldots\ldots,$$

in which the coefficients β_n^j include the constants A and B. Thus in the vicinity of the end points z_j of the cracks the structure of ϕ and Ω have the form

$$
\left.\begin{array}{c}\phi(z)\\[2mm]\Omega(z)\end{array}\right\} = \frac{\beta_0^j}{(z-z_j)^{\frac{1}{2}}} + \beta_1^j(z-z_j)^{\frac{1}{2}} + \beta_2^j(z-z_j)^{3/2} + \ldots\ldots\ldots \mp C
$$

$$
= \frac{\beta_0^j}{(z-z_j)^{\frac{1}{2}}} \mp C + O(|z-z_j|^{\frac{1}{2}}) , \qquad z_j \epsilon R_j, \quad j=1,2. \quad (2.38)
$$

Equations for the elastic stress and displacements in the crack-tip region can now be expressed in the standard form. This may be accomplished most economically by introduction of a pair of polar coordinate systems originating at the ends of the crack by writing $z-z_j = re^{i\theta}$, with the stipulation that, at the end $z_2 = b$ the angle θ is to be measured counter clockwise from the real axis, whereas at the end $z_1 = a$ it is to be taken clockwise. Accordingly, from Eqs. (2.1) and (2.38)

$$t_{yy} + t_{xx} = 4Re\left(\frac{\beta_0^j}{r^{\frac{1}{2}}} e^{-i\theta/2}\right) - 4Re\ C + O(r^{\frac{1}{2}})$$

$$t_{yy} - t_{xx} + 2it_{xy} = \frac{2\left(\overline{\beta_0^j} - \beta_0^j\right)}{r^{\frac{1}{2}}} e^{-i\theta/2} + 2i\frac{\beta_0^j}{r^{\frac{1}{2}}} e^{-i\frac{3\theta}{2}}\sin\theta \qquad (2.39)$$

$$+ 4Re\ C + O(r^{\frac{1}{2}}).$$

Consistent with standard notation, the coefficient β_0^j can be expressed in the form of a complex elastic stress intensity factor as

-17-

$$\beta_0^j = \frac{1}{2(2\pi)^{\frac{1}{2}}}\left(K_{1j} - iK_{2j}\right) . \tag{2.40}$$

Equations (2.39) and (2.40) then yield the characteristic forms

$$t_{xx} \cong \frac{K_{1j}}{(2\pi r)^{\frac{1}{2}}}\cos\frac{\theta}{2}\left(1-\sin\frac{\theta}{2}\sin\frac{3\theta}{2}\right) - \frac{K_{2j}}{(2\pi r)^{\frac{1}{2}}}\sin\frac{\theta}{2}\left(2+\cos\frac{\theta}{2}\cos\frac{3\theta}{2}\right)$$
$$+ \sigma(1-k)\cos 2\alpha .$$

$$t_{yy} \cong \frac{K_{1j}}{(2\pi r)^{\frac{1}{2}}}\cos\frac{\theta}{2}\left(1+\sin\frac{\theta}{2}\sin\frac{3\theta}{2}\right) + \frac{K_{2j}}{(2\pi r)^{\frac{1}{2}}}\sin\frac{\theta}{2}\cos\frac{\theta}{2}\cos\frac{3\theta}{2} . \tag{2.41}$$

$$t_{xy} \cong \frac{K_{1j}}{(2\pi r)^{\frac{1}{2}}}\sin\frac{\theta}{2}\cos\frac{\theta}{2}\cos\frac{3\theta}{2} + \frac{K_{2j}}{(2\pi r)^{\frac{1}{2}}}\cos\frac{\theta}{2}\left(1-\sin\frac{\theta}{2}\sin\frac{3\theta}{2}\right)$$

for $z\epsilon R_j$, $j=1,2$.

At the inner and outer ends of the cut, respectively,

$$K_{1j} = K_{11} \equiv K_1(a) \quad , \quad K_{1j} = K_{12} \equiv K_1(b)$$

$$K_{2j} = K_{21} \equiv K_2(a) \quad , \quad K_{2j} = K_{22} \equiv K_2(b) . \tag{2.42}$$

Considering the manner in which angle θ is defined, Eqs. (2.38) and (2.40) afford explicit determination of the stress intensity factors according to the relations

$$\left.\begin{array}{r} i\left(K_{1j}-iK_{2j}\right)_{j=1} \\ \left(K_{1j}-iK_{2j}\right)_{j=2} \end{array}\right\} = \lim_{z\to z_j}\left[2(2\pi)^{\frac{1}{2}}(z-z_j)^{\frac{1}{2}}\Phi(z)\right] , \tag{2.42a}$$

from which

$$K_1(a) = \frac{\sigma\sqrt{\pi a}[b^2\lambda(p)-a^2]}{2a(b^2-a^2)^{\frac{1}{2}}}[(1+k)-(1-k)\cos 2\alpha]$$

$$K_2(a) = \frac{\sigma\sqrt{\pi a}[b^2\lambda(p)-a^2]}{2a(b^2-a^2)^{\frac{1}{2}}}(1-k)\sin 2\alpha \tag{2.43}$$

-18-

and

$$K_1(b) = \frac{\sigma\sqrt{\pi b}\ b[1-\lambda(p)]}{2(b^2-a^2)^{\frac{1}{2}}}\ [(1+k)-(1-k)\cos 2\alpha]$$

$$K_2(b) = \frac{\sigma\sqrt{\pi b}\ b[1-\lambda(p)]}{2(b^2-a^2)^{\frac{1}{2}}}\ (1-k)\sin 2\alpha \qquad (2.44)$$

for $0<a<b$. The variation of $K_1(a)/K_1(b)$ and $K_2(a)/K_2(b)$ with crack spacing is shown in Fig. 8. When the distance between the cracks is the equivalent of the crack length, interaction of the inner crack-tip stress fields is just about negligible, $K_1(a)$ and $K_2(a)$ being only two percent greater than $K_1(b)$ and $K_2(b)$. For crack spacing at about three tenths the crack length or less, the stress intensity at the inner crack ends increase rapidly relative to the outer ends.

For horizontally oriented cracks,

$$K_1(a) = \frac{\sigma(\pi a)^{\frac{1}{2}}[b^2\lambda(p)-a^2]}{a(b^2-a^2)^{\frac{1}{2}}}$$

$$K_1(b) = \frac{\sigma(\pi b)^{\frac{1}{2}}b[1-\lambda(p)]}{(b^2-a^2)^{\frac{1}{2}}} \qquad (2.45)$$

$$K_2(a) = K_2(b) = 0$$

independent of the load biaxiality.

From Eqs. (2.1), (2.2) and (2.38), $\phi(z)$ and $\omega(z)$ can be represented by the series

$$\left.\begin{array}{c}\phi(z)\\[2mm]\omega(z)\end{array}\right\} = \ 2\beta_0^j(z-z_j)^{\frac{1}{2}} + Cz + 0(|z-z_j|^{3/2})$$

$$\qquad (2.46)$$

$$= 2\beta_0^j r^{\frac{1}{2}}e^{i\theta/2} + Cz_j\left(\frac{r}{z_j}\ e^{i\theta} + 1\right) + 0\left(r^{3/2}\right)\quad.$$

-19-

Substitution of Eqs. (2.46), (2.38) and (2.40) into (2.1)$_3$ yields the following expressions for the displacements components in the immediate vicinity of the ends of the cracks:

$$u_x \approx \frac{K_{1j}}{\mu}\left(\frac{r}{2\pi}\right)^{\frac{1}{2}}\cos\frac{\theta}{2}\left[\frac{1}{2}(\kappa-1)+\sin^2\frac{\theta}{2}\right]+\frac{K_{2j}}{\mu}\left(\frac{r}{2\pi}\right)^{\frac{1}{2}}\sin\frac{\theta}{2}\left[\frac{1}{2}(\kappa+1)+\cos^2\frac{\theta}{2}\right]$$

$$+\frac{\sigma(1-k)}{4\mu}\left[\frac{1}{2}(\kappa+1)z_j\cos2\alpha-r\sin\theta\sin2\alpha+\frac{1}{2}r\left\{\kappa\cos(\theta+2\alpha)+\cos(\theta-2\alpha)\right\}\right]$$

$$(2.47)$$

$$u_y \approx \frac{K_{1j}}{\mu}\left(\frac{r}{2\pi}\right)^{\frac{1}{2}}\sin\frac{\theta}{2}\left[\frac{1}{2}(\kappa+1)-\cos^2\frac{\theta}{2}\right]+\frac{K_{2j}}{\mu}\left(\frac{r}{2\pi}\right)^{\frac{1}{2}}\cos\frac{\theta}{2}\left[\frac{1}{2}(1-\kappa)+\sin^2\frac{\theta}{2}\right]$$

$$+\frac{\sigma(1-k)}{4\mu}\left[\frac{1}{2}(\kappa+1)z_j\sin2\alpha-r\sin\theta\cos2\alpha+\frac{1}{2}r\left\{\kappa\sin(2\alpha+\theta)+\sin(2\alpha-\theta)\right\}\right],$$

where $j=1,2$ and $z_1=a$, $z_2=b$.

The same comments that were made for the single crack concerning the presence of the horizontal load $k\sigma$ in the approximations for the crack tip region stress and displacements, apply verbatim for the double crack geometry, as Eqs. (2.37), (2.38), (2.41)-(2.47) indicate.

2.3 SHEAR PANEL

The centrally cracked sheet subject to pure shear along the outer boundary (cf. Fig. 9)

$$t_{yy}'(\infty)=0, \qquad t_{xx}'(\infty)=0, \qquad t_{xy}'(\infty)=\tau \qquad (2.48)$$

relative to the $(x'-y')$ coordinate system, can be transformed to a biaxial boundary condition

$$t_{yy}(\infty)=-\tau\sin2\beta, \qquad t_{xx}(\infty)=\tau\sin2\beta, \qquad t_{xy}(\infty)=\tau\cos2\beta \qquad (2.49)$$

relative to the $(x-y)$ coordinate system. The boundary condition along the interior crack boundary is specified by Eq. (2.7)

The solution to the above problem is given by [8]

$$\left.\begin{matrix}\phi(z)\\ \\ \Omega(z)\end{matrix}\right\} = -\frac{1}{2}i\tau e^{-2i\beta}\left(\frac{z}{(z^2-a^2)^{\frac{1}{2}}} \mp 1\right) \quad , \qquad (2.50)$$

so that

$$\left.\begin{matrix}\phi(z)\\ \\ \omega(z)\end{matrix}\right\} = -\frac{1}{2}i\tau e^{-2i\beta}\left[(z^2-a^2)^{\frac{1}{2}} \mp z\right] \quad . \qquad (2.51)$$

Relative to the polar coordinate system at the crack tip $z-a=\zeta=re^{i\theta}$ (cf. Fig. 2), Φ has the power series expansion

$$\Phi(\zeta) = -\frac{1}{2}i\tau e^{-2i\beta}\frac{1}{(2)^{\frac{1}{2}}}\left\{\left(\frac{\zeta}{a}\right)^{-\frac{1}{2}} - (2)^{\frac{1}{2}}\left(\frac{\zeta}{a}\right)^0 + \frac{3}{4}\left(\frac{\zeta}{a}\right)^{\frac{1}{2}} - \dots\dots\right\}$$

$$= \frac{K_1-iK_2}{2(2\pi\zeta)^{\frac{1}{2}}} + \frac{1}{2}i\tau e^{-2i\beta} + O\left(\left|\frac{\zeta}{a}\right|^{\frac{1}{2}}\right) , \qquad (2.52)$$

where by means of Eqs. (2.16) and (2.50)

$$K_1-iK_2 = -i\tau(\pi a)^{\frac{1}{2}}e^{-2i\beta} \quad . \qquad (2.53)$$

Thus for $0<|\zeta/a|=(r/a)<<1$, up to terms of order $(r/a)^{\frac{1}{2}}$, the stress functions become, (analogous to Eqs. (2.18)),

$$\left.\begin{matrix}2\Phi(\zeta)\\ \\ 2\Omega(\zeta)\end{matrix}\right\} \approx \frac{K_1-iK_2}{(2\pi r)^{\frac{1}{2}}}e^{-i(\theta/2)} \pm i\tau e^{-2i\beta} \quad . \qquad (2.54)$$

Similarly, for $\phi(\zeta)$ and $\omega(\zeta)$ up to terms of order $(r/a)^{3/2}$, (analogous to Eqs. (2.20)),

$$\left.\begin{matrix}\phi(\zeta)\\ \\ \omega(\zeta)\end{matrix}\right\} \approx (K_1-iK_2)\left(\frac{r}{2\pi}\right)^{\frac{1}{2}}e^{i(\theta/2)} \pm \frac{1}{2}i\tau a\left(\frac{r}{a}e^{i\theta}+1\right)e^{-2i\beta} \quad . \qquad (2.55)$$

The elastic stress and displacement in the vicinity of the crack tip follow from Eqs. (2.1), (2.54) and (2.55) as

-21-

$$t_{xx} \cong \frac{K_1}{(2\pi r)^{\frac{1}{2}}} \cos\frac{\theta}{2}\left(1-\sin\frac{\theta}{2}\sin\frac{3\theta}{2}\right) - \frac{K_2}{(2\pi r)^{\frac{1}{2}}} \sin\frac{\theta}{2}\left(2+\cos\frac{\theta}{2}\cos\frac{3\theta}{2}\right) + 2\tau\sin\beta$$

$$t_{yy} \cong \frac{K_1}{(2\pi r)^{\frac{1}{2}}} \cos\frac{\theta}{2}\left(1+\sin\frac{\theta}{2}\sin\frac{3\theta}{2}\right) + \frac{K_2}{(2\pi r)^{\frac{1}{2}}} \sin\frac{\theta}{2} \cos\frac{\theta}{2} \cos\frac{3\theta}{2} \qquad (2.56)$$

$$t_{xy} \cong \frac{K_1}{(2\pi r)^{\frac{1}{2}}} \sin\frac{\theta}{2} \cos\frac{\theta}{2} \cos\frac{3\theta}{2} + \frac{K_2}{(2\pi r)^{\frac{1}{2}}} \cos\frac{\theta}{2}\left(1-\sin\frac{\theta}{2} \sin\frac{3\theta}{2}\right)$$

and

$$u_x \cong \frac{K_1}{\mu}\left(\frac{r}{2\pi}\right)^{\frac{1}{2}} \cos\frac{\theta}{2}\left[\frac{1}{2}(\kappa-1)+\sin^2\frac{\theta}{2}\right] + \frac{K_2}{\mu}\left(\frac{r}{2\pi}\right)^{\frac{1}{2}} \sin\frac{\theta}{2}\left[\frac{1}{2}(\kappa+1)+\cos^2\frac{\theta}{2}\right]$$

$$+ \frac{\tau}{4\mu}[(\kappa+1)(r\cos\theta+a)\sin2\beta-(\kappa+3)r\sin\theta\cos2\beta]$$

$$(2.57)$$

$$u_y \cong \frac{K_1}{\mu}\left(\frac{r}{2\pi}\right)^{\frac{1}{2}} \sin\frac{\theta}{2}\left[\frac{1}{2}(\kappa+1)-\cos^2\frac{\theta}{2}\right] + \frac{K_2}{\mu}\left(\frac{r}{2\pi}\right)^{\frac{1}{2}} \cos\frac{\theta}{2}\left[\frac{1}{2}(1-\kappa)+\sin^2\frac{\theta}{2}\right]$$

$$+ \frac{\tau}{4\mu}[(\kappa+1)(r\cos\theta+a)\cos2\beta+(\kappa-5)r\sin\theta\sin2\beta] \quad ,$$

where from Eq. (2.53)

$$K_1 = -\tau(\pi a)^{\frac{1}{2}}\sin2\beta \quad , \qquad K_2 = \tau(\pi a)^{\frac{1}{2}}\cos2\beta \quad . \qquad (2.58)$$

It will be instructive to again focus attention on the second term of the series expansion approximations given by Eqs. (2.54) and (2.55), which lead to the $2\tau\sin\beta$ contribution to Eqs. (2.56) for the stress, and to the second lines of Eqs. (2.57) for the displacement. As for the biaxially loaded cracked bodies, failure to retain these terms in the series approximations for the crack tip stress and displacement can lead to significant error in describing the mechanical state about the crack tip. For example, for the displacements at the tip of the inclined crack

$$
\begin{Bmatrix} u_x \\ u_y \end{Bmatrix}_{r=0} \approx \frac{\tau(\kappa+1)a}{4\mu} \begin{Bmatrix} \sin 2\beta \\ \cos 2\beta \end{Bmatrix} \quad , \tag{2.59}
$$

which according to the usual one-term series approximation should be zero.

SECTION 3

ISOSTATS FOR MAXIMUM SHEAR STRESS

The maximum shear stress at any point of a body in plane stress or plane strain is determined by

$$\tau_m^2 = \frac{1}{4}(t_{yy} - t_{xx})^2 + t_{xy}^2 \quad . \tag{3.1}$$

3.1 SINGLE CRACK

For the maximum shear stress near the tip of the inclined crack Eq. (2.21) may be substituted into Eq. (3.1) with the result

$$\tau_m^2 \cong \frac{1}{8\pi r}\left[K_1^2\sin^2\theta + K_2^2(4-3\sin^2\theta) + 4K_1 K_2 \sin\theta\cos\frac{\theta}{2}\right]$$

$$- \frac{1}{2}\sigma(1-k)\cos 2\alpha\left[\frac{K_1}{(2\pi r)^{\frac{1}{2}}}\sin\theta\sin\frac{3\theta}{2} + \frac{K_2}{(2\pi r)^{\frac{1}{2}}}\left(\sin\theta\cos\frac{3\theta}{2} + 2\sin\frac{\theta}{2}\right)\right.$$

$$\left. - \frac{1}{2}\sigma(1-k)\cos 2\alpha\right] \quad . \tag{3.2}$$

With the crack horizontally oriented, the maximum shear stress becomes

$$\left(\tau_m^2\right)_{\alpha=\pi/2} \cong \frac{1}{8\pi r}K_1^2\sin^2\theta + \frac{K_1}{2(2\pi r)^{\frac{1}{2}}}\sin\theta\sin\frac{3\theta}{2}\sigma(1-k) + \frac{\sigma^2}{4}(1-k)^2 . \tag{3.3}$$

If the customary singular approximation for stress were employed in Eq. (3.1), i.e., Eq. (2.21) without the $\sigma(1-k)\cos 2\alpha$ contribution, only the first line of Eq. (3.2) would appear for the inclined crack and only the first term of (3.3) would appear for the horizontal crack. Designating the latter by

$$\left(\tau_m^{*2}\right)_{\alpha=\pi/2} = \frac{1}{8\pi r}K_1^2\sin^2\theta \quad , \tag{3.4}$$

where $K_1^2 = \sigma^2 \pi a$, it is seen that the effect of the horizontal load $k\sigma$ on the maximum shear stress disappears entirely. The ratio of Eq. (3.3) to Eq. (3.4)

$$\left(\frac{\tau_m}{\tau_m^*}\right)_{\alpha = \pi/2} = \frac{\left[\left(\frac{a}{r}\right)\sin^2\theta + 4(1-k)\left(\frac{a}{2r}\right)^{\frac{1}{2}}\sin\theta\sin\frac{3\theta}{2} + 2(1-k)^2\right]^{\frac{1}{2}}}{\left(\frac{a}{r}\right)^{\frac{1}{2}}\sin\theta} \qquad (3.5)$$

gives a measure of the error for the maximum shear stress that is associated with use of Eq. (3.4). The ratio given by Eq. (3.5) is plotted in Fig. 10 along the radial line $\theta = 20^O$.

Equation (3.2) together with Eq. (2.23) can be rearranged to the following more convenient form for the purposes of drawing lines of constant maximum shear stress near the crack tip.

$$\left\{\left(\frac{\tau_m}{\sigma}\right)^2 - \left[\frac{(1-k)\cos2\alpha}{2}\right]^2\right\}\left(\frac{r}{a}\right)$$

$$+ \frac{1}{4(2)^{\frac{1}{2}}}\left\{\left[(1-k^2)\cos2\alpha - (1-k)^2\cos^2 2\alpha\right]F_1(\theta) + \left[(1-k)^2\sin4\alpha\right]F_2(\theta)\right\}\left(\frac{r}{a}\right)^{\frac{1}{2}}$$

$$- \frac{1}{32}\left\{\left[(1+k)^2 - 2(1-k^2)\cos2\alpha + (1-k)^2\cos^2 2\alpha\right]F_3(\theta) + \left[(1-k)^2\sin^2 2\alpha\right]F_4(\theta)\right.$$

$$\left. + \left[4(1-k^2)\sin2\alpha - 2(1-k)^2\sin4\alpha\right]F_5(\theta)\right\} = 0, \qquad (3.6)$$

where

$$F_1(\theta) = \sin\theta\sin\frac{3\theta}{2} \qquad\qquad F_4(\theta) = (4 - 3\sin^2\theta)$$

$$F_2(\theta) = \sin\theta\cos\frac{3\theta}{2} + 2\sin\frac{\theta}{2} \qquad F_5(\theta) = \sin\theta\cos\frac{\theta}{2} \qquad (3.7)$$

$$F_3(\theta) = \sin^2\theta$$

For $\alpha = \pi/2$, Eqs. (3.6) reduce to

$$\left\{\left(\frac{\tau_m}{\sigma}\right)^2 - \left(\frac{1-k}{2}\right)^2\right\}\left(\frac{r}{a}\right) - \left\{\frac{(1-k)}{2(2)^{\frac{1}{2}}} \sin\theta\sin\frac{3\theta}{2}\right\}\left(\frac{r}{a}\right)^{\frac{1}{2}} - \frac{1}{8}\sin^2\theta = 0. \qquad (3.8)$$

The pronounced effect that the load biaxiality has on the maximum shear stress near the crack tip is shown in Figures 11-13. It is observed in Fig. 11 that as the load biaxiality passes from tension-tension to uniaxial tension to tension-compression, the extent of high level shear about the end of the crack increases appreciably. Moreover, since plastic yield is strongly influenced by the maximum shear stress (c.f. the yield conditions of Tresca and Mises,) the plastic yield region about the crack tip should show a similar pattern of variation with load biaxiality, that is, should increase in size as load biaxiality varies from tension-tension to tension-compression.

3.2 TWO COLLINEAR CRACKS

Equation (2.41) combined with Eq. (3.1) produces exactly the same form for the square of the maximum shear stress as Eq. (3.2) for the single crack, except that K_1 and K_2 in (3.2) is now replaced by K_{1j} and K_{2j} as defined by Eq. (2.42) and (2.43). When these expressions for the stress intensity factors are explicitly introduced, the equation defining the isostats of maximum shear stress, analogous to Eq. (3.6), becomes

$$\left\{\left(\frac{\tau_m}{\sigma}\right)^2-\left[\frac{(1-k)\cos 2\alpha}{2}\right]^2\right\}\left(\frac{r}{z_j}\right)$$

$$+\frac{1}{4(2)^{\frac{1}{2}}}\,L_j(p)\left\{[(1-k^2)\cos 2\alpha-(1-k)^2\cos^2 2\alpha]F_1(\theta)+\left[\frac{(1-k)^2}{2}\sin 4\alpha\right]F_2(\theta)\right\}\left(\frac{r}{z_j}\right)^{\frac{1}{2}}$$

$$-\frac{1}{32}\,L_j^2(p)\left\{[(1+k)^2\cos 2\alpha+(1-k)^2\cos^2 2\alpha]F_3(\theta)\right.$$

$$\left.+[(1-k)^2\sin^2 2\alpha]F_4(\theta)+[(1-k^2)\sin 2\alpha-\frac{(1-k)^2}{2}\sin 4\alpha]F_5(\theta)\right\}=0,\quad j=1,2,\qquad (3.9)$$

where

$$L_1(p)=\frac{b^2\lambda(p)-a^2}{a(b^2-a^2)^{\frac{1}{2}}}\ ,\qquad\qquad L_2(p)=\frac{b[1-\lambda(p)]}{(b^2-a^2)^{\frac{1}{2}}}\ ,\qquad (3.10)$$

and the $F_k(\theta)$, $k=1,2,\ldots,5$ are as defined by Eq. (3.7). Figures 14-16 give an indication of the variation of the normalized maximum shear stress with load biaxiality for cracks of unit length inclined at $\alpha=45^\circ$ and spaced at $2a=0.20$.

3.3 SHEAR PANEL

For the cracked shear panel the maximum shear stress near the crack tip is determined from Eqs. (2.56) and (3.1) as

$$\tau_m^2\cong\frac{1}{8\pi r}\left[K_1{}^2\sin^2\theta+K_2{}^2(4-3\sin^2\theta)+4K_1K_2\sin\theta\cos\frac{\theta}{2}\right]$$

$$-\tau\sin 2\beta\left[\frac{K_1}{(2\pi r)^{\frac{1}{2}}}\sin\theta\sin\frac{3\theta}{2}+\frac{K_2}{(2\pi r)^{\frac{1}{2}}}\left(\sin\theta\cos\frac{3\theta}{2}+2\sin\frac{\theta}{2}\right)+\tau\sin 2\beta\right].$$

$$(3.11)$$

Again, if the customary singular approximation for the stress were used in Eq.(3.1), i.e., Eq. (2.56) without the $2\tau\sin 2\beta$ contribution, the result would be only the first line of Eq. (3.11). Designating the first line of Eq. (3.11) by τ_m^*,

$$\tau_m^* = \frac{1}{8\pi} \left[K_1^2 \sin^2\theta + K_2^2 (4 - 3\sin^2\theta) + 4K_1 K_2 \sin\theta\cos\frac{\theta}{2} \right] \quad , \quad (3.12)$$

a measure of the error involved by the use of Eq. (3.12) rather than Eq. (3.11) is provided by

$$\left(\frac{\tau_m}{\tau_m^*}\right)^2 = 1 - \left[32\left(\frac{r}{a}\right)\right]^{\frac{1}{2}} \left\{ \frac{\cos2\beta\left(\sin\theta\sin\frac{3\theta}{2} + 2\sin\frac{\theta}{2}\right) - \sin2\beta\sin\theta\sin\frac{3\theta}{2}}{\sin2\beta\sin^2\theta + \cot2\beta\cos2\beta(4 - 3\sin^2\theta) - 4\cos2\beta\sin\theta\cos\frac{\theta}{2}} \right\}$$

$$- 8\left(\frac{r}{a}\right)\left\{ \frac{1}{\sin^2\theta + \cot^2 2\beta(4 - 3\sin^2\theta) - 4\cot2\beta\sin\theta\cos\frac{\theta}{2}} \right\} \quad , \quad (3.13)$$

which is illustrated by Fig. 17.

Equation (3.11), in which K_1 and K_2 are given by Eq. (2.58), can be written as

$$\left\{ \left(\frac{\tau_m}{\tau}\right)^2 + \sin2\beta\right\}\left(\frac{r}{a}\right) - \frac{1}{(2)^{\frac{1}{2}}} \left\{ \sin^2 2\beta F_1(\theta) - \sin2\beta\cos2\beta F_2(\theta) \right\} \left(\frac{r}{a}\right)^{\frac{1}{2}}$$

$$- \frac{1}{8}\left\{ \sin^2 2\beta F_3(\theta) + \cos^2 2\beta F_4(\theta) - 4\sin2\beta\cos2\beta F_5(\theta) \right\} = 0 \quad , \quad (3.14)$$

where the $F_k(\theta)$, $k = 1, 2, \ldots, 5$, are as defined by Eq. (3.7). Equation (3.14) may be used to draw isostats of normalized maximum shear stress as shown in Fig. 18.

SECTION 4

ANGLE OF INITIAL CRACK EXTENSION

The maximum tensile stress criterion may be used to obtain
an estimate of the angle at which a crack extension will begin
to take place. Although the criterion itself cannot be considered
to be wholly satisfactory, it nevertheless has been shown to
offer resonably good correlations with experimental data under
tensile loading [9,10], and can serve as a means of demonstrating
the influence of load biaxiality on the direction of crack
extension.

Designating θ_0 as the angle which locates the tangent to
the direction of initial crack extension, the criterion predicts
crack extension along the radial line normal to the direction
of the maximum tensile stress or, equivalently, along the dir-
ection parallel to the plane upon which the tangential stress
component $t_{\theta\theta}$ attains maximum value. A mathematical statement
of the criterion requires that at some arbitrarily small radial
distance $0<r_0<<1$ from the crack tip, the angle of crack exten-
sion is determined by simultaneous satisfaction of the con-
ditions:

$$t_{\theta\theta}(r_0,\theta_0)>0, \quad \frac{\partial t_{\theta\theta}(r_0,\theta_0)}{\partial\theta}=0, \quad \frac{\partial^2 t_{\theta\theta}(r_0,\theta_0)}{\partial\theta^2}<0 . \quad (4.1)$$

The unspecified radial dimension r_0 is necessitated by the
singular nature of the stress at the crack tip and introduces,
thereby, a small measure of arbitrariness in the predictions.
It should also be observed that no elastic material parameters
appear in the equations for stress in the plane theory of

linear elasticity (neglecting body force), consequently, the above criterion predicts the same angles for all materials.

A series expansion for the tangential stress component $t_{\theta\theta}$ can be shown to have the following form [3] (up to terms of order $(\frac{r}{a})^{\frac{1}{2}}$)

$$\frac{t_{\theta\theta}}{t} \cong A(r)\left\{B_1\left(\sin\frac{\theta}{2}+\sin\frac{3\theta}{2}\right)+B_2\left(3\cos\frac{\theta}{2}+\cos\frac{3\theta}{2}\right)\right\}+B_3\sin^2\theta \qquad (4.2)$$

where the stress t, the function $A(r)$ and the coefficients B_1, B_2, B_3, are defined below for each particular load-crack geometry. Insertion of Eq.(4.2) into the conditions (4.1) leads to the set of requirements

$$A(r_0)\left\{B_1\left[\sin\frac{\theta_0}{2}+\sin\frac{3\theta_0}{2}\right]+B_2\left[3\cos\frac{\theta_0}{2}+\cos\frac{3\theta_0}{2}\right]\right\}+B_3\sin^2\theta_0 > 0$$

$$A(r_0)\left\{B_1\left[3\cos\theta_0-1\right]-3B_2\sin\theta_0\right\}+4B_3\sin\frac{\theta_0}{2}\cos\theta_0 = 0 \qquad (4.3)$$

$$A(r_0)\left\{B_1\sin\frac{\theta_0}{2}\left[9\sin^2\frac{\theta_0}{2}-7\right]+B_2\cos\frac{\theta_0}{2}\left[6-9\cos^2\frac{\theta_0}{2}\right]\right\}+2B_3\cos2\theta_0 > 0$$

which, when satisfied collectively, determine the crack extension angle θ_0.

4.1 SINGLE CRACK

For the single inclined crack the undefined quantities appearing in Eqs. (4.2) and (4.3) are as follows:

$$t = \sigma$$

$$A(r) = \left\{\frac{1}{32}\left(\frac{a}{r}\right)\right\}^{\frac{1}{2}}$$

$$B_1 = (k-3)\sin\alpha\cos\alpha$$

$$B_2 = k+(1-k)\sin^2\alpha$$

$$B_3 = (1-k)\cos2\alpha$$

-30-

A summary of the variation of the angle of crack extension, θ_0, with crack inclination, α, and load biaxiality, k, is shown by Fig. 19, for which the arbitrary value of r_0 was chosen such that $(a/r_0) = 0.01$.

4.2 TWO COLLINEAR CRACKS

For the collinear cracks, the undefined quantities become

$$t = \sigma$$

$$A(r) = A_j(r) \cdot L_j(p), \qquad j = 1, 2$$

$$A_1(r) = \left\{ \frac{1}{32}\left(\frac{a}{r}\right) \right\}^{\frac{1}{2}}, \qquad L_1(p) = \frac{b^2 \lambda(p) - a^2}{a(b^2 - a^2)^{\frac{1}{2}}}$$

$$A_2(r) = \left\{ \frac{1}{32}\left(\frac{b}{r}\right) \right\}^{\frac{1}{2}}, \qquad L_2(p) = \frac{b[1 - \lambda(p)]}{(b^2 - a^2)^{\frac{1}{2}}}$$

$$B_1 = (k-3)\sin\alpha\cos\alpha$$
$$B_2 = k + (1-k)\sin^2\alpha$$
$$B_3 = (1-k)\cos2\alpha$$

$$\left(\frac{a}{r_0}\right) = \left(\frac{b}{r_0}\right) = 0.01$$

Figures 20 and 21 illustrate the variation of crack extension angle with load biaxiality and inclination of the cracks. Figure 20 is for the inner crack tip $z_1 = a$ and Fig. 21 for the outer crack tip $z_2 = b$. The crack spacing was taken at $2a = 0.20$. According to Fig. 20, the inner crack ends, although closely spaced, will not extend along their original directions to join together when the cracks are inclined, except under equal

-31-

tension-tension biaxial load, k=1, or when the cracks are horizontal, $\alpha=\pi/2$, and $k \leq 2$.

4.3   SHEAR PANEL

For the cracked shear panel, the undefined quantities become

$$t = \tau$$

$$A(r) = -\left\{ \frac{1}{32}\left(\frac{a}{r}\right) \right\}^{\frac{1}{2}}$$

$$B_1 = 3\cos 2\beta$$

$$B_2 = \sin 2\beta$$

$$B_3 = 2B_2$$

$$\left(\frac{a}{r_0}\right) = 0.01.$$

The variation of crack extension angle with crack orientation is shown in Fig. 22, along with experimental data for 7075 and 2024 aluminum alloys reported by Liu [11].

SECTION 5

DISPLACEMENT OF THE CRACK BORDER, COLLINEAR CRACKS

The components of displacement for the points defining the borders of either one of the inclined collinear cracks can be determined using Eq. (2.36) for $\phi(z)$ and $\omega(z)$ in Eq. $(2.1)_3$ for the points along the x-axis for which $a<x<b$. Approaching the crack from the positive side one obtains*

$$2\mu\left[u_x^{(+)}(x,0)+iu_y^{(+)}(x,0)\right] = (\kappa-1)A\left[\psi^{(+)}(x)-B\chi^{(+)}(x)\right]-(\kappa+1)Cx, \tag{5.1}$$

where

$$\psi(x) = \int_a^x \frac{x^2 dx}{[(x^2-a^2)(x^2-b^2)]^{\frac{1}{2}}} = \frac{1}{i}\left\{bE(\phi,p)-\frac{1}{x}(b^2-x^2)(x^2-a^2)\right\}^{\frac{1}{2}} \tag{5.2}$$

$$\chi(x) = \int_a^x \frac{dx}{[(x^2-a^2)(x^2-b^2)]^{\frac{1}{2}}} = \frac{1}{ib}F(\phi,p) .$$

$F(\phi,p)$ and $E(\phi,p)$ are the elliptic integrals of the first and second kind, respectively, with modulus p. Substitution of Eqs. (5.2) and (2.37) into (5.1) gives for the displacement components along the positive border of the cut

---

*Approaching the cut from the negative side, it may be shown that

$$\psi^{(-)}(x) = -\psi^{(+)}(x), \qquad \chi^{(-)}(x) = -\chi^{(+)}(x)$$

$$u_x^{(+)}(x,0) = -\frac{\sigma}{8\mu}(1-k)\left\{(\kappa-1)b\left[E(\phi,p) - \frac{x}{b}\left\langle\left[\left(\frac{b}{x}\right)^2-1\right]\left[1-\left(\frac{a}{x}\right)^2\right]\right\rangle^{\frac{1}{2}} - \lambda(p)F(\phi,p)\right]\sin 2\alpha\right.$$
$$\left. - (\kappa+1) \, x \cos 2\alpha\right\}$$

$$(5.3)$$

$$u_y^{(+)}(x,0) = -\frac{\sigma}{8\mu}\left\{(\kappa-1)b\left[E(\phi,p) - \frac{x}{b}\left\langle\left[\left(\frac{b}{x}\right)^2-1\right]\left[1-\left(\frac{a}{x}\right)^2\right]\right\rangle^{\frac{1}{2}} - \lambda(p)F(\phi,p)\right][(1+k)\right.$$
$$\left. - (1-k)\cos 2\alpha] - (\kappa+1)(1-k)x\sin 2\alpha\right\}.$$

For horizontally oriented cracks $u_x^{(+)}=u_x^{(-)}$, $u_y^{(+)}=-u_y^{(-)}$, and with this understanding

$$u_x(x,0) = -\frac{\sigma}{8\mu}(1-k)(\kappa+1) \, x \tag{5.4}$$

$$u_y(x,0) = -\frac{\sigma}{4\mu}(\kappa-1)b\left\{E(\phi,p) - \frac{x}{b}\left\langle\left[\left(\frac{b}{x}\right)^2-1\right]\left[1-\left(\frac{a}{x}\right)^2\right]\right\rangle^{\frac{1}{2}} - \lambda(p)F(\phi,p)\right\}.$$

In the limit $a \to 0$ leaving a single crack of length 2b, u_x remains the same and Eq. $(5.4)_2$ reduces to

$$u_y(x,0) = \frac{\sigma}{4\mu}(\kappa-1)(b^2-x^2)^{\frac{1}{2}} \quad , \tag{5.5}$$

which coincides with the result obtained from the single crack solution. Equation $(5.4)_2$ for the double crack, and Eq. (5.5) for the single crack, are shown in Fig. 23, each plotted for a crack of unit length, illustrating the effect of the presence of the second crack on the u_y component of the crack border displacement for a crack spacing $2a=0.2$. The influence of the horizontal load $k\sigma$ on the crack border displacements is evident from the above equations.

SECTION 6

GRIFFITH CRACK INSTABILITY CRITERION

The criterion for fracture introduced by Griffith initially
in 1921 [12], and restated in 1924 [13], is expressed as follows:

> "The fundamental conception of the new theory
> is this. Just as in a liquid, so in a solid the
> bounding surfaces possess a surface tension which
> implies the existence of a corresponding amount of
> potential energy. If owing to the action of a stress
> a crack is formed, or a pre-existing crack is caused
> to extend, therefore, a quantity of energy proportion-
> al to the area of the new surface must be added, and
> the condition that this shall be possible is that such
> addition of energy shall take place without any in-
> crease in the total potential energy of the system.
> This means that the increase of potential energy due
> to the surface of the crack must be balanced by the
> decrease in the potential of the strain energy and
> the applied forces."

The total potential energy of the system is stipulated to
be a maximum at the point of incipient fracture (unstable crack
extension), or

$$\frac{dP}{da} = 0 \tag{6.1}$$

at the onset of crack instability. When applied to an elastic-
ally deformed body with an existing crack of length (a), the
total potential energy of the system consists of the elastic
potential energy, V, and the crack surface energy, Γ,

$$P = V + \Gamma , \tag{6.2}$$

where

$$V = \int_R \frac{1}{2} t_{jk} e_{jk} dV - \left(\int_S T_k u_k dA + \int_R b_k u_k dV \right) , \quad j,k = 1,2,3 \tag{6.3}$$

and

$$U = \int_R \frac{1}{2} t_{jk} e_{jk} dV \tag{6.4}$$

is the elastic strain energy of the body, which is subjected to the body force b_k and the surface traction T_k applied over the region R bound by the surface S. By virtue of Clapeyron's theorem [14] however,

$$\int_S T_k u_k dA + \int_R b_k u_k dV = 2U, \qquad (6.5)$$

allowing the total potential energy of the system to be equivalently expressed as

$$P = \Gamma - U , \qquad (6.6)$$

with the corresponding condition for crack instability

$$\frac{d}{d\varepsilon}(\Gamma - U) = 0. \qquad (6.7)$$

Since Griffith assumes the surface energy Γ to be a linear function of the crack surface area multiplied by a constant surface energy density, γ, application of the fracture cri-terion is reduced to determining dU/da, the derivative of the elastic strain energy of the entire body with respect to the crack dimension.

SECTION 7

ELASTIC STRAIN ENERGY DERIVATIVE

An estimation of the load that must be applied sufficient
to cause an existing crack in a structure to become unstable,
that is, to suddenly propagate and cause, thereby, complete
separation of the body, can be obtained from application of
Griffith's fracture criterion. As indicated in the previous
section, all that is necessary in order to apply the criterion
is knowledge of the rate at which the elastic strain energy
of the body changes with extension of the crack size, i.e., a
calculation of the derivative

$$\lim_{(a'-a)\to 0}\left(\frac{U'-U}{a'-a}\right) = \frac{dU}{da} , \qquad (7.1)$$

in which U and U´ represent the elastic strain energy of the
body having the crack lengths (2a) and (2a´), respectively, and
where the crack length difference $\Delta a = a' - a$ is arbitrarily small.

In the case of two collinear cracks, an assumption must
be made at the outset as to which of the crack tips is first
anticipated to extend. It would appear on the basis of the
ratio of the crack-tip stress intensity factors at the inner
and outer crack ends, Fig. 8, that for relatively closely
spaced cracks, crack growth should be expected first at the
inner crack ends. Thus, corresponding to the strain energies
U and U´ are the initial and extended crack lengths (b-a) and
$(b-a')=b-(a-\Delta a)$, respectively, from which

$$\lim_{(b-a')\to(b-a)}\left[\frac{U'-U}{(b-a')-(b-a)}\right] = \frac{dU}{da} . \qquad (7.2)$$

Consider the plane body with a single horizontally oriented crack, (2a), and let R designate an arbitrary region of the plane bound by the arbitrary simple closed curves C_1, C_2 that enclose the crack (cf. Fig. 24). For the plane body with horizontally oriented collinear cracks, (b-a), the region R is bound by three arbitrary simple closed curves, C_k, k=1,2,3, that enclose both cracks (cf. Fig. 25).

The difference of elastic strain energy (per unit thickness) of the region R of the body having incrementally differing crack sizes is

$$U'(R) - U(R) = \iint \frac{1}{2}(t'_{jk}e'_{jk} - t_{jk}e_{jk})dA, \qquad j,k=1,2. \qquad (7.3)$$

From the linear elastic constitutive relations

$$e_{jk} = \frac{(1+\nu)}{E} t_{jk} - \frac{\nu}{E} t_{\ell\ell}\delta_{jk} \qquad (7.4)$$

the following identity is easily established

$$t'_{jk}e'_{jk} - t_{jk}e_{jk} = (t_{jk}+t'_{jk})(e'_{jk}-e_{jk}) = (t'_{jk}-t_{jk})(e'_{jk}+e_{jk}), \qquad (7.5)$$

which allows Eq. (7.3) to be given the equivalent expressions

$$U'(R)-U(R) = \frac{1}{2}\iint_R (t'_{jk}+t_{jk})(e'_{jk}-e_{jk})dA, \qquad j,k=1,2, \qquad (7.6)$$

or

$$U'(R)-U(R) = \frac{1}{2}\iint_R (t'_{jk}-t_{jk})(e'_{jk}+e_{jk})dA, \qquad j,k=1,2. \qquad (7.7)$$

Either expression (7.6) or (7.7) can be used in performing the differentiation indicated in Eqs. (7.1) and (7.2).

Momentarily writing $t_{jk}^{'}+t_{jk}=t_{jk}^*$, $e_{jk}^{'}-e_{jk}=e_{jk}^*$, and $u_k^{'}-u_k=u_k^*$, the first of the equivalent expressions, Eq. (7.6), may then be written as

$$U^{'}(R)-U(R) = \frac{1}{2}\iint_R t_{jk}^* \, e_{jk}^* \, dA$$

$$= \frac{1}{2}\iint_R \left\{ t_{xx}^* \frac{\partial u_x^*}{\partial x} + t_{yy}^* \frac{\partial u_y^*}{\partial y} + t_{xy}^* \left(\frac{\partial u_x^*}{\partial y} + \frac{\partial u_y^*}{\partial x} \right) \right\} \, dxdy. \qquad (7.8)$$

The open set of points defining the domain of the mathematical analysis, which consists of the extended complex plane with the points $Re(z)=|x|<a$ defining the crack removed (or for the two collinear cracks with the points $|a|<Re(z)=|x|<|b|$ removed), is a multiply connected domain, as may be seen by recourse to sterographic projection of the extended cut complex plane onto the Riemann sphere [15]. Thus upon application Green's theorem for the multiply connected domain [16], taken in conjunction with the equations of equilibrium and the assumption of zero body force, the multiple integral given in Eq. (7.8) over the region R may be transformed into the following sum of line integrals about the bounding contours C_k

$$U^{'}(R)-U(R)=\frac{1}{2}\sum_{k=1}^{N}\oint_{C_k}\left(\left[t_{xx}^* u_x^* + t_{xy}^* u_y^*\right]dy - \left[t_{yy}^* u_y^* + t_{xy}^* u_x^*\right]dx\right), \qquad (7.9)$$

or

$$U^{'}(R)-U(R)=\frac{1}{2}\sum_{k=1}^{N}\oint_{C_k}\left\{\left[(t_{xx}^{'}+t_{xx})(u_x^{'}-u_x)+(t_{xy}^{'}+t_{xy})(u_y^{'}-u_y)\right]dy\right.$$

$$\left.-\left[(t_{yy}^{'}+t_{yy})(u_y^{'}-u_y)+(t_{xy}^{'}+t_{xy})(u_x^{'}-u_x)\right]dx\right\}, \qquad (7.10)$$

where N=2 for the single crack and N=3 for the multiple crack geometries.

The boundary contours C_k are arbitrary, hence they may be chosen to facilitate computation. The outer boundary, C_1, may be taken to be a circle centered at the origin with an arbitrary radius r_0 sufficiently large so as to allow the circle to completely enclose the crack (or cracks). The first of the sum of line integrals in Eq. (7.10) then has the circular line integral form

$$\left[U'(R)-U(R)\right]_{C_1} = \frac{1}{2}r_0\oint_{-\pi}^{\pi}\left\{\left[(t'_{xx}+t_{xx})(u'_x-u_x)+(t'_{xy}+t_{xy})(u'_y-u_y)\right]_{r=r_0}\cos\theta\right.$$

$$\left.+\left[(t'_{yy}+t_{yy})(u'_y-u_y)+(t'_{xy}+t_{xy})(u'_x-u_x)\right]_{r=r_0}\sin\theta\right\}d\theta . \qquad (7.11)$$

The inner boundary (or boundaries) of the region R can be taken to coincide with the boundary of the extended crack (or cracks). Accordingly, the second of the sum of line integrals in Eq. (7.10) will involve integration along the x-direction only, and thus leave the reduced form

$$\left[U'(R)-U(R)\right]_{C_2} = -\frac{1}{2}\oint_{C_2}\left\{(t'_{yy}+t_{yy})(u'_y-u_y)+(t'_{xy}+t_{xy})(u'_x-u_x)\right\}dx \qquad (7.12)$$

for the single crack geometry, and

$$\left[U'(R)-U(R)\right]_{C_2+C_3} = -\frac{1}{2}\left(\oint_{C_2}+\oint_{C_3}\right)\left\{(t'_{yy}+t_{yy})(u'_y-u_y)+(t'_{xy}+t_{xy})(u'_x-u_x)\right\}dx \qquad (7.13)$$

for the multiple crack geometry.

7.1 SINGLE CRACK

Further evaluation of the line integrals of Eqs. (7.11) and (7.12) requires expressions for the stress and displacement, which can be obtained from Eqs. (2.11), (2.12) and (2.1). The result, expressed in series form, is as follows:

$$t_{xx} = \frac{\sigma}{2}\left\{2k + \left(\frac{a}{r}\right)^2 [\cos2\theta - 2\sin\theta\, \sin3\theta]\right.$$
$$\left. + 3\left(\frac{a}{4}\right)^4 [\frac{1}{4}\cos4\theta - \sin\theta\, \sin5\theta] + \ldots\ldots\right\}$$

$$t_{yy} = \frac{\sigma}{2}\left\{2 + \left(\frac{a}{r}\right)^2 [\cos2\theta + 2\sin\theta\, \sin3\theta]\right.$$
$$\left. + 3\left(\frac{a}{r}\right)^4 [\frac{1}{4}\cos4\theta + \sin\theta\, \sin5\theta] + \ldots\ldots\right\} \tag{7.14}$$

$$t_{xy} = \sigma\left\{\left(\frac{a}{r}\right)^2 \sin\theta\, \cos3\theta + \frac{3}{2}\left(\frac{a}{r}\right)^4 \sin\theta\, \cos5\theta + \ldots\right\} \quad,$$

and

$$u_r = \frac{\sigma}{4\mu}\left\{\frac{1}{2}[\kappa(1+k)+k-3]\, r\, \cos\theta + \left(\frac{a^2}{r}\right)[\sin\theta\sin2\theta - \left(\frac{\kappa-1}{2}\right)\cos\theta]\right.$$
$$\left. + \frac{1}{4}\left(\frac{a^4}{r^3}\right)[3\sin\theta\sin4\theta - \left(\frac{\kappa-1}{2}\right)\cos3\theta] + \ldots\ldots\right\} \tag{7.15}$$

$$u_y = \frac{\sigma}{4\mu}\left\{\frac{1}{2}[\kappa(1+k)+(1-3k)]\, r\, \sin\theta + \left(\frac{a^2}{r}\right)[\left(\frac{\kappa+1}{2}\right)-\cos2\theta]\sin\theta\right.$$
$$\left. + \frac{1}{4}\left(\frac{a^4}{r^3}\right)[\frac{1}{2}(\kappa+1)\sin3\theta - 3\sin\theta\, \cos4\theta] + \ldots\ldots\right\} \quad,$$

for $(a/r) < 1$.

Along the circle C_1 with $r = r_0$, it follows from Eqs. (7.14) and (7.15) that

-41-

$$t'_{xx} + t_{xx} = \sigma \left\{ 2k + \frac{a^2 + a\Delta a}{r_0^2} [\cos 2\theta - 2\sin\theta \sin 3\theta] \right.$$

$$\left. + \frac{3(a^4 + 2a^3 \Delta a)}{r_0^4} \left[\frac{1}{4} \cos 4\theta - \sin\theta \sin 5\theta \right] + \ldots \ldots \right\}$$

$$t'_{yy} + t_{yy} = \sigma \left\{ 2 + \frac{(a^2 + a\Delta a)}{r_0^2} [\cos 2\theta + 2\sin\theta \sin 3\theta] \right. \qquad (7.16)$$

$$\left. + \frac{3(a^4 + 2a^3 \Delta a)}{r_0^4} \left[\frac{1}{4} \cos 4\theta + \sin\theta \sin 5\theta \right] + \ldots \ldots \right\}$$

$$t'_{xy} + t_{xy} = \sigma \left\{ \frac{2(a^2 + a\Delta a)}{r_0^2} \sin\theta \cos 2\theta + \frac{3(a^4 + 2a^3 \Delta a)}{r_0^4} \sin\theta \cos 5\theta + \ldots \ldots \right\} ,$$

and

$$u'_x - u_x = \frac{\sigma}{4\mu} \left\{ \frac{2a\Delta a}{r_0} [\sin\theta \sin 2\theta - \left(\frac{\kappa - 1}{2} \right) \cos\theta] \right.$$

$$\left. + \frac{a^3 \Delta a}{r_0^3} [3\sin\theta \sin 4\theta - \left(\frac{\kappa - 1}{2} \right) \cos 3\theta] + \ldots \ldots \right\}$$

$$(7.17)$$

$$u'_y - u_y = \frac{\sigma}{4\mu} \left\{ \frac{2a\Delta a}{r_0} \left[\left(\frac{\kappa + 1}{2} \right) - \cos 2\theta \right] \sin\theta \right.$$

$$\left. + \frac{a^3 \Delta a}{r_0^3} \left[\left(\frac{\kappa + 1}{2} \right) \sin 3\theta - 3\sin\theta \cos 4\theta \right] + \ldots \ldots \right\} .$$

Note that in the above expressions terms to order $(\Delta a)^2$ and higher are omitted. This entails no loss of accuracy because Δa may be taken arbitrarily small, and approaches zero in the limit process. Substitution of Eqs. (7.16) and (7.17) into Eq. (7.11) leaves

$$\left[U^{\hat{}}(R) - U(R)\right]_{C_1} = \frac{1}{2} \frac{\sigma^2}{4\mu} \int_{-\pi}^{\pi} \left\{ 4a\Delta a\left[k(\sin\theta \sin2\theta \cos\theta - \left(\frac{\kappa-1}{2}\right)\cos^2\theta\right) \right.$$

$$\left. + \left(\frac{\kappa+1}{2}\right)\sin^2\theta - \cos2\theta \sin^2\theta\right] + a\Delta a \sum_{n=1}^{\infty} \left(\frac{a}{r_0}\right)^{2n} H_n(\theta;k)\right\} d\theta \ . \tag{7.18}$$

The functions $H_n(\theta;k)$, $n=1,2,3,\ldots$, appearing in the integrand are products of and sums of sine and cosine functions, which are finite for $-\pi \leq \theta \leq \pi$. In addition, the sequence of positive constants $\{(a/r_0)^{2n}\}$ approaches zero monotonically as $n \to \infty$. Accordingly for each n and $-\pi \leq \theta \leq \pi$, it is always possible to find numbers M and N such that the bound functions $H_n(\theta;k)$ satisfy $|H_1(\theta;k) + \ldots + H_n(\theta;k)| < M$ for any $n > N$. It follows from the Dirichlet test for convergence [17] that the infinite series appearing in the integrand of Eq. (7.18) converges uniformly for all $-\pi \leq \theta \leq \pi$. The order of integration with summation in Eq. (7.18) may therefore be interchanged, allowing it to be reduced to

$$\left[U^{\hat{}}(R) - U(R)\right]_{C_1} = \frac{\sigma^2 \pi(1+\nu)}{2E} \ [k(2-\kappa) + \kappa + 2] \ \Delta a$$

$$+ \frac{\sigma^2 a \Delta a}{8\mu} \sum_{n=1}^{\infty} \left(\frac{a}{r_0}\right)^{2n} \int_{-\pi}^{\pi} H_n(\theta;k)d\theta \ . \tag{7.19}$$

For the infinite sheet geometry, the outer boundary contour C_1 of R must approach infinity. In the limit as $r_0 \to \infty$ the infinite series appearing in Eq. (7.19) converges to the value zero, i.e.

$$\lim_{r_0 \to \infty} \sum_{n=1}^{\infty} \left(\frac{a}{r_0}\right)^{2n} \int_{-\pi}^{\pi} H_n(\theta;k)d\theta = \lim_{r_0 \to \infty} \left\{ \left(\frac{a}{r_0}\right)^2 H_1^*(k) + \left(\frac{a}{r_0}\right)^4 H_2^*(k) + \ldots \right\} = 0$$

$$\tag{7.20}$$

because each of the quantities $H_n^*(k)$, from the integrated bound functions $H_n(\theta;k)$, is a finite number and $r_0 > a$.

In Eq. (7.12) C_2 represents the crack border with crack size $2a$ or $2a' = 2(a+\Delta a)$. Along the cut $|x| < |a|$, $y=0$, the stress free surfaces require $t_{yy} = t_{xy} = 0$. Likewise for the extended crack $|x| < |a+\Delta a|$, $y=0$, $t_{yy}' = t_{xy}' = 0$. From Eqs. (7.14) and (7.15) it is clear that along $y=0$ and $|x| < |a|$, $t_{xy} = u_y = 0$. Because of the symmetry of t_{yy} relative to the crack plane $t_{yy}^{(+)} = t_{yy}^{(-)}$, whereas for the displacements in the y-direction $u_y'^{(+)} = -u_y'^{(-)}$. The positive and negative superscripts designate the opposite faces of the crack. With these considerations in mind, Eq. (7.12) can be reduced to

$$\left[U'(R) - U(R)\right]_{C_2} = -4 \int_a^{a+\Delta a} \tfrac{1}{2} t_{yy}^{(+)} \cdot u_y'^{(+)} dx. \tag{7.21}$$

By means of Eqs. (2.11), (2.12) and (2.1),

$$\left[t_{yy}\right]_{\substack{y=0 \\ x>a}} = \sigma x (x^2 - a^2)^{-\frac{1}{2}}, \tag{7.22}$$

$$\left[u_y'\right]_{\substack{y=0 \\ x<a(a+\Delta a)}} = \frac{\sigma(\kappa+1)}{4\mu} \left[2a\Delta a - (x^2 - a^2)\right]^{\frac{1}{2}}, \tag{7.23}$$

so that

$$\left[U'(R) - U(R)\right]_{C_2} = -\frac{\sigma^2(\kappa+1)}{2\mu} \int_a^{a+\Delta a} \left\{\frac{2a\Delta a - (x^2 - a^2)}{x^2 - a^2}\right\}^{\frac{1}{2}} x \; dx$$

$$= -\frac{\sigma^2 \pi a (1+\nu)(\kappa+1)}{2E} \Delta a. \tag{7.24}$$

The change of the elastic strain energy with change of crack dimension for the infinite plane body can be obtained by substitution of Eqs. (7.19), (7.20) and (7.23) in the

limits $(a'-a)=\Delta a \to 0$ and $r_0 \to \infty$:

$$\frac{dU}{da} = \lim_{(a'-a)\to 0}\left(\frac{U'-U}{a'-a}\right) = \lim_{\substack{\Delta a \to 0 \\ r_0 \to \infty}} \sum_{k=1}^{2} \frac{[U'(R)-U(R)]}{\Delta a} C_k$$

$$= \frac{\sigma^2 \pi a (1+\nu)}{2E}[k(2-\kappa)+\kappa+2] - \frac{\sigma^2 \pi a (1+\nu)}{2E}(\kappa+1) \qquad (7.25)$$

$$= \frac{\sigma^2 \pi a (1+\nu)}{2E}[1+k(2-\kappa)] \quad .$$

The derivation of Eq. (7.25) proceeded from the first of the two equivalent expressions, Eqs. (7.6) and (7.7), for the strain energy difference. A calculation beginning with Eq. (7.7) instead, involves only a difference in signs for the terms appearing in the integrands of the line integrals of Eq. (7.12). In place of terms such as $(t'_{xx}+t_{xx})(u'_x-u_x)$ there now appears $(t'_{xx}-t_{xx})(u'_x+u_x)$, and so on. Stress sums are replaced by stress differences, while displacemnt differences are replaced by displacement sums. The remaining part of the calculation is identical in every respect to the one above. The result is the same, although the contributing terms are slightly different, i.e.,

$$\frac{dU}{da} = \frac{\sigma^2 \pi a (1+\nu)}{2E}\left[k(2-\kappa)-\kappa\right] + \frac{\sigma^2 \pi a (1+\nu)}{2E}(\kappa+1)$$

$$= \frac{\sigma^2 \pi a (1+\nu)}{2E}\left[1+k(2-\kappa)\right] \quad . \qquad (7.26)$$

The first term of the first line is the contribution from the outer circular boundary C_1 in the limit as $r_0 \to \infty$, while the second is from the integral about the boundary C_2 when it coincides with the crack boundary.

-45-

If one can imagine crack extension during which the outer boundary of the body remains fixed (a so-called 'fixed-grips' condition), then the displacement differences $(u_x'-u_x)$, $(u_y'-u_y)$ are zero along the outer boundary and the contribution to the strain energy difference from the integration about the outer boundary C_1 vanishes. This leaves only the second term of the second line of Eq. (7.25) for the strain energy derivative, which comes from the line integration about the crack border boundary C_2, i.e.,

$$\left(\frac{dU}{da}\right)_{\substack{\text{fixed} \\ \text{grips}}} = -\frac{\sigma^2 \pi a(1+\nu)}{2E}\,(\kappa+1) < 0, \text{ for } (\kappa+1) > 0.$$

The elastic strain energy of the body decreases if a crack extends under 'fixed-grips', and its rate of decrease is independent of the load biaxiality.

If one can imagine crack extension during which the tractions along the outer boundary of the body remain unchanged (a so-called 'dead-load' condition), then the traction differences $(t_{xx}'-t_{xx})$, $(t_{yy}'-t_{yy})$ are zero along the outer boundary and the contribution to the strain energy difference from the integration about the outer boundary C_1 vanishes. This leaves only the second term of the first line of Eq. (7.26) for the strain energy derivative, which also comes from the line integration about the crack border boundary C_2, i.e.,

$$\left(\frac{dU}{da}\right)_{\substack{\text{dead} \\ \text{load}}} = \frac{\sigma^2 \pi a(1+\nu)}{2E}\,(\kappa+1) > 0, \text{ for } (\kappa+1) > 0.$$

The elastic strain energy of the body increases if a crack extends under 'dead-load', and its rate of increase is independent of the load biaxiality.

These two quantities, opposite in sign but identical in magnitude, are, to within a factor of two, what is often identified in the literature as Irwin's "strain energy release rate" G [18].

The right side of Eq. (7.25) expressing the strain energy derivative dU/da can be viewed as a continuous function of the crack size, $F(a;\sigma, k, \kappa)$, with σ, k and κ (or ν) assuming the role of parameters. It is apparent from the form of Eq. (7.25) that for any crack size, a, and applied load, σ, the values assumed by the strain energy derivative may be positive or negative or zero, depending on the values of the parameters k and κ. The latter occurs when

$$k = \frac{1}{\kappa - 2} = \begin{cases} (1+\nu)/(1-3\nu) & , \quad \text{for plane stress} \\ \\ 1/(1-4\nu) & , \quad \text{for plane strain.} \end{cases} \tag{7.27}$$

Since Griffith's fracture criterion requires solving for the extreme value of the potential energy by setting dP/da = $d(\Gamma-U)/da$ = 0, the vanishing of one of the two contributions entering into this expression renders the calculation meaningless. Therefore, for the condition given by Eq. (7.27) Griffith's crack instability criterion is inapplicable.

7.2 TWO COLLINEAR CRACKS

Because of the symmetry of the applied loads and the crack geometry relative to the x-axis (horizontally oriented cracks, $\alpha = \pi/2$) Eqs. (2.1) may be shown [3,19] to simplify to

$$t_{xx} = Re(2\Phi(z)) - y \ Im \ (2\Phi'(z)) + S$$

$$t_{yy} = Re(2\Phi(z)) + y \ Im \ (2\Phi'(z)) - S \qquad (7.28)$$

$$t_{xy} = -y \ Re \ (2\Phi'(z))$$

and

$$2\mu u_x = (\kappa-1) \ Re(\phi(z)) - y \ Im \ (2\Phi(z)) + S \ x$$
$$\qquad (7.29)$$
$$2\mu u_y = (\kappa+1) \ Im(\phi(z)) - y \ Im \ (2\Phi(z)) - S \ y.$$

The constant S is required by boundary conditions (2.6) to have the value

$$S = -\frac{1}{2} \ \sigma(1-k) \qquad . \qquad (7.30)$$

Equations (2.35)-(2.37) and (7.28)-(7.30) lead to the following series expansions for the stress and displacement components

$$t_{xx} = \frac{\sigma}{2}\left[2k + N(\lambda) \ \frac{b^2}{r^2} \ (\cos2\theta - 2\sin\theta \ \sin3\theta)\right.$$

$$\left. + 3M(\lambda) \ \frac{b^4}{r^4} \left(\frac{1}{4} \cos4\theta - \sin\theta \ \sin5\theta\right) + 0\left(\frac{b^6}{r^6}\right)\right]$$

$$t_{yy} = \frac{\sigma}{2}\left[2 + N(\lambda) \ \frac{b^2}{r^2} \ (\cos2\theta + 2\sin\theta \ \sin3\theta)\right. \qquad (7.31)$$

$$\left. + 3M(\lambda) \ \frac{b^4}{r^4} \left(\frac{1}{4} \cos4\theta + \sin\theta \ \sin5\theta\right) + 0\left(\frac{b^6}{r^6}\right)\right]$$

$$t_{xy} = \sigma\left[N(\lambda) \ \frac{b^2}{r^2} \ \sin\theta \ \cos3\theta + \frac{3}{2}M(\lambda) \ \frac{b^4}{r^4} \ \sin\theta \ \cos5\theta + 0\left(\frac{b^6}{r^6}\right)\right] \ ,$$

and

$$u_x = \frac{\sigma}{4\mu}\left[\frac{1}{2}\Big(\kappa(1+k)+k-3\Big)r\cos\theta+N(\lambda)\frac{b^2}{r}\Big(\sin\theta\sin2\theta-\Big(\frac{\kappa-1}{2}\Big)\cos\theta\Big)\right.$$

$$\left.+\frac{1}{4}M(\lambda)\frac{b^4}{r^3}(3\sin\theta\sin4\theta-\Big(\frac{\kappa-1}{2}\Big)\cos3\theta)+0\Big(\frac{b^6}{r^6}\Big)\right]$$

$$u_y = \frac{\sigma}{4\mu}\left[\frac{1}{2}\Big(\kappa(1+k)+1-3k\Big)r\sin\theta+N(\lambda)\frac{b^2}{r}\Big(\Big(\frac{\kappa+1}{2}\Big)\sin\theta-\sin\theta\cos2\theta\Big)\right.$$

$$\left.+\frac{1}{4}M(\lambda)\frac{b^4}{r^3}\Big(\Big(\frac{\kappa+1}{2}\Big)\sin3\theta-3\sin\theta\cos4\theta\Big)+0\Big(\frac{b^6}{r^5}\Big)\right] \qquad (7.32)$$

where r>b and

$$N(\lambda) = [(a/b)^2 + 1 - 2\lambda(p)]$$

$$M(\lambda) = \left[(a/b)^4 + \frac{2}{3}(a/b)^2 + 1 - \frac{4}{3}\Big(\frac{a^2+b^2}{b^2}\Big)\lambda(p)\right] . \qquad (7.33)$$

Since the crack size increment (Δa) is arbitrarily small, terms of order (Δa)^2 and higher may be ignored in writing

$$t_{jk}' = t_{jk} + \frac{\Delta t}{\Delta a}jk\ (\Delta a)$$

$$j,k=1,2$$

$$u_k' = u_k + \frac{\Delta u}{\Delta a}k\ (\Delta a)\ ,$$

which in conjunction with Eqs. (7.31) and (7.32) lead to the following expressions for the integrand of the line integral in Eq. (7.11) along the circle C_1, $r=r_0$:

-49-

$$\left(t'_{xx}+t_{xx}\right)=\sigma\left\{2k+\left[N(\lambda)+\frac{1}{2}\frac{\Delta N}{\Delta a}(\Delta a)\right]\frac{b^2}{r_0^2}(\cos2\theta-2\sin\theta\sin3\theta)\right.$$

$$\left.+3\left[M(\lambda)+\frac{1}{2}\frac{\Delta M}{\Delta a}(\Delta a)\right]\frac{b^4}{r_0^4}\left(\frac{1}{4}\cos4\theta-\sin\theta\sin5\theta\right)+0\left(\frac{b^6}{r_0^6}\right)\right\}$$

$$\left(t'_{yy}+t_{yy}\right)=\sigma\left\{2+\left[N(\lambda)+\frac{1}{2}\frac{\Delta N}{\Delta a}(\Delta a)\right]\frac{b^2}{r_0^2}(\cos2\theta+2\sin\theta\sin3\theta)\right.$$

$$\left.+3\left[M(\lambda)+\frac{1}{2}\frac{\Delta N}{\Delta a}(\Delta a)\right]\frac{b^4}{r_0^4}\left(\frac{1}{4}\cos4\theta+\sin\theta\sin5\theta\right)+0\left(\frac{b^6}{r_0^6}\right)\right\}$$

$$\left(t'_{xy}+t_{xy}\right)=\sigma\left\{\left[N(\lambda)+\frac{\Delta N}{\Delta a}(\Delta a)\right]\frac{b^2}{r_0^2}\sin\theta\cos3\theta\right. \tag{7.34}$$

$$\left.+\frac{3}{2}\left[M(\lambda)+\frac{\Delta M}{\Delta a}(\Delta a)\right]\frac{b^4}{r_0^4}\sin\theta\cos5\theta+0\left(\frac{b^6}{r_0^6}\right)\right\}$$

and

$$\left(u'_x-u_x\right)=\frac{\sigma}{4\mu}\left\{\frac{\Delta N}{\Delta a}(\Delta a)\frac{b^2}{r_0}\left(\sin\theta\sin2\theta-\left(\frac{\kappa-1}{2}\right)\cos\theta\right)\right.$$

$$\left.+\frac{1}{4}\frac{\Delta M}{\Delta a}(\Delta a)\frac{b^4}{r_0^3}(3\sin\theta\sin4\theta-\left(\frac{\kappa-1}{2}\right)\cos3\theta)+0\left(\frac{b^6}{r_0^5}\right)\right\}$$

$$u'_y-u_y=\frac{\sigma}{4\mu}\left\{\frac{\Delta N}{\Delta a}(\Delta a)\frac{b^2}{r_0}\left(\left(\frac{\kappa+1}{2}\right)\sin\theta-\sin\theta\cos2\theta\right)\right. \tag{7.35}$$

$$\left.+\frac{1}{4}\frac{\Delta M}{\Delta a}(\Delta a)\frac{b^4}{r_0^3}\left(\left(\frac{\kappa+1}{2}\right)\sin3\theta-3\sin\theta\cos4\theta\right)+0\left(\frac{b^6}{r_0^5}\right)\right\}\quad.$$

The above expression, when substituted into Eq. (7.11), give

$$\left[U'(R)-U(R)\right]_{C_1} = \frac{\sigma^2 b^2}{4\mu} \int_{-\pi}^{\pi} \left\{ k[\sin\theta \cos\theta \sin2\theta - \left(\frac{\kappa-1}{2}\right)\cos^2\theta] \right.$$

$$+ \left[\left(\frac{\kappa+1}{2}\right)\sin^2\theta - \sin^2\theta \cos2\theta\right] \frac{\Delta N}{\Delta a}(\Delta a)$$

$$\left. + (\Delta a)\sum_{n=1}^{\infty} \left(\frac{b}{r_0}\right)^{2n} T_n(\theta;F(p),E(p),k) \right\} d\theta \quad . \qquad (7.36)$$

The functions $T_n(\theta;F(p),E(p),k)$ include products of sine and cosine functions and of the complete elliptic integrals. As such they are bound function for $0<a<b$ and $-\pi\leq\theta\leq\pi$. It may be shown that derivatives of $N(\lambda)$ and $M(\lambda)$, which involve the elliptic integrals, again produce elliptic integrals, and are, therefore, also bound quantities for $0<a<b$. Accordingly, by the same argument given in Section (7.1), the series converges uniformly on the interval $[-\pi,\pi]$ and it follows that

$$\left[U'(R)-U(R)\right]_{C_1} = \frac{\sigma^2\pi b^2}{8\mu}[k(2-\kappa) + \kappa + 2] \frac{\Delta N}{\Delta a}(\Delta a)$$

$$\qquad (7.36a)$$

$$+ \frac{\sigma^2 b^2}{4\mu}(\Delta a)\sum_{n=1}^{\infty} \left(\frac{b}{r_0}\right)^{2n} \int_{-\pi}^{\pi} T_n(\theta;F(p),E(p)k)\, d\theta \quad .$$

In the limit $r_0\to\infty$ the infinite series appearing in the above equation converges to zero, i.e.,

$$\lim_{r_0\to\infty} \sum_{n=1}^{\infty} \left(\frac{b}{r_0}\right)^{2n} \int_{-\pi}^{\pi} T_n(\theta;F(p),E(p),k)d\theta$$

$$\qquad (7.37)$$

$$= \lim_{r_0\to\infty}\left\{\left(\frac{b}{r_0}\right)^2 T_1^*(F(p),E(p),k) + \left(\frac{b}{r_0}\right)^4 T_2^*(F(p),E(p),k)+\ldots\ldots\right\} = 0$$

because each of the quantities $T_n^*(F(p),E(p),k)$, from the integrated bound functions $T_n(\theta;F(p),E(p),k)$, is a finite number.

In the two line integrals of Eq. (7.13), the inner boundary contours C_2 and C_3 coincide with the borders of the cracks. For the extended cracks the boundary conditions on the crack surfaces require that $t_{yy}^- = t_{xy}^- = 0$ for $|a-\Delta a| < |x| < |b|$, while for the unextended cracks $t_{yy} = t_{xy} = 0$ for $|a| < |x| < |b|$. Because of symmetry considerations $u_y = 0$ for $|x| < |a|$, $u_y^{-(+)} = -u_y^{-(-)}$ and $t_{yy}^{(+)} = t_{yy}^{(+)}$. Consequently, Eq. (7.13) may be reduced to

$$\left[U^-(R) - U(R) \right]_{C_2+C_3} = -2\int_a^a t_{yy}^{(+)} u_y^{(+)} dx = -2\int_0^{\Delta a} t_{yy}^{(+)} u_y^{-(+)} dt \ . \qquad (7.38)$$

The crack-tip expressions Eqs. $(2.41)_2$ and $(2.47)_2$ may be employed to evaluate Eq. (7.38) since the interval of integration is over the crack-tip region. Thus for the stress just ahead of the unextended crack-tip

$$[t_{yy}]_{\substack{r=t \\ \theta=0}} = \frac{K_1(a)}{(2\pi t)^{\frac{1}{2}}} \ , \qquad (7.39)$$

while for the displacement just beyond the extended crack tip

$$[u_y]_{\substack{r=\Delta a-t \\ \theta=\pi}} = \frac{K_1(a^-)(\kappa+1)}{2\mu} \left(\frac{\Delta a-t}{2\pi}\right)^{\frac{1}{2}} \qquad (7.40)$$

where $K_1(a^-) = K_1(a-\Delta a)$. Evaluation of Eq. (7.38) can now proceed to give

$$\left[U^-(R) - U(R) \right]_{C_2+C_3} = \frac{K_1(a)K_1(a-\Delta a)(\kappa+1)}{4\mu} \Delta a. \qquad (7.41)$$

-52-

Substitution of Eqs. (7.36), (7.37) and (7.41) into Eq. (7.2) in the limits as $(b-a') \to (b-a)$ or $\Delta a \to 0$, and $r_0 \to \infty$, yields

$$\frac{dU}{da} = \lim_{(b-a') \to (b-a)} \left\{ \frac{U' - U}{(b-a') - (b-a)} \right\} = \lim_{\substack{\Delta a \to 0 \\ r_0 \to \infty}} \sum_{k=1}^{3} \frac{[U'(R) - U(R)]}{\Delta a} C_k$$

$$= \frac{\sigma^2 \pi b^2}{8\mu} [k(2-\kappa) + \kappa + 2] \frac{dN(\lambda)}{da} - K_1^2(a) \frac{(\kappa+1)}{4\mu} . \qquad (7.42)$$

By means of the following derivative formulas

$$\frac{dF(p)}{da} = + \frac{1}{ap^2} [E(p) - \left(\frac{a}{b}\right)^2 F(p)]$$

$$\frac{dE(p)}{da} = + \frac{(a/b)^2}{ap^2} [E(p) - F(p)] , \qquad (7.43)$$

and the defining Eqs. (2.37) and $(7.33)_1$, it follows that

$$\frac{dN(\lambda)}{da} = + 2\frac{[\lambda(p) - (a/b)^2]^2}{a[1 - (a/b)^2]} . \qquad (7.44)$$

From Eq. $(2.43)_1$, where $\alpha = \pi/2$, and Eq. (7.44) it is seen that

$$K_1^2(a) = \sigma^2 \pi b^2 \frac{[\lambda(p) - (a/b)^2]^2}{a[1 - (a/b)^2]} = + \frac{\sigma^2 \pi b^2}{2} \frac{dN(\lambda)}{da} . \qquad (7.45)$$

Consequently, substitution of Eqs. (7.44) and (7.45) into Eq. (7.42) leaves

$$\frac{dU}{da} = + \frac{\sigma^2 \pi b^2}{4\mu} [1 + k(2-\kappa)] \frac{[\lambda(p) - (a/b)^2]^2}{a[1 - (a/b)^2]} . \qquad (7.46)$$

It will be recalled that calculation of Eq. (7.46) proceeded from the first of the two equivalent expressions (7.6) and (7.7). Were the derivation to have followed from Eq. (7.7) instead of Eq. (7.6), the only difference would involve the

-53-

signs appearing in the integrands of the line integrals in Eq. (7.10). In place of terms such as $(t_{xx}^{'}+t_{xx})(u_y^{'}-u_x)$ one would have $(t_{xx}^{'}-t_{xx})(u_x^{'}+u_x)$ and so on, i.e., the stress sums are replaced by stress differences and the displacement differences by displacement sums. The remaining part of the calculation would be similar in every respect, with the result that

$$\frac{dU}{da} = \frac{\sigma^2 \pi b^2}{8\mu} \ [k(2-\kappa)-\kappa] \ \frac{dN(\lambda)}{da} + K_1^2(a) \ \frac{(\kappa+1)}{4\mu} \ ,$$

in place of Eq. (7.42). However when this is combined with Eqs. (7.44) and (7.45), Eq. (7.46) is reproduced.

As in the case with the single crack, the derivative dU/da given by Eq. (7.46) may be positive or negative or zero, depending on the values of the parameters k and κ. The latter possibility occurs when the load biaxiality has the values given by Eq. (7.27), and for which Griffith's crack instability criterion becomes meaningless.

7.3 SHEAR PANEL

For the cracked shear panel, (cf. Fig. 9), the strain energy difference expressed by Eq. (7.10) for the bound region R shown by Fig. 26, may be reduced to

$$U^{\prime}(R) - U(R) = [U^{\prime}(R) - U(R)]_{C_1} + [U^{\prime}(R) - U(R)]_{C_2}$$

$$= \frac{1}{2}\int_{-\pi}^{\pi}\left\{\left[(t_{xx}^{\prime}+t_{xx})(u_x^{\prime}-u_x)+(t_{xy}^{\prime}+t_{xy})(u_y^{\prime}-u_y)\right]_{r=r_o}\cos\theta\right.$$

$$\left.+\left[(t_{yy}^{\prime}+t_{yy})(u_y^{\prime}-u_y)+(t_{xy}^{\prime}+t_{xy})(u_x^{\prime}-u_x)\right]_{r=r_0}\right\}\sin\theta\ r_0 d\theta$$

$$-4\int_{a}^{a+\Delta a}\frac{1}{2}\left(t_{yy}^{(+)}u_y^{\prime(+)}+t_{xy}^{(+)}u_x^{\prime(+)}\right)dx \qquad (7.47)$$

when the outer boundary C_1 is again a circle, and the inner boundary C_2 coincides with the borders of the crack.

The stress and displacement, obtained from Eqs. (2.50), (2.51) and (2.1), are given by

$$t_{xx}=\frac{\tau}{2}\left\{2\sin2\beta+\left(\frac{a}{r}\right)^2[-2(\sin\theta\cos3\theta+\sin2\theta)\cos2\beta\right.$$

$$\left.+2(\cos2\theta-2\sin\theta\sin3\theta)\sin2\beta]+f_x(\theta;\beta)O\left(\frac{a^4}{r^4}\right)\right\}$$

$$t_{yy}=\frac{\tau}{2}\left\{-2\sin2\beta+\left(\frac{a}{r}\right)^2[2\sin\theta\cos3\theta\cos2\beta\right.$$

$$\qquad\qquad (7.48)$$

$$\left.-(2\sin\theta\sin3\theta+\cos2\beta)\sin2\beta]+f_y(\theta;\beta)O\left(\frac{a^4}{r^4}\right)\right\}$$

$$t_{xy}=\frac{\tau}{2}\left\{2\cos2\beta+\left(\frac{a}{r}\right)^2[(\cos2\theta-2\sin\theta\sin3\theta)\cos2\beta\right.$$

$$\left.-2\sin\theta\cos3\theta\sin2\beta]+f_{xy}(\theta;\beta)O\left(\frac{a^4}{r^4}\right)\right\}$$

and

$$u_x = \frac{\tau}{2\mu}\left\{r(\sin\theta\cos2\beta+\cos\theta\sin2\beta)\right.$$

$$+\frac{1}{4}\frac{a^2}{r}[\{(\kappa+1)\sin\theta+2\sin\theta\cos2\theta\}\cos2\beta$$

$$\left.+\{(\kappa-1)\cos\theta-2\sin\theta\sin2\theta\}\sin2\beta]+g_x(\theta;\beta)O\left(\frac{a^4}{r^3}\right)\right\}$$

$$(7.49)$$

$$u_y = \frac{\tau}{2\mu}\left\{r(\cos\theta\cos2\beta-\sin\theta\sin2\beta)+\frac{1}{4}\frac{a^2}{r}[\{(\kappa-1)\cos\theta\right.$$

$$+2\sin\theta\sin2\theta\}\cos2\beta-\{(\kappa+1)\sin\theta-2\sin\theta\cos2\theta\}\sin2\beta]$$

$$\left.+g_y(\theta;\beta)O\left(\frac{a^4}{r^3}\right)\right\},$$

where the function f_x, f_y, g_x and g_y are sine and cosine functions of the variable θ and the parameter β.

From Eqs. (7.48) it may be seen that when terms of higher order in the arbitrarily small increment of crack extension Δa are ignored, then along the circular boundary C_1

$$(t_{yy}'+t_{yy})=-\tau\left\{2\sin2\beta+\frac{a^2+a\cdot\Delta a}{r_0^2}[2\sin\theta\cos3\theta\cos2\beta\right.$$

$$\left.+(\cos2\theta-2\sin\theta)\sin2\beta]+f_y(\theta;\beta)O\left(\frac{a^4}{r_0^4}\right)\right\}$$

$$(t_{xx}'+t_{xx})=\tau\left\{2\sin2\beta+\frac{a^2+a\cdot\Delta a}{r_0^2}[2(\sin\theta\cos3\theta-\sin2\theta)\cos2\beta\right.$$

$$\left.-(2\sin\theta\sin3\theta+\cos2\theta)\sin2\beta]+f_x(\theta;\beta)O\left(\frac{a^4}{r_0^4}\right)\right\}$$

$$(7.50)$$

$$(t_{xy}'+t_{xy})=\tau\left\{2\cos2\beta+\frac{a^2+\Delta a}{r_0^2}[(\cos2\theta+2\sin\theta\sin3\theta)\cos2\beta\right.$$

$$\left.+2\sin\theta\cos3\theta\sin2\beta]+f_{xy}(\theta;\beta)O\left(\frac{a^4}{r_0^4}\right)\right\}$$

while from Eqs. (7.49)

$$(u_x^{\prime}-u_x)=\frac{\tau}{4\mu}\left\{\frac{a\cdot\Delta a}{r_0}\left[\left\langle(\kappa+1)\sin\theta-2\sin\theta\cos2\theta\right\rangle\cos2\beta\right.\right.$$

$$\left.\left.+\left\langle(\kappa-1)\cos\theta+2\sin\theta\sin2\theta\right\rangle\sin2\beta\right]+g_x(\theta;\beta)O\left(\frac{a^3}{r_0^3}\right)\right\}$$

$$(7.51)$$

$$(u_y^{\prime}-u_y)=\frac{\tau}{4\mu}\left\{\frac{a\cdot\Delta a}{r_0}\left[\left\langle(\kappa-1)\cos\theta-2\sin\theta\sin2\theta\right\rangle\cos2\beta\right.\right.$$

$$\left.\left.-\left\langle(\kappa+1)\sin\theta+2\sin\theta\cos2\theta\right\rangle\sin2\beta\right]+g_y(\theta;\beta)O\left(\frac{a^3}{r_0^3}\right)\right\}\ .$$

Substitution of Eqs. (7.50) and (7.51) into the first of the line integrals of Eq. (7.47) yields

$$[U^{\prime}(R)-U(R)]_{C_1}=\frac{\tau^2}{4\mu}\int_{-\pi}^{\pi}\{a\cdot\Delta a[\kappa+\sin^2\theta-\cos^2\theta$$

$$+\ (\sin^2 2\beta-\cos^2 2\beta)(2\cos2\theta\sin^2\theta+\sin^2 2\theta)+\sin4\beta\qquad(7.52)$$

$$+\sin4\beta(2\sin2\theta\sin^2\theta-\tfrac{1}{2}\sin4\theta)]+a\cdot\Delta a\sum_{n=1}^{\infty}\left(\frac{a}{r_0}\right)^{2n}G_n(\theta;\beta)\}d\theta\ .$$

The functions $G_n(\theta;\beta)$ are sums and products of sine and cosine functions, so that, as before, the series may be shown to converge uniformly over $[-\pi,\pi]$. Thus

$$\left[U^{\prime}(R)-U(R)\right]_{C_1}=\frac{\tau^2\pi a}{4\mu}2\kappa\cdot\Delta a+\frac{\tau^2 a}{4\mu}\cdot\Delta a\sum_{n=1}^{\infty}\left(\frac{a}{r_0}\right)^{2n}\int_{-\pi}^{\pi}G_n(\theta;\beta)d\theta\ ,\qquad(7.53)$$

where it is clear that after term by term integration, the resulting infinite sum of bound quantities will converge to zero as $r_0\to\infty$:

$$\lim_{r_0 \to \infty} \sum_{n=1}^{\infty} \left(\frac{a}{r_0}\right)^{2n} \int_{-\pi}^{\pi} G_n(\theta; \beta) d\theta \to 0 . \tag{7.54}$$

Because the crack extension increment Δa is arbitrarily small, the second of the integrals of Eq. (7.47) can be evaluated using Eqs. (2.56), (2.57) and (2.58). These give

$$\left[t_{yy}^{(+)}\right]_{\substack{\theta=0 \\ r=x}} = -\frac{\tau\sqrt{a}}{\sqrt{2x}} \sin 2\beta, \quad \left[t_{xy}^{(+)}\right]_{\substack{\theta=0 \\ r=x}} = \frac{\tau\sqrt{a}}{\sqrt{2x}} \cos 2\beta \tag{7.55}$$

for the unextended crack, and

$$\left[u_y^{\prime(+)}\right]_{\substack{\theta=\pi \\ r=(\Delta a-x)}} = -\frac{\tau\sqrt{\pi(a+\Delta a)}\sin 2\beta(\kappa+1)}{2\mu}\sqrt{\frac{\Delta a-x}{2\pi}}$$

$$+ \frac{\tau}{4\mu} (\kappa+1)(x+a)\cos 2\beta$$

$$\tag{7.56}$$

$$\left[u_x^{\prime(+)}\right]_{\substack{\theta=\pi \\ r=(\Delta a-x)}} = \frac{\tau\sqrt{\pi(a+\Delta a)}\cos 2\beta(\kappa+1)}{2\mu}\sqrt{\frac{\Delta a-x}{2\mu}}$$

$$+ \frac{\tau}{4\mu} (\kappa+1)(x+a)\sin 2\beta$$

for the extended crack. The second integral of Eq. (7.47) thus gives

$$\left[U^{\prime}(R)-U(R)\right]_{C_2} = -\frac{\tau^2 a(\kappa+1)}{2\mu} \int_0^{\Delta a} \sqrt{\frac{\Delta a-x}{x}} \, dx$$

$$\tag{7.57}$$

$$= -\frac{\tau^2 \pi a(\kappa+1)}{4\mu} \cdot \Delta a .$$

The change of elastic strain energy with change of crack size for the infinite cracked shear panel is obtained from Eqs. (7.1), (7.53), (7.54) and (7.57) in the limits $r_0 \to \infty$ and $\Delta a \to 0$, with the result that

$$\frac{dU}{da} = \frac{\pi^2 \pi a}{4\mu}(2\kappa) - \frac{\tau^2 \pi a}{4\mu}(\kappa+1) = \frac{\tau^2 \pi a}{4\mu}(\kappa-1) . \tag{7.58}$$

It is noted that for $\kappa=1$, or for $\nu=1$ in plane stress, or for $\nu=\frac{1}{2}$ in plane strain, $dU/da=0$.

SECTION 8

ALTERNATIVE CALCULATION OF THE ELASTIC
STRAIN ENERGY DERIVATIVE

A determination of the elastic strain energy derivative, dU/da, can be approached in a somewhat different manner, that is, by calculating the strain energy, U, of the entire cracked body first, and then obtaining its change with respect to the crack dimension by a formal differentiation.

Referring to Fig. (24) for the single crack, Fig. (25) for the collinear cracks, and Fig. (26) for the shear panel, the elastic strain energy (per unit thickness) of the region R is specified by

$$U(R) = \frac{1}{2} \iint\limits_{R} \left[t_{xx}\frac{\partial u_x}{\partial x} + t_{yy}\frac{\partial u_y}{\partial y} + t_{xy}\left(\frac{\partial u_x}{\partial y} + \frac{\partial u_y}{\partial x}\right) \right] dxdy. \qquad (8.1)$$

Integration over the plane region can be transformed into line integrations about the boundary curves C_k by application of Green's theorem as discussed in the previous section:

$$U(R) = \frac{1}{2}\sum_{k=1}^{N} \oint_{C_k} \left([t_{xx}u_x + t_{xy}u_y]dy - [t_{yy}u_y + t_{xy}u_x]dx \right) , \qquad (8.2)$$

where N=2 for the single crack and N=3 for two collinear cracks. Again, the arbitrary outer boundary C_1 can be taken to be a circle of arbitrarily large radius r_0, while the inner boundary (or boundaries) may be taken to coincide with the crack borders. For the single crack and shear panel geometries such choices will give

$$U(R) = I_1 + I_2 \qquad (8.3)$$

-60-

$$I_1 = \frac{1}{2} r_0 \int_{-\pi}^{\pi} \left\{ [t_{xx}u_x + t_{xy}u_y]_{r=r_0} \cos\theta + [t_{yy}u_y + t_{xy}u_x]_{r=r_0} \sin\theta \right\} d\theta \qquad (8.4)$$

$$I_2 = -\frac{1}{2} \oint [t_{yy}u_y + t_{xy}u_x] dx = 0 \quad , \qquad (8.5)$$

and

$$U(R) = I_1 + I_2 + I_3 \qquad (8.6)$$

$$I_1 = \text{Eq. } (8.4)$$

$$I_2 = -\frac{1}{2} \left(\oint_{C_2} + \oint_{C_3} \right) [t_{yy}u_y + t_{xy}u_x] dx = 0 \qquad (8.8)$$

for the collinear crack geometry. The integrals I_2 about the crack borders vanish because of the stress free crack boundary conditions.

8.1 SINGLE CRACK

Utilizing Eqs. (7.14) and (7.15) along the circle $r = r_0$, Eq. (8.4) gives

$$I_1 = \frac{\sigma^2}{16\mu} \int_{-\pi}^{\pi} \left\{ r_0^2 F(\theta;k) + a^2 G(\theta;k) + a^2 \sum_{n=1}^{\infty} \left(\frac{a}{r_0}\right)^{2n} H_n(\theta;k) \right\} d\theta \quad , \quad (8.9)$$

in which

$$F(\theta;k) = k[\kappa(1+k)+k-3]\cos^2\theta + [\kappa(1+k)+(1-3k)]\sin^2\theta$$

$$G(\theta;k) = 2k[\sin\theta\cos\theta\sin2\theta - \frac{1}{2}(\kappa-1)\cos^2\theta]$$

$$+ [\kappa(1+k)+(1-3k)]\cos3\theta\cos\theta\sin^2\theta + [(\kappa+1)-2\cos2\theta]\sin^2\theta$$

$$+ \frac{1}{2}[\kappa(1+k)+(k-3)][\cos2\theta - 2\sin\theta\sin3\theta]\cos^2\theta$$

$$+ \frac{1}{2}[\kappa(1+k)+(1-3k)][\cos2\theta + 2\sin\theta\sin3\theta]\sin^2\theta$$

$$+ [\kappa(1+k)+(k-3)]\cos\theta\cos3\theta\sin^2\theta \quad ,$$

and the functions $H_n(\theta;k)$, $n=1,2,3\ldots$ which are products and sums of sine and cosine functions, are bound over the interval $-\pi \le \theta \le \pi$. The infinite series in the integrand of Eq. (8.9) is similar in form to the series appearing in the integrand of Eq. (7.18), and may be proved to converge uniformly over the interval of integration by the same argument. Consequently, integration of the first two terms of the integrand followed by interchange of the order of integration with summation of the series leaves

$$I_1 = \frac{\sigma^2 \pi r_0^2 (1+\nu)}{8E} \left[(\kappa+1)k^2 + 2(\kappa-3)k + \kappa + 1 \right] + \frac{\sigma^2 \pi a^2 (1+\nu)}{4E} \left[1 + k(2-\kappa) \right]$$

$$+ \frac{\sigma^2 a^2 (1+\nu)}{8E} \sum_{n=1}^{\infty} \left(\frac{a}{r_0} \right)^{2n} \int_{-\pi}^{\pi} H_n(\theta;k)\,d\theta \quad . \tag{8.10}$$

The infinite series in Eq. (8.10) vanishes in the limit $r_0 \to \infty$ in the same manner as shown by Eq. (7.20).

By means of Eqs. (8.3)-(8.5) and Eq. (8.10), the elastic strain energy for the entire infinite body is obtained in the limit $r_0 \to \infty$:

$$U = \lim_{r_0 \to \infty} \left(I_1 \right) + I_2 \quad ,$$

with the result

$$U = U_0 + \Delta U, \tag{8.11}$$

where

$$U_0 = \lim_{r_0 \to \infty} \left\{ \frac{r_0^2 \sigma^2 \pi (1+\nu)}{8E} \left[(\kappa+1)(1+k^2) + 2k(\kappa-3) \right] \right\}$$

and $\tag{8.12}$

$$\Delta U = \frac{\sigma^2 \pi a^2 (1+\nu)}{4E} \left[1 + k(2-\kappa) \right] \quad .$$

-62-

The first term, U_0, which is independent of the crack dimen-
sion, represents the strain energy of the infinite non-cracked
body with boundary tractions applied as in Fig. 1. The second
term, which includes the crack dimension, indicates that the
elastic strain energy of an infinite sheet of unit thickness
containing a centrally located line crack is different from
that of a continuous sheet by the amount ΔU. It is, therefore,
often referred to in the literature as the energy of the
crack. Formal differentiation of Eqs. (8.11) and (8.12) with
respect to the crack dimension gives

$$\frac{dU}{da} = \frac{d}{da}(U_0 + \Delta U) = \frac{\sigma^2 \pi a (1+\nu)}{2E} [1 + k(2 - \kappa)] , \qquad (8.13)$$

which concides with Eq. (7.25).

It should be noted that for equal tension-tension loads,
$k=1$, ΔU given by Eq. (8.12) is identical to Griffith's result
of 1921 [12], and to Swedlow's calculation in 1965 [20]. For
uniaxial load, $k=0$, Eq. (8.12) reduces to the expression
obtained by Wolf [21].

8.2 TWO COLLINEAR CRACKS

Substitution of Eqs. (7.31) and (7.32) into (8.7) produces

$$I_1 = \frac{\sigma^2}{16\mu} \int_{-\pi}^{\pi} \left\{ r_0^2 F(\theta;k) + N(\lambda) b^2 G(\theta;k) + b^2 \sum_{n=1}^{\infty} \left(\frac{b}{r_0}\right)^{2n} H_n(\theta;\lambda(p),k) \right\} d\theta \qquad , \qquad (8.14)$$

in which

$$F(\theta;k) = k[\kappa(1+k)+(k-3)]\cos^2\theta+[\kappa(1+k)+(1-3k)]\sin^2\theta \quad ,$$

$$G(\theta;k) = 2k[\sin\theta\sin2\theta - \frac{(\kappa-1)}{2}\cos\theta]\cos\theta+[\kappa(1+k)+(1-3k)]\cos\theta\cos3\theta\sin^2\theta$$

$$+ \frac{1}{2}[\kappa(1+k)+(k-3)][\cos2\theta-2\sin\theta\sin3\theta]\cos^2\theta+[(\kappa+1)-2\cos2\theta]\sin^2\theta$$

$$+ \frac{1}{2}[\kappa(1+k)+(1-3k)][\cos2\theta+2\sin\theta\sin3\theta]\sin^2\theta$$

$$+[\kappa(1+k)+(k-3)]\cos\theta\cos3\theta\sin^2\theta \quad .$$

The functions $H_n(\theta;\lambda(p),k)$ are products and sums of sine and
cosine iunctions and the complete elliptic integrals, and
are bound functions over $-\pi\leq\theta\leq\pi$ and $0<a<b$. The infinite series
in Eq. (8.14) is similar in form to the series appearing in
Eq. (7.36), and may therefore be proved to converge uniformly
over the interval of integration by the same argument. Con-
sequently, integration of the first two terms of the integrand
followed by interchange of the order of integration with
summation of the series leaves

$$I_1 = \frac{\sigma^2\pi r_0^2}{16\mu}[(\kappa+1)k^2+2(\kappa-3)k+\kappa+1] + \frac{\sigma^2\pi b^2}{8\mu} N(\lambda)[1+k(2-\kappa)]$$

$$+ \frac{\sigma^2 b^2}{16\mu} \int_{-\pi}^{\pi}\sum_{n=1}^{\infty} \left(\frac{b}{r_0}\right)^{2n} H_n(\theta;\lambda(p),k)\ d\theta \quad . \tag{8.15}$$

The infinite series in Eq. (8.15) vanishes in the limit as
$r_0\to\infty$ in the same manner as shown by Eq. (7.37).

By means of Eqs. (8.6)-(8.8), Eq. (8.14) and Eq. (8.15),
the elastic strain energy for the infinite body follows in
the limit as $r_0\to\infty$:

$$U = \lim_{r_0\to\infty}\left(I_1\right) + I_2 + I_3$$

giving

$$U = U_0 + \Delta U \quad , \qquad (8.16)$$

where

$$U_0 = \lim_{r_0 \to \infty} \left\{ \frac{\sigma^2 \pi r_0^2}{16\mu} \left[(\kappa+1)k^2 + 2(\kappa-3)k + \kappa + 1 \right] \right\}$$

$$\qquad\qquad (8.17)$$

and

$$\Delta U = \frac{\sigma^2 \pi b^2}{8\mu} N(\lambda)[1 + k(2-\kappa)] \quad .$$

In these expression U_0 and ΔU have the same interpretation as given in Section 8.1 for the single crack. In the limit as $a \to 0$, leaving a single crack of length 2b, $N(\lambda) \to 1$ and ΔU assumes the value appropriate to a single crack, i.e., Eq. $(8.12)_2$. For crack lengths $(b-a) = \ell$ held fixed while the crack spacing $2a \to \infty$, leaving the infinite body without cracks, $N(\lambda) \to 0$ and $U = U_0$. A formal differentiation of Eqs. (8.16) and (8.17), utilizing Eq. (7.44), reproduces Eq. (7.46)

$$\frac{dU}{da} = \frac{d}{da} (U_0 + \Delta U) = + \frac{\sigma^2 \pi b^2}{4\mu} [1 + k(2-\kappa)] \frac{[\lambda(p) - (a/b)^2]^2}{a[1 - (a/b)^2]} \quad . \qquad (8.18)$$

8.3 SHEAR PANEL

Substitution of Eqs. (7.48) and (7.49), with $r = r_0$, into Eq. (8.4) gives

$$I_1 = \frac{\tau^2}{4\mu} \int_{-\pi}^{\pi} \left[r_0^2 (\cos^2 2\beta + \sin^2 2\beta) \right.$$

$$\qquad\qquad (8.19)$$

$$\left. + \frac{a^2}{4} F(\theta;3) + a^2 \sum_{n=1}^{\infty} \left(\frac{a}{r_0} \right)^{2n} G_n(\theta;\beta) \right] d\theta$$

-65-

where

$$F(\theta;\beta) = (1-4\cos^2 2\beta)\sin^2 2\theta - (4\sin^2\theta\cos 4\beta$$

$$+2\cos^2\theta+1)\cos 2\theta - 2(2\sin\theta\sin 3\theta+\sin 4\theta\sin 4\beta)+\kappa$$

and $G_n(\theta;\beta)$, $n=1,2,\ldots$, represent functions composed of products and powers of sine and cosine functions. Integration of the first two terms of Eq. (8.19) leaves

$$I_1 = \frac{\tau^2\pi r_0^2}{2\mu} + \frac{\tau^2\pi a^2}{8\mu}(\kappa-1) + \frac{\tau^2 a^2}{4\mu}\int_{-\pi}^{\pi}\sum_{n=1}^{\infty}\left(\frac{a}{r_0}\right)^{2n}G_n(\theta;\beta)d\theta \quad . \qquad (8.20)$$

The infinite sum in Eq. (8.20), as in Eq. (7.15), converges uniformly over $-\pi\le\theta\le\pi$ by the same argument given previously. Thus upon interchange of integration and summation, it follows that in the limit $r_0\to\infty$

$$\lim_{r_0\to\infty}\left\{a^2\sum_{n=1}^{\infty}\left(\frac{a}{r_0}\right)^{2n}\int_{-\pi}^{\pi}G_n(\theta;\beta)d\theta\right\}$$

$$\qquad (8.21)$$

$$=\lim_{r_0\to\infty}\left\{a^2\left[\left(\frac{a}{r_0}\right)^2 G_1^*(\beta) + \left(\frac{a}{r_0}\right)^4 G_2^*(\beta)+\ldots\right]\right\} = 0$$

since each of the numbers $G_n^*(\beta)$ are bound quantities.

From Eqs. (8.3)-(8.5), Eq. (8.20) and Eq. (8.21), the elastic strain energy for the infinite cracked shear panel is determined in the limit as $r_0\to\infty$:

$$U = \lim_{r_0\to\infty}\left(I_1\right) + I_2$$

from which

$$U = U_0 + \Delta U \quad , \qquad (8.22)$$

where

$$U_0 = \lim_{r_0 \to \infty} \left(\frac{\tau^2 \pi r_0^2}{2\mu} \right)$$

and   (8.23)

$$\Delta U = \frac{\tau^2 \pi a^2}{8\mu} (\kappa - 1) \quad .$$

Formal differentiation of Eqs. (8.22) and (8.23) recovers
Eq. (7.56):

$$\frac{dU}{da} = \frac{d}{da} (U_0 + \Delta U) = \frac{\tau^2 \pi a^2}{4\mu} (\kappa - 1) \quad .$$ (8.24)

SECTION 9

FRACTURE LOAD

The tensile load necessary to cause onset of crack instability (fast crack propagation) according to the Griffith crack instability criterion may be determined from Eq. (6.7). The surface energy of the crack (per unit thickness) is assumed to be equal to a constant surface energy density, γ, multiplied by the surface area of the crack.

$$\Gamma = 4\gamma a \quad . \tag{9.1}$$

9.1 SINGLE CRACK

For the single (horizontally oriented) crack, Eqs. (7.25), (9.1) and (6.7) lead to the critical applied tensile stress values

$$\sigma_c = \left\{ \frac{8E\gamma}{\pi a} \left[\frac{1}{(3\nu-1)k+(1+\nu)} \right] \right\}^{\frac{1}{2}} \qquad \text{plane stress}$$

and $\hspace{9cm}$ (9.2)

$$\sigma_c = \left\{ \frac{8E\gamma}{\pi a(1+\nu)} \left[\frac{1}{(4\nu-1)k+1} \right] \right\}^{\frac{1}{2}} \qquad \text{plane strain.}$$

The variation of the fracture load with load biaxiality and Poisson's ratio for plane stress and plane strain is shown by Figs. 27 and 28. Referring to Fig. 27, for Poisson ratio values $\nu<1/3$, σ_c increases with increasing load biaxiality, while for values greater than one-third it decreases as the load increases. In the range of values $0.3<\nu<0.4$, which encompasses most structural materials, the biaxial effect on the fracture load, while present, is rather small for the k variation $-1 \leq k \leq 1$.

For values of k equal to those given by Eq. (7.27), the
unbound value for σ_c indicated by Eq. (9.2) should not be
interpreted as meaning that these equations predict an
infinite fracture stress. As remarked in Section 7, for
the plane infinite centrally-cracked body at these particular
values of the load biaxiality, dU/da is zero and Griffith's
fracture criterion becomes inapplicable.

9.2 TWO COLLINEAR CRACKS

For the (horizontally oriented) collinear cracks, Eqs.
(7.46), (9.1) and (6.7) give

$$\sigma_c = \frac{\{a[1-(a/b)^2]\}^{\frac{1}{2}}}{\lambda(p)-(a/b)^2} \left\{\frac{16\mu\gamma}{\pi b^2} \frac{1}{[1+k(2-\kappa)]}\right\}^{\frac{1}{2}} . \qquad (9.3)$$

The variation of σ_c with load biaxiality k in the case of
plane stress is shown by Fig. 29. For materials with Poisson's
ratio less than one-third, the breaking stress must be in-
creased as tensile loads of increasing magnitude are applied
parallel to the cracks. This trend is reversed when the
Poisson's ratio value is greater than one-third. The curves
shown in Fig. 29 for the multiple-crack are very similar to
those determined for the single crack, i.e., Fig. 27. The
comments given above concerning load biaxiality values at
$k=1/(\kappa-2)$ for the single crack, apply in the same way for
the collinear cracks.

To gain some idea of the influence of the crack spacing
on the breaking load, b can be assumed to be fixed with the
value b=1, so that the pair of cracks have the fixed lengths

$\ell = (1-a)$. The corresponding critical normal tensile load for a single crack of length $(1-a)$ is

$$\sigma_c^* = \left(\frac{2}{1-a}\right)^{\frac{1}{2}} \left\{ \frac{16\mu\gamma}{\pi} \frac{1}{[1+k(2-\kappa)]} \right\}^{\frac{1}{2}} . \tag{9.4}$$

The ratio

$$\frac{\sigma_c}{\sigma_c^*} = \frac{[a(1-a)(1-a^2)]^{\frac{1}{2}}}{(2)^{\frac{1}{2}}[\lambda(p)-a^2]} \tag{9.5}$$

provides a measure of the degree to which the body is weakened by the presence of the second crack. The variation of Eq. (9.5) with the ratio of the distance between the cracks to the crack length, i.e., $\rho = (2a/\ell)$, is shown in Fig. 30, from which the following important observation can be made: As the spacing between the collinear cracks approaches four times the individual crack length, the critical load for the doubly-cracked body is just about the same as the critical load of the body with a single crack of the same length. Thus a pair of widely spaced collinear cracks in a relatively large body behave, with respect to instability, as if the body contained only a single crack having the length of one of the collinear cracks.

The critical load for collinear cracks, each of length $\ell = (1-a)$, can be compared to the critical load for a single crack having the greater length, $\ell = 2 > 2(1-a)$, by the ratio

$$\frac{\sigma_c}{\sigma_c^*} = \frac{\{a(1-a^2)\}^{\frac{1}{2}}}{\lambda(p)-a^2} \geq 1 \quad , \tag{9.6}$$

c.f. Fig. 31. For cracks relatively closely spaced, the
critical normal tensile load necessary to cause the inner
crack ends to extend and join exceeds the critical load for
the resulting longer crack. Fracture of the collinear cracks
will therefore proceed in two stages: The inner crack ends
will extend first to join up forming the larger single crack,
whereupon the sustained load level will be sufficient to
cause the second stage, onset of fracture from the ends of
the newly formed single crack. From these observations the
assumption of crack instability for the doubly-cracked body
in terms of initial extension of the inner crack ends is
justified.

9.3 SHEAR PANEL

The critical applied tensile stress for the cracked
shear panel has, by virtue of Eqs. (7.58), (9.1) and (6.7),
the value

$$\sigma_c = \left\{ \frac{8E\gamma}{\pi a(1+\nu)(\kappa-1)} \right\}^{\frac{1}{2}} , \qquad (9.7)$$

which is seen to be independent of the angle of crack
orientation. Note that for $\kappa=1$, or equivalently, for $\nu=1$
in plane stress or $\nu=\frac{1}{2}$ in plane strain, $dU/da=0$ and the
above expression is meaningless, that is, Griffith's crack
instability hypothosis is no longer applicable.

SECTION 10

EFFECT OF LOAD BIAXIALITY ON
FATIGUE CRACK GROWTH RATES

The phenomenon of crack formation and the subsequent incremental extension of such cracks under repeated or cyclic load application until catastrophic fracture ensues, may be usefully thought of as three hypothetically distinct or separate physical events: (i) micro-crack nucleation, terminated by the appearance of macro-cracks, followed by (ii) crack 'propagation' (which is here taken to mean very minute incremental crack extensions caused by cyclic load application), and finally at the critical crack size (iii) onset of rapid crack propagation to fracture. This somewhat artificial division has proven to be fruitful, nevertheless, because it allows for the introduction of fracture mechanics concepts that have been able to correlate a wide range of fatigue crack growth experimental data appropriate to category (ii) semi-empirically, in a more or less satisfactory manner.

10.1 SEMI-EMPIRICAL FATIGUE CRACK PROPAGATION LAWS

According to the generally accepted micro structural theory concerning fatigue crack development and growth, the basic mechanism of crack nucleation and crack extension under cyclic load is cyclic slip (micro-plasticity), with slip bands (multiple slip planes). Crystalline slip results from the motions of dislocation which are generated by the action of shear stresses along potential slip planes. Fatigue micro

crack nucleation, which leads to the development of a
macroscopic crack by coalesence of many micro-cracks, and
the subsequent propagation of this crack under continued
cyclic load application, appears, therefore, to be intimately
related to the extent of plastic deformation that developes
around the crack tip.

This realization has served as the physical basis for
the development of a variety of semi-empirical fatigue
crack propagation laws, evolving ultimately into the widely
used form [22-26]

$$\frac{da}{dN} = B(\Delta K_1)^n \quad , \tag{10.1}$$

where (a) is the current crack length, N the number of load
cycles and $\Delta K_1 = (K_1)_{max} - (K_1)_{min}$, a measure of the applied load
range. On a log-log graph this relation plots as a straight
line

$$\ln \frac{da}{dN} = \ln B + n \ln(\Delta K_1) \quad , \tag{10.2}$$

for which B represents the $\Delta K_1 = 1$ intercept and n the slope
of the straight line. Relation (10.1) has been shown to
correlate a broad range of fatigue crack growth data in the
moderate to high ΔK_1 range, where the data was obtained mostly
from tests performed on center cracked sheets (with horizontal
crack orientation) cycled in uniaxial tension between $(K_1)_{max}$
and $(K_1)_{min} = 0$, that is, for the load ratio $\bar{R} = (K_1)_{min}/(K_1)_{max} = \sigma_{min}/\sigma_{max} = 0$.

Over the full range of crack growth rates, however, ranging from 10^{-3} to 10^{-9} inches per load cycle, fatigue crack growth rates are not observed to fall along a straight line (cf. Fig. 32). At the higher load levels, as the fatigue crack approaches the critical crack size, the increment of crack growth per cycle of load increases causing an upward inflection away from the straight line, and characterizes the passage from the fatigue crack propagation stage of category (ii) to the fast fracture stage of category (iii). Here as the curve asymptotically approaches the upper vertical line $(da/dN) \to \infty$. At the lower end, the downward inflection from the straight line represents progressively smaller crack growth increments per load cycle, so small as to be considered negligible, i.e., $(da/dN) \approx 0$. The asymptotic approach to the lower vertical line is therefore interpreted as defining a fatigue threshold value, ΔK_0, below which fatigue crack propagation cannot take place [27].

To take account of the frequently observed effect of the load ratio, $\bar{R}$, on the growth rates, [28], as well as to incorporate the departure from linearity of the upper end of the growth rate curve, Eq. (10.1) may be modified in the manner proposed by Forman [29]

$$\frac{da}{dN} = \frac{C(\Delta K_1)^m}{(1-\bar{R})K_c - \Delta K_1} \qquad , \qquad (10.3)$$

where the parameters C and m are determined in the same way as the parameters B and n of Eq. (10.1). As $(K_1)_{max} \to K_c$,

-74-

indicating the onset of fast fracture, the denominator of (10.3) approaches zero and $(da/dN) \to \infty$. The deviation from linearity at both ends of the spectrum of fatigue crack growth rate can be accounted for by the form proposed by Hartman and Schijve [30].

$$\frac{da}{dN} = \frac{C(\Delta K_1 - \Delta K_0)^m}{(1-\overline{R})K_c - \Delta K_1} \qquad . \qquad (10.4)$$

According to this expression, as the value of the load range ΔK_1 approaches the lower limit or fatigue threshold value, ΔK_0, $(da/dN) \to 0$. This is represented in Fig. 32 by the asymptotic approach to the vertical at negligibly small crack growth rates approximating $(da/dN) \approx 0$.

10.2 EFFECT OF LOAD BIAXILITY

Any survey of the large body of existing fatigue crack growth data identifies many factors that can possibly effect fatigue crack propagation [28, 31]. These may be grouped into the following broad categories:

(i) Geometry - including crack size, shape and orientation, specimen thickness and relative size.

(ii) Loading - including load magnitude, max-min. load ratio, biaxiality, sequence, cyclic frequency.

(iii) Material Properties - including the elastic modulus, uniaxial yield and ultimate stresses, cyclic stress-strain properties.

(iv) Environment.

Such a large number of possibilities probably explains why for any given one of them, one almost invariably encounters conflicting experimental data. Some of the factors no doubt must mitigate, or entirely nullify, their effects on fatigue crack growth rate when considered jointly. Without the benefit of a comprehensive rational theory of fatigue crack propagation that can explicitly account for many of these factors and, thereby, provide a basis for weighing their relative contributing effects, development of a full understanding of fatigue crack phenomena must continually entail partial understanding and accompanying confusion.

With respect to the influence that load biaxiality might have on fatigue crack propagation, qualitatively important insights and expectations may be gotten from the information provided in the previous sections. The belief that the elastic stress intensity factor K_1 (assuming here a horizontal crack orientation) is sufficient to completely determine the stress about the crack-tip, is shown by equations (2.24) and (3.3) to be incorrect in situations where loads are biaxially applied. Figure 11 demonstrates the pronounced effect that the horizontal load σk has on the intensity and spatial distribution of the maximum shear stress which, in turn, must cause a qualitatively similar pattern of dependence on σk of the plastic deformation around the tip of the crack. Thus, the pattern of variation of the lines of maximum shear stress with increasing tension-tension load biaxiality implies

-76-

correspondingly reduced plastic deformation and, therefore, a correspondingly reduced fatigue crack growth rate.

Equation $(9.2)_1$ and Fig. 27 indicate that for materials with a Poisson ratio in the vicinity of 0.30, the fracture stress σ_c increases approximately linearly with increase of tensile load biaxiality in the load range $-1 < k < 2.5$. The plane stress fracture toughness for a horizontally oriented center-cracked sheet of finite width should therefore also show a similar dependency on k, i.e.,

$$K_c(k) = \sigma_c(k)(\pi a)^{\frac{1}{2}} f(a/w) = [\sigma_c(0) + \beta k](\pi a)^{\frac{1}{2}} f(a/w) \qquad (10.5)$$

where β is the slope of the σ_c vs. k curve of Fig. 27 and $f(a/w)$ is the correction factor for the finite width, w, of the test specimen. A similar argument can be made for the plane strain fracture toughness K_{1C} based on Eq. $(9.2)_2$ and Fig. 28. The semi-empirical expressions (10.3)-(10.5) thus appear to indicate that an increase in the tensile load biaxiality should cause a reduction of the fatigue crack growth rate relative to the growth rate for uniaxially cycled load.

The reduced crack-tip plasticity associated with increasing tension-tension load biaxiality might possibly diminish the effect of crack closure that is believed to accompany crack propagation through cyclically loaded and unloaded plastically deformed regions [27]. Any such miti-gation or lessening of their effect would have the consequence

of increasing the crack growth rate, offsetting thereby, to some extent, the anticipated crack growth rate decrease with horizontal tensile load increase indicated above.

PART II.   EXPERIMENT

The agenda for the experimental part of the research program was determined by selection of those tests that could provide directly measureable, or observeable, information on the influence of load biaxiality on conditions near the crack-tip and on fracture. The tests that were performed involved crack-tip photoelasticity, measurements of angles of initial crack extension, fracture load and fatigue crack propagation rates, all under varying levels of horizontal load application.

SECTION 11

DEVELOPMENT OF THE BIAXIAL TEST FACILITY

To be able to perform the indicated tests, it was necessary at the outset to design and assemble a biaxial test specimen, and a testing system compatible with it. Several of the more important features of this part of the test program are described initially.

11.1 SPECIMEN DESIGN

The preliminary biaxial test specimen design was based upon a specimen configuration developed by Radon and co-workers, [32], which was shown to provide a relatively large uniform stress field for the given specimen size. Several other designs, [33-37], were also examined, which suggested several minor changes in the preliminary design. A photo-elastic study was employed to ensure that the design would be adequate to provide the desired uniform stress field through out a large central portion of the center cracked specimen over a wide range of the biaxial load ratio. The specimen configuration that was finally adopted is shown in Fig. 33. A second large specimen was also designed in the event that a larger working area became necessary. This alternate design is shown in Fig. 34. It was also noted from this initial photoelastic study that the biaxiality of the applied load has a clearly observeable effect on the crack-tip stress field that is in qualitative agreement with the

predictions of the analysis. These results will be pre-
sented and discussed in a following section.

It was also necessary to design and purchase (or
fabricate) grips to interface between the test system and
the specimen. The specially designed grips that were pur-
chased performed satisfactorily throughout the testing
program.

11.2 TEST SYSTEM DEVELOPMENT

The second phase involved designing a biaxial test
system, which was comprised of an existing MTS testing system
of 100 kips capacity as the vertical axis, a portable test
frame of 50 kip capacity as the horizontal axis, and a control
system capable of controlling both axis. Since only two
independent actuators were planned for this test system
(rather than four), the center of the test specimen would
not remain stationary but would move in response to the
motion of each actuator. In order to prevent this motion
from introducing side loads on the specimen, the horizontal
axis was suspended in its working position by elastic ropes.
In this manner the test frame could move relatively freely
with the center of the specimen. However, the motion of the
frame under rapid fatigue loading conditions could introduce
dynamic loads which would be transmitted to the specimen.
The magnitudes of these loads were calculated for the ex-
pected worst case conditions and were found to be small
enough to be neglected.

The test system design incorporated considerable versatility so that a wide range of tests could be performed. The control system purchased as part of the second channel (horizontal axis) was designed and connected so that it could control both actuators for applying phased static or cyclic loads, with the phase angle readily adjustable to any desired value. Since the specimen could serve as a load path between the two control channels, a specially designed pair of service manifolds was incorporated into the syst m, effectively eliminating "cross-talk" between the channels. These service manifolds also permit completely independent operation of the two channels so that different types of load programs could be applied to each channel. For example, a randomly varying cyclic load could be applied to one axis while a constant amplitude fatigue load or a static load could be applied to the other. The two systems could also be operated independently when biaxial tests were not being performed.

In order that the horizontal axis be lightweight and relatively easy to manage, the horizontal load frame was designed and manufactured from aluminum structural sections and high-strength aluminum plates. The load frame design was completed and the components were fabricated in the school machine shop. The assembled test system weighed less than 1000 pounds, of which the actuator alone weighed approximately 600 pounds. After assembly of the horizontal

test system, this system was operated for a brief check-out period and then interconnected with the existing test system. The combined system was then checked out and found to operate as designed. A schematic drawing of the combined test system is seen in Fig. 35, and photographs of the completed system are shown in Fig. 36.

SECTION 12

EFFECT OF BIAXIAL LOADS ON THE CRACK-TIP
ISOCHROMATIC PATTERNS

As the biaxial test specimen design and the biaxial
test system was being developed, an initial photoelastic
study was performed for the purpose of: (1) examining
photoelastically several aspects of the test specimen design,
and (2) providing preliminary information about the possible
effects of biaxial load on the crack-tip stress field.

The photoelastic study sought to answer several ques-
tions that concerned important details needed to complete
the design of the test specimen. The first parameter
examined was the radius of the fillet between two adjacent
load tangs. Initial biaxial specimen designs developed
by other researchers employed large circular radii or hyper-
bolic curves between the load tangs. Consequently, a large
radius was employed initially for the first photoelastic
specimens. In this series of experiments it was seen that
the biaxial forces did have a significant effect on the crack-
tip isochromatic pattern, however, the quantitative agreement
between the theoretically predicted isochromatic patterns
and the photoelastic results was not very good. Subsequent
study showed that the large fillet radius introduced inter-
actions between the stresses parallel and perpendicular to
the crack. Other studies [38] have confirmed this condition,
and have also shown that there was significant nonuniformity

-84-

of the stress field along the width of the tang. Additional studies by other researchers have been made into the effects of different geometrical details at the intersection of two adjacent tangs [39]. The effects of different, small radii, and of undercutting were examined and it was concluded that employing a small fillet, as in Fig. 33, provided the optimum configuration in the intersection region.

The second parameter examined was the crack length-to-specimen width (a/w) ratio. The biaxial photoelastic specimens were fabricated initially with small crack lengths and after photoelastic examination, the cracks were extended and subsequent photoelastic examinations performed. The results of these studies showed that the extent of the biaxial effect was not altered by changes in the (a/w) ratio. As expected, the crack-tip stress fields were affected by the (a/w) ratio, with the fringe patterns increasing in size as the crack length was increased. However, the effect of load biaxiality on the fringe patterns was not significantly affected by changes in the (a/w) ratio.

The third parameter to be studied was the crack-tip radius, with two different notch radii, and a natural crack employed in the study. The notch radii were filed using screw-head files of different.radii, while the natural crack was produced by means of a razor blade. As with the (a/w) study, it was determined that the sharpness of the crack-tip radius had a significant effect on the crack-tip stress

fields. However, the magnitude of the load biaxiality effect was not measurably influenced by variation of the crack-tip radius.

Since the effects of several important test parameters were shown to have insignificant interaction with the presence of the horizontal loads, a study of the biaxial load effects on the crack-tip maximum shear stress was then performed. The most extensive data were taken from one of the early photoelastic specimens having an (a/w) ratio of approximately 0.5, a natural crack-tip, and a large fillet radius. The variation of the lines of maximum shear stress with load biaxiality indicated by the analysis of Section 3.1, and summarized in Fig. 11, provides a basis for comparison between the theoretically predicted patterns and the photoelastically observed patterns. The observed patterns are shown in Fig. 37 for k=0, 0.5 and 1.0. A comparison of Figs. 11 and 37 show good agreement for the angular shift in the stress profiles, and careful measurements confirmed the agreement. The change in the size of the isostatic loops with increasing tensile load biaxiality agreed with the predicted pattern, although the magnitudes did not initially correlate very well. However, when a correction factor appropriate to the large fillet radius was applied, the sizes of the isostatic loops and the associated stress intensity factors agreed much more closely with the theoretical predictions.

SECTION 13

FRACTURE TESTING OF SPECIMENS WITH HORIZONTAL CRACKS

Upon completion of the test system development, test
specimen design and photoelastic verification, the fracture
testing program was initiated. It was determined that three
initial test series would be performed and approximately forty
specimens were prepared for testing. Two of the test series
were performed on 7075-T6 aluminum, 0.063 inch thick, with
the center slot oriented perpendicular to the rolling direc-
tion for one series and parallel to the rolling direction for
the other. The material chosen for the third test series
was 0.25 inch thick plexiglass, because its material pro-
perties were quite different from 7075-T6.

Thin center slots were machined in all specimens and the
slot tips were subsequently sharpened to a tip radius of
0.003-0.005 inch by use of a screw head file. The 7075-T6
specimens were tested with the slot tips in this condition
(no fatigue precracking) since prior uniaxial testing ex-
perience with this material indicated that subcritical crack
growth occurs prior to unstable fracture. With the existence
of subcritical crack growth, unstable fractures initiated
from the existing crack and, therefore, were not influenced
by the notch tip radius. In contrast, the plexiglass speci-
mens fractured in a manner apparently more brittle than the
7075-T6 specimens. It was anticipated that variations in
the crack tip radius could cause significant differences in

-87-

the fracture behavior of the plexiglass. Consequently, natural cracks were introduced into these specimens by pressing the slot ends with a suitably reinforced razor blade. The final crack length-to-specimen width ratio was between 0.4 and 0.5 for all of these tests.

Since 7075-T6 is a relatively brittle aluminum alloy it was decided to perform two additional test series on 2024-T3 aluminum. The interest in performing the 2024-T3 tests was based on two considerations. First, 2024-T3 is an important material for aerospace applications, and it is often treated as a prototype material for the 2xxx series of aluminum alloys. Second, the additional ductility provided by 2024-T3 was desirable because finite element calculations by others suggest that the biaxial effect on fracture load is increased with increased material plasticity. These specimens were made according to the same design and were also machined from 0.063 inch sheets. A total of fifteen tests were performed on 2024-T3, in which the starter slot was parallel to the roll direction for seven tests and perpendicular to the roll direction for eight tests.

In performing these fracture tests, ramp loads were applied to the two perpendicular pairs of specimen tangs in porportion to the desired biaxiality ratio, k. For the 7075-T6 specimens the biaxiality ratios varied in the range $0 < k \leq 1.8$ and for the plexiglass specimens the range was $-0.5 \leq k \leq 2.0$. For the tests on 7075-T6 and 2024-T3 the loading

was interrupted periodically for the purpose of recording

the loads and displacements on both axis with the use of a

datalogger. In addition, the loads and displacements per-

pendicular to the slot were recorded continuously on an x-y

plotter. For the plexiglass tests the loading was not

interrupted, due to the time-rate effects associated with

this material. Only the loads and displacements perpendicular

to the crack were recorded on the plotter.

13.1 FRACTURE TEST RESULTS FOR 7075-T6

For the two 7075-T6 test series, the effect of load

biaxiality on the fracture load (perpendicular to the plane

of the starter slot) is seen in Figs. 38 and 39. The speci-

men thickness, B=0.063 in., was considered to be sufficiently

small to establish a plane stress situation. This assump-

tion was confirmed by the mode of fracture, in which the

fracture surfaces were oriented at 45° to the lateral sur-

face of the specimen (100 percent oblique fracture). For

both test series the critical fracture load increased 15-20

percent as k was increased from 0 to 1.8. Higher k values

could not be tested successfully, because the horizontal tabs

pulled off before unstable crack propagation, thus releasing

the biaxial constraint. Since the crack length and specimen

dimensions were identical for all specimens, the critical

stress and K_c values increase proportionally. The linear

regression fit to the data also showed the same increasing

trend in both test series, with the slope of the lines

exhibiting the same general uptrend. Poisson's ratio for this
material is approximately 0.30. For this value of Poisson's
ratio Fig. 27 predicts a small increase of the fracture load,
which is confirmed by the experimental results. The difference
in results between Figs. 38 and 39 is attributed to the aniso-
tropy introduced by the rolling process.

13.2 FRACTURE TEST RESULTS FOR PLEXIGLASS

The predicted variation of critical fracture load (or
K_{1c}) with k shown in Fig. 28 suggests that failure under
plane strain conditions (square fracture surfaces), combined
with values of Poisson's ratio greater than 0.25, should
produce the reverse trend of decreasing critical load (or
K_{1c}) with increasing k. Therefore a test series was per-
formed on plexiglass specimens with B=0.25 in., a thickness
which was large enough to cause plane strain fracture.
Poisson's ratio for this material is high, $0.40 < \nu < 0.47$,
so that in view of the test data trend obtained for the 7075
aluminum alloy, a definite decreasing trend in the K_{1c} data
would provide a strong confirmation of the results of the
theoretical analysis. The results of the plexiglass tests
are shown in Fig. 40, and do exhibit a trend of decreasing
fracture toughness with increasing load biaxiality. These
results are presented in terms of critical K_I rather than
critical load since the length of the natural cracks was
not the same for all specimens. Although there was a greater
amount of scatter in this data, the linear regression confirms
the decreasing trend.

Additional confirmation of the plexiglass data can be
found in the test results recently published by Radon, et al,
[40, 41], although they did not come to the same conclusion,
possibly due to the lack of a linear regression analysis of
their data. The results of forty tests on polymethylmeth-
acrylate (PMMA), which is essentially the same material as
plexiglass, are shown in Fig. 41. The best fit straight line
was added to their reported data, and it is seen that the two
test series agree remarkably well with regard to the magni-
tudes, the trends, (decreasing slopes), and the scatter in
the toughness values. Although the extent of test data re-
ported here is insufficient for definitive conclusions,
nevertheless, the qualitative agreement with the predicted
trends for both materials offers considerable evidence as
to the presence of biaxial load effects on the fracture
stresses and the associated K values.

13.3 FRACTURE TEST RESULTS FOR 2024-T3

In order to correlate as closely as possible with the
7075-T6 tests, one series of seven specimens was prepared
with the starter slot parallel to the rolling direction and
a second series of eight specimens was prepared with the
starter slot perpendicular to the rolling direction. The
specimen geometry, the slot length and notch tip radius and
the test procedure were the same as for the 7075-T6 tests.

The effect of the biaxiality ratio, k, on the fracture
load for 2024-T3 is shown in Figs. 42 and 43 for the starter

slot oriented parallel and perpendicular respectively to the rolling direction of the material. The behavior of these two test series is clearly self consistent in that they both display a peak in the critical fracture load corresponding to k values around 0.5 to 0.75. The rate of variation of critical load with k is greater in the range of 0<k<0.75 than was evidenced by the 7075-T6 results, and suggests that the increased biaxial effect may be due to the greater ductility of the material. However, the reasons for the existence of a peak value and subsequent decrease in critical load with increasing k is not apparent. One possible explanation for this behavior is that the increased ductility of the material was responsible for the tangs parallel to the starter slot to fail first, thus eliminating the biaxial constraint. This behavior would lead to the prediction that, at the higher k values, the breaking load would approach the result for uniaxial tension, k=0. It is seen that both tests series do display this type of behavior, with the exception of the test at k=1.25 in Fig. 42. There is some further experimental evidence to support this type of behavior, although these observations need considerably more study before reliable conclusions can be drawn. The difference in critical load between the two test series is due to the anisotropy effect and is of the same order of magnitude as the effect for 7075-T6.

SECTION 14

FRACTURE OF ANGLE-CRACKED SPECIMENS OF 7075-T6 ALUMINUM

Since a crack in a structure subjected to biaxial applied loads will not normally be aligned with either of the principal loading directions, knowledge of biaxial load effects on angle-cracked specimens is of considerable practical importance. The loads on both axis of the angle cracked specimens must be considered because the loads on each axis can be resolved into components parallel and perpendicular to the starter slot. The component perpendicular to the starter slot represents the principal force causing fracture, while the other component coincides with the horizontal (biaxial) load for the flat crack geometry.

Two test series were performed on 7075-T6 aluminum sheets, 0.063 in. thick, with the starter slot oriented 45 degrees to either of the load axis. Four tests were performed in each test series, with one test at each of the biaxiality ratios of $k = 0$, 0.25, 0.5 and 1.0. In one series the primary (larger load) axis was aligned with the rolling direction, while for the other the primary axis was perpendicular to the rolling direction. Figure 44 shows the broken specimens from the equal biaxial tests ($k=1.0$) for both test series, where the principal load direction is indicated by the arrow.

The specimen and starter slot were prepared in the same manner as for the specimens having the starter slots oriented perpendicular to the primary load axis. The same testing procedure employed previously for the aluminum test series was also followed for these tests. The load versus displacement for the principal axis was plotted continuously on an x-y recorder, and the loading ramp was interrupted periodically for the purpose of recording the load and displacement values for each axis using a datalogger. The critical or maximum load in the principal loading direction was also recorded using a digital multimeter with memory capability.

According to the analysis of the angle-cracked specimen given in Section 2, the opening-mode stress intensity factor is given by [cf. Eq. (2.23)]

$$K = \frac{\sigma(\pi a)^{\frac{1}{2}}}{2} [(1+k) - (1-k)\cos 2\alpha],$$

corresponding to an infinite sheet geometry, where the angle
of crack inclination α is defined in Fig. 1. For these tests
$\alpha=45^{\circ}$. In addition, a finite-width correction factor must be
appended to the above expression, which then becomes

$$K = \frac{\sigma(\pi a)^{\frac{1}{2}}}{2}(1+k)f\left(\frac{a}{w}\right) . \tag{14.1}$$

If the critical value of the applied stress, obtained as
described above, is inserted into Eq. (14.1) K becomes the
plane-stress fracture toughness, K_c,

$$K_c = \frac{\sigma_c(\pi a)^{\frac{1}{2}}}{2} (1+k)f\left(\frac{a}{w}\right) . \tag{14.2}$$

Since the a/w ratio was identical for all specimens, the value
of the finite-width correction factor was the same for all tests.
Consequently the finite width correction factor had no influence
on the relative magnitudes and trend of the biaxial load effect.

Equation (14.2) shows the dependence of K_c on k as being
linear with the factor (1+k) increasing from one to two as
k is increased from zero to one. Therefore the K_c value
would be expected to approximately double over the range of
k values employed in these tests. The test results shown in
Fig. 45 are in very good agreement with this predicted trend,
and offer a further confirmation of the analytical portion
of this work.

SECTION 15

EFFECT OF BIAXIAL LOADS ON THE ANGLE
OF INITIAL CRACK EXTENSION

Another effect of load biaxiality on fracture behavior,
one which is directly measurable and can be compared with
the analytical predictions, is the influence of k on the angle
of initial crack extension. The calculations of this angle,
based on the maximum tensile stress criterion, are displayed
graphically in Fig. 19 for different orientations of the
crack (or starter slot). The fractured specimesn of all of
the test series were examined for comparison with the analyti-
cal predictions, and the results are presented in this section.

15.1 ANGLE OF INITIAL CRACK EXTENSION FOR THE ANGLE-CRACKED
SPECIMENS

The effect of applied load biaxiality on K_c for the two
series of tests on 7075-T6 aluminum in which the starter slot
was oriented at 45° was discussed in the previous section.
The broken specimens from these tests were examined to
aetermine the angle of initial crack propagation for compari-
son with the analytical predictions contained in Fig. 19.
As noted in Section 13, the material from which these speci-
mens were made exhibited a measurable amount of anisotropy.
It was anticipated therefore that this could have some in-
fluence on the direction of initial crack extension. In
much the same manner that the average of the two test results
at each biaxiality ratio minimized the effect of material

-96-

anisotropy on the K_c data shown in Fig. 45, the average of the two angles of initial crack extension for any k value should provide a result relatively free of the material anisotropy effects.

A good appreciation of the influence of material anisotorpy on the angle of initial crack extension can be obtained from Fig. 44. The analytical predications indicate that, for $\alpha=45^O$ and k=1.0, the crack angle should not deviate from the plane of the starter slot ($\theta_0=0^O$). Figure 44 shows, however, that the cracks propagated at an angle of approximately $\pm25^O$ from the starter slot toward the rolling direction. If the angles measured from the two tests are averaged, they approximately cancel each other leaving a net measured value of approximately $\theta_0=3^O$. This procedure was followed for the other three pairs of tests and the results of all eight tests are summarized in Table I. It is seen from this table that the agreement between the predicted and measured values of θ_0 is quite good, with the only significant deviation being for k=0.5.

15.2 ANGLE OF INITIAL CRACK EXTENSION FOR HORIZONTALLY
     SLOTTED 7075-T6 SPECIMENS

Additional comparison between the predicted and measured values of initial crack propagation can be obtained from the fracture test series discussed in Section 13. For these tests the biaxiality ratio was varied from zero to 1.8, with $\alpha=90^O$. Examination of the predicted values of θ_0 (for $\alpha=90^O$)

-97-

given in Fig. 19 shows that, at the higher positive values of k the predicted values of θ_0 begin to increase rapidly as k exceeds values of three, and approach values of 80° to 90° as k assumes values between five and nine. A greater accuracy of prediction is difficult because of the very high slopes (rates of change) of the curves at $\alpha=90^{\circ}$. About all that can be certain is that the expected angle of initial crack extension increases with increasing k.

A qualitative confirmation of the above statement can be seen in Fig. 45, which shows the effect of increasing k on the angle of initial crack extension for the 7075-T6 specimens. For these tests the starter slot was perpendicular to the rolling direction. It is seen in Fig. 45a ($k=0$) that the crack extended essentially parallel to the starter slot, while in Fig. 44b ($k=1.5$) the angle of initial crack extension had increased significantly. When k was further increased to 1.8, it is seen in Fig. 44c that the crack very quickly changed orientation to become more normal to the direction of maximum tensile stress.

15.3 ANGLE OF INITIAL CRACK EXTENSION FOR PLEXIGLASS SPECIMENS

Since the material anisotropy associated with the 7075-T6 tests has some effect on the angle of initial crack extension (especially for $\alpha=90^{\circ}$), the plexiglass specimens were also examined because they do not exhibit significant anisotropy, and because higher k values could be employed in the tests. A large number of tests were performed so that

many specimens were available for the purpose of examining the angle of initial crack extension. The results, however, for any given k value were quite consistent, consequently, only three of the typical results are presented in Fig. 46. The broken specimen from test B20 (k=0) is shown in Fig. 46a, where it is seen that the crack extended with only slight deviation from the plane of the starter slot. Fig.46b shows the broken test from test B17 (k=1.0), in which significant deviation from the starter slot is evident. For test B19 (k=2.0), Fig. 46c shows that the deviation from the plane of the starter slot is quite strong, as the crack attempts to align itself normal to the direction of maximum tensile stress. All of the plexiglass specimens exhibited similar tendencies and confirm the qualitative agreement with the predicted trend that was observed for the 7075-T6 specimens with initially horizontal crack orientation. Additional observations of the angle of initial crack extension have been made for PMMA by Leevers, Radon and Culver [42], who obtained results in generally good agreement with those presented here.

SECTION 16

BIAXIAL FATIGUE CRACK GROWTH RATE TESTS

Because of the importance of fatigue crack growth laws in determining the residual life of structures and the relative merits of many structural materials subjected to cyclic loading, one of the objectives of this research program was to examine the influence of biaxial loads on the fatigue crack growth rates. Most fundamental studies of fatigue crack growth under cyclic loading conditions [43] conclude that the size of the crack-tip plastic zone is a critical factor influencing the fatigue crack growth rates. Since the present study has shown that increasing k values lead to reduced crack-tip plastic zone sizes, it follows that higher k values should cause reduced fatigue crack growth rates.

Experimental data about the effect of load biaxiality on fatigue crack growth rates are currently quite limited and somewhat inconsistent in their assessment of biaxial effects. Most test results reported in the literature were performed at zero or positive $\overline{R}$ values ($\overline{R} = F_{min}/F_{max}$) although some exceptions have been reported. In tests conducted on a high strength aluminum alloy, RR58, Hopper and Miller [44] reported a decrease in fatigue crack growth rates as k increased from -1.0 to 1.0. Kibler and Roberts [35] observed the same qualitative trend for 6061-T4 and T6 aluminum alloys as k was increased from 0 to 0.33. Leevers,

Radon and Culver [45] reported fatigue crack growth rates in PMMA to be reduced by a factor of two to three as k increased from 0 to 2.0. For all of the test results just cited the biaxial loads were in-phase cyclic loads.

On the other hand, a variation of the static lateral load from k=0 to k=2.0 appeared to have little effect on the fatigue crack growth rates of the more ductile PVC (polyvinylchloride)[45]. Similarly, Liu, Allison, Dittmer and Yamane, observed negligible effects on the crack growth rates of 7075-T7351 and 2024-T351 aluminum alloys as k was varied from -1.5 to 1.75 [46], while Pook and Holmes found little lateral load effect on the growth rates of nickel alloy plates as k was varied from 0 to 2.0 [47]. Because of the lack of agreement between the results of these studies it was considered desirable to perform some experiments to provide additional data about the nature of biaxial effects.

16.1 BIAXIAL FATIGUE TESTING PROGRAM

In order to gain initial insight into the effect of biaxial cyclic loads on the fatigue crack growth rates, a preliminary testing program involving four specimens made from thin sheets of 2024-T3 aluminum was initiated. For these tests two specimens were tested with the starter slot parallel to the rolling direction (k=0 and 1.0) and two were tested with the starter slot perpendicular to the rolling direction (k=0 and 1.0). The specimens were made identical to those for the static tests and the loads were varied in

-101-

a sinusoidal manner, with both axis loaded in phase. The load ratio, $\bar{R}$, was approximately zero for all four tests. The test frequency was 12 Hz and, with the exception of the first test, the crack growth measurements were made while the test was running. An arbitrary initial cyclic load level was imposed until the fatigue crack initiated from the starter slot and the load level was then reduced until a reasonable crack growth rate was obtained. This load level was then maintained until the specimen fractured. The crack size was recorded as a function of the number of cycles and calculations were then made for the crack growth rate, $\frac{da}{dN}$, as a function of the applied stress intensity range, ΔK.

The experimental results of fatigue crack growth rate, plotted on logarithmic scale, versus ΔK is given in Figs. 48-51, in which each figure represents the test results for one specimen. Thus Figs. 48 and 49 represent the data for the two tests on 2024-T3 with the starter slot perpendicular to the rolling direction and k equal to 0 and 1.0 respectively. It can be seen that there is a significant biaxial effect on the fatigue crack growth rates, but determination of the magnitude of the effect is difficult because of the scatter in the data. The scatter was apparently due primarily to the lack of experience in collecting fatigue crack growth data on these biaxial specimens, since it was considerably re- duced in subsequent tests.

In order to obtain a better appreciation for the extent of the biaxial effect, a few specific comparisons will also

-102-

be presented. In both pairs of tests, increasing the k value from zero to 1.0 caused a significant reduction in the fatigue crack growth rates. For example, for the tests with the starter slot parallel to the rolling direction, the crack growth rates corresponding to the same value of ΔK were approximately 1.8×10^{-5} in/cycle for k=0 and 1.4×10^{-5} in/cycle for k=1.0. From these results it is seen that the decrease in fatigue crack growth rates was approximately 25 percent for an increase in k from zero to 1.0. The other pair of tests with the starter slot perpendicular to the rolling direction exhibited a greater dependence of the fatigue crack growth rates on k. For example the fatigue crack growth rates corresponding to a fixed ΔK were approximately 4.2×10^{-5} in/cycle for k=0 and 2.0×10^{-5} in/cycle for k=1.0, which represents a change of 100 percent in the fatigue crack growth rates. However, the procedure for taking crack growth measurements for the k=0 test was different from the k=1.0 test in that the test system was stopped while the measurements were made. For all subsequent tests the crack growth measurements were made while the test was running. A number of subsequent tests were then performed for the purpose of obtaining additional data about the biaxial effects.

These data are presented in a different way in Figs. 52 and 53, in which $\frac{da}{dN}$ is still represented on the ordinate (vertical axis) but the half-crack length, a, is plotted on the abscissa. The data shown in this manner for k=0 and 1.0 illustrate quite clearly the biaxial effect. The number

-103-

of data points have been reduced in these figures by averaging several adjacent $\frac{da}{dN}$ values, and it is seen that the scatter is reduced markedly.

The results of these four tests are also shown with $\frac{da}{dN}$ plotted linearly on the ordinate and the half-crack length plotted on the abscissa. The results are given in Figs. 54 and 55, and again exhibit the significant biaxial influence already indicated. These results also show very effectively the acceleration in fatigue crack growth rates that is characteristic of these tests. Since these results could be easily misinterpreted if different initial crack sizes or different loads were employed in the testing program, results similar to Figs. 54 and 55 are not presented for the subsequent tests.

16.2 BIAXIAL FATIGUE TESTS ON 7075-T6 ALUMINUM

The next test series that was performed was planned to provide fatigue crack growth rate data over a larger range of k values. Thus, four additional tests were performed on 7075-T6 alumunim sheets, 0.063 in. thick, in which the starter slots were parallel to the rolling direction. The starter slots were also considerably shorter than for the prior tests so that more data could be collected. Also for these tests, after an initial set of data were taken at low crack growth rates, the load was increased in several steps so that a larger range of ΔK values could be examined. The cyclic frequency for these tests was decreased from 15 to

-104-

10 Hz as the test progressed and the crack growth rates increased. The $\bar{R}$ value was 0.1 for all four tests.

The effects of load biaxiality on the fatigue crack growth rates, $\frac{da}{dN}$, as a function of ΔK for the four biaxialities, k=0, 0.5, 1.0 and 1.5 are shown in Figs. 56-59. It is seen from these figures that the data points exhibited reasonable scatter and that a biaxial effect is clearly evident. As a measure of the effect of load biaxiality, the fatigue crack growth rates for all four tests at two selected values of ΔK are given in Table II. The results at both values of ΔK exhibited a definite biaxial effect, although the primary effect seems to have occurred between k=0 and 0.5. Because of the scatter that is usually associated with fatigue crack growth rate testing, the primary conclusion from these data is that, although there is a clear biaxial effect, the trend in the variation of $\frac{da}{dN}$ with k will need additional testing before it is clearly understood. The results for the first three tests, k=0, 0.5 and 1.0 have been combined into one plot as shown in Fig. 60, where ΔK has also been plotted on a logarithmic scale. The test for k=1.5 was not included because of the very limited amount of data that had been collected before the specimen failed by breaking one of the tangs parallel to the starter slot. The very strong biaxial effect is more evident in this figure, although the close agreement between the results for k=0.5 and 1.0 is difficult to interpret.

A different presentation of these results is also given in Fig. 61. In this figure, the half-crack length, a, is

plotted on the ordinate using a linear scale and ΔK is
plotted linearly on the abscissa. This presentation also
illustrates clearly the magnitude of the biaxial effect on
the fatigue crack growth rates.

16.3 BIAXIAL FATIGUE TESTS ON 2024-T3 ALUMINUM

Since it was considered likely that accurate fatigue
crack growth rates are more difficult to obtain in more
brittle materials, three additional tests were preformed on
2024T-3 aluminum with biaxiality ratios of 0, 0.5 and 1.0.
The starter slots were parallel to the rolling direction and
$\bar{R}=0.1$ for all three tests. The same general procedures estab-
lished in the previous tests were followed for these tests
also. The results of the crack growth rates as a function
of ΔK for the three k values are given in Figs. 62-64, where
these data have been plotted on semi-log paper. The same
data were also plotted in Figs. 65-67 on a log-log plot
which, as was seen in the 7075-T6 results, tends to make the
biaxial effect less apparent. Again for direct comparison
purposes, the values of $\frac{da}{dN}$ as a function of k are given in
the Table III. The ΔK values of 10 and 40 ksi $\sqrt{in}$ provided a
large range of values for additional comparison purposes.
It is seen in these results that a significant biaxial effect
exists, although the magnitude of the effect is approximately
30 percent, rather than a factor of 10 as exhibited for the
7075-T6 data. Also the limited differences between the values
for k=0.5 and 1.0 render interpretation difficult. The

-106-

closeness of the k=0.5 and 1.0 values for both alloys is a
matter that can only be a subject for speculation with the
limited data that are available.

PART III. CONCLUSIONS

SECTION 17

SUMMARY AND CONCLUSIONS

The plane problem of linear elasto-statics is a boundary
value problem for the solution of the biharmonic partial
differential equation that must, in addition, satisfy given
conditions of stress or displacement that are prescribed on
the boundaries of the body. This problem can be reformulated
into one of finding a pair of analytic functions $\Phi(z)$ and $\Omega(z)$
of the complex variable, z, that must satisfy the same pre-
scribed conditions of boundary stress or displacement. Once
these functions have been determined, the problem may be
considered to be solved because all of the quantities that
define the mechanical state of the elastic body are derivable
from Φ and Ω.

For the boundary value problem represented by the biaxially
loaded infinite sheet with an inclined centrally located crack,
[cf. Fig. 1], the solution functions Φ and Ω are given by Eqs.
(2.8) and (2.9). For the horizontally oriented crack they
are given by Eq. (2.11), while for the pair of collinear
cracks, by Eqs. (2.35) and (2.37). In all of these expressions
for Φ and Ω, both of the boundary load parameters, σ and k,
appear, as they must, if Φ and Ω are to represent solutions of
a boundary value problem. Consequently it follows directly
from Eqs. (2.1) and (2.2) that the stress, displacement, strain,
maximum shear stress and the strain energy density at every

point of the body must, likewise, show dependency on the biaxial load parameter, k. The same must also be true of integrals of these quantities, yielding the elastic strain energy and the elastic potential energy of the entire body. When the elastic strain energy of the body is differentiated with respect to the crack size, the resulting derivative representing the change of the elastic strain energy with increasing crack size, must also exhibit a dependence on the horizontal load parameter, k, when the body is biaxially loaded. Since every quantity defining the mechanical state of the cracked body is thus shown to be influenced by the presence of the horizontal load, the conclusion that the fracture behavior of the body must also be so influenced is inescapable. These conclusions, which are here drawn from general considerations only, are clearly illustrated by the extensive analytical results appearing in the body of the report, and by the experimental data that is presented, which quantitatively and qualitatively confirm the findings of the analysis.

Stress and Displacement Near the Crack-Tip

The expressions for the elastic stress and displacement in the immediate vicinity of the crack tip when properly derived, will show a dependence on the horizontal load parameter, k. Examination of the series expansions of the solution functions Φ, Ω (and also for ϕ, ω) reveal that a two-term approximation of the infinite series representations

is necessary if proper account of the presence of the horizontal load is to be reflected in the crack-tip stress and displacement approximations, [e.g., Eqs. (2.17), (2.19), (2.21)-(2.23) for the inclined crack, Eqs. (2.24)-(2.26) for the horizontal crack, and Eqs. (2.41)-(2.47) for the pair of collinear cracks].

When the crack is horizontal, the second term of the series expansion of Φ is the only term of the expansion that includes the parameter k. Consequently, the usual one-term (singular) approximation for the crack-tip stress, and also for the displacement, is incapable of incorporating the presence of the horizontal load, $k\sigma$, in a biaxial load situation for this crack geometry.

Maximum Shear Stress Near The Crack Tip

The maximum shear stress about the crack tip is shown to be strongly influenced by the presence of load applied parallel to the crack [c.f. Eqs. (3.1),(3.8)]. The predicted pattern of variation of the maximum shear stress contours with load biaxiality, Fig. 11, is confirmed by the photoelastic maximum shear stress isochromatics that were obtained for the biaxial load range $0 \leq k \leq 1.0$, shown by Fig. 37.

Because of the relation between maximum shear stress and plastic yield, the plastic yield region about the crack tip should show a qualitatively similar pattern of variation with load biaxiality to that shown by Fig. 11, that is, as the horizontal load varies from tension to compression the extent

of the plastic yield region about the crack tip should in-
crease. (This predicted effect has been observed from the
finite-element (NASTRĀN) elastic-plastic calculations con-
ducted by Liu and Dittmer [52] for a biaxially loaded
cruciform shaped specimen.)

Angle of Initial Crack Extension

Utilizing the maximum tensile stress criterion, the
influence of load biaxiality on the angle of initial crack
extension was calculated for different orientations of the
crack, with the results summarized in Fig. 19. Test results
for cracks initially horizontal are shown in Fig. 46. These
photographs show clearly the pattern of turning of the angle
of initial crack extension with increasing horizontal tensile
load, in qualitative agreement with the predicted trend shown
in Fig. 19 at $\alpha = \pi/2$. For the crack inclined at $\alpha = 45^O$, c.f.
Fig. 44, the measured angles of initial crack extension are in
generally good agreement with the predicted values, summarized
in Table I.

Fracture Load and Fracture Toughness

A calculation of the theoretical fracture stress, σ_c,
based upon Griffith's crack instability hypothesis, shows
the critical stress to be dependent on both the load biaxiality,
and the Poisson ratio of the material, c.f. Eqs. (9.2) and
(9.3), and Figures 27, 28 and 29. In the case of plane stress,
for materials with Poisson ratio less than one-third, the

breaking stress increases with increasing horizontal tensile load. However for values of Poisson ratio greater than one-third, this trend is reversed. A similar patter of variation holds for plane strain.

The results of fracture tests performed on 7075-T6 aluminum with Poisson ratio about 0.30, and plexiglass with Poisson ratio about 0.40-0.45, are shown in Figures 38 thru 40. Additional fracture test data on PMMA specimens (similar to plexiglass) that were obtained elsewhere are shown in Fig. 41. These test results confirm, qualitatively, the predicted influence of the Poisson ratio on the pattern of variation of the critical stress with variation of the horizontal load.

Plane stress fracture toughness tests for determination of K_c values, on 7075-T6 aluminum sheets with the crack inclined at 45° and the horizontal load parameter varying between $0 \leq k \leq 1.0$, show a pronounced dependence on the load biaxiality. The predicted variation of K_c with k, given by Eq. (14.2), which shows K_c as approximately doubling in value in a linear manner as k varies from zero to one, is in excellent agreement with the experimental data given in Fig. 45.

Fatigue Crack Growth Rates

The reduction of the rate of fatigue crack growth with increase of the horizontal load, which is implied by the decrease in size of the crack-tip plastic zone for such biaxial load variation, is demonstrated by the experimental data given in Figures 48 through 67, and in Tables II and III. These

results are consistent with the generally accepted view that
the size or extent of the plastic yield region at the crack
tip is a major factor in influencing fatigue crack growth
rates. The reduction of the crack growth rate as k was varied
from 0.0 to 0.5 was observed to be much greater than the re-
duction in rate that accompanied the change of k from 0.5 to
1.0. At this time no explanation for this surprising differ-
ence can be offered.

SECTION 18

RECOMMENDATIONS FOR FURTHER RESEARCH

Although a considerable amount of research effort has by
now been directed toward examining the effects of biaxial
applied loads on the fracture characteristics of materials,
many facets of this effect have yet to be clarified and
fully understood. A number of suggestions for further research
in this area which appear to be important are indicated below.

1. A finite-element analysis that would take this particu-
    lar specimen geometry into consideration should be per-
    formed. This analysis would serve to provide more
    accurate correlations between the anlytical and experi-
    mental results. Such an analysis should also lead to
    further clarification of some of the observed trends in
    some of the experimental results, such as the interactions
    between Poisson's ratio and load biaxiality on the
    fracture strength.

2. The finite-element analysis should be extended to include
    elastic-plastic material behavior and subcritical crack
    growth. An analysis of this kind should provide a
    greater appreciation of biaxial load effects on crack-
    tip plasticity, and its consequent effect on the fracture
    characteristics. The subcritical crack growth capability
    of the finite element analysis would also serve to pro-
    vide more information for comparison with the experi-
    mentally-observed angles of initial crack extension.

3. The interaction between Poisson's ratio and load biaxility and their influence on the fracture strength should be examined further. The reversal of trend of the fracture load, σ_c, versus k, observed for aluminum and plexiglass needs to be examined in more detail under both plane stress and plane strain conditions.

4. Fracture tests should be performed on specimens containing two collinear cracks since no tests of this type have been performed. It would be desirable to perform tests with horizontal starter slots as well as with the starter slots at an angle.

5. More fatigue crack growth tests need to be conducted to examine in more detail the biaxial effects on $\frac{da}{dN}$ in the range $0<k<1.0$, since nearly all of the biaxial effect that was observed in the GWU tests occurred as k was increased from zero to 0.5. These test results should also be examined and used, in conjunction with existing data, to formulate modifications to existing semi-empirical fatigue crack growth rate laws that would explicitly include k as a factor. At present it appears that the dependence on k of $\frac{da}{dN}$ would be highly nonlinear.

6. Additional angle-cracked tests should be performed so that crack orientation angles other than $\alpha = 45^{\circ}$ and 90° could be studied. These results would have considerable practical significance since actual cracks in biaxially-loaded structures (such as pressure vessels, etc) will

not normally be aligned with the principal loading directions.

7. A wider range of structural materials, including titanium and steel alloys, should be tested in order to determine quantitatively the relevance of the biaxial effect on these structurally important materials. Such tests could provide for greater variations in important variables such as crack-tip plasticity, subcritical crack growth and plane stress versus plane strain conditions, within the context of a biaxial loading situation.

REFERENCES

1. N. Muskhelishvili, Some Basic Problems of the Mathema-
   tical Theory of Elasticity. Noordhoff, Groningen, 1963.

2. J. Eftis and N. Subramonian, The Inclined Crack Under
   Biaxial Load. Engng. Fracture Mechanics. Vol. 10, 1978,
   pp. 43-67.

3. J. Eftis, N. Subramonian and H. Liebowitz, Crack Border
   Stress and Displacement Equations Revisited. Engng.
   Fracture Mechanics. Vol. 9, 1977, pp. 189-210.

4. P.C. Paris and G.C. Sih, Stress Analysis of Cracks. ASTM
   STP 381, 1965, pp. 30-81.

5. J. Eftis, N. Subramonian and H. Liebowitz, Biaxial Load
   Effects On The Crack Border Elastic Strain Energy And
   Strain Energy Rate. Engng. Fracture Mechanics. Vol. 9,
   1977, pp. 753-764.

6. G.C. Sih, A Special Theory Of Crack Propagation. In
   Mechanics of Fracture. (Ed. G.C. Sih). Vol. I, Noordhoff,
   Leyden, 1973.

7. J. Eftis, Influence Of Load Biaxiality On The Fracture
   Characteristics Of Two Collinear Cracks. (Submitted
   for publication.)

8. J. Eftis and N. Subramonian, The Cracked Shear Panel.
   AIAA Jornal, Vol. 18, No. 3, 1980, pp. 324-332.

9. J.G. Williams and P.D. Ewing, Fracture Under Complex
   Stress-The Angled Crack Problem. Journ. Fracture
   Mechanics. Vol. 8, 1972, pp. 441-445.

10. I. Finnie and A. Saith, A Note On The Angled Crack
    Problem And The Directional Stability Of Cracks. Journ.
    Fracture Mechanics. Vol. 9, 1973, pp. 484-486.

11. A.F. Liu, Crack Growth And Failure Of Aluminum Plate
    Under In-Plane Shear. AIAA Journal, Vol. 12, 1974,
    pp. 180-185.

12. A.A. Griffith, The Phenomena Of Rupture And Flow In
    Solids. Phil. Trans., Royal Society London, Vol. 221,
    1921, pp. 163-198.

13. A.A. Griffith, The Theory Of Rupture. Proc. 1st Int'l
    Congress Of Applied Mechanics, Delft. 1924, pp. 55-63.

REFERENCES (con't)

14. I.S. Sokolnikoff, Mathematical Theory Of Elasticity.
    McGraw Hill, New York, 1956.

15. L.L. Pennisi, Elements of Complex Variables. Holt,
    Rinehart and Winston, New York, 1963.

16. D.V. Widder, Advanced Calculus. Prentice-Hall, Englewood
    Cliffs, New Jersey, 1961.

17. R.G. Bartle, The Elements of Real Analysis. J. Wiley,
    New York, 1964.

18. G.R. Irwin, Analysis of Stresses and Strains Near the
    End of a Crack Traversing a Plate. Trans. ASME, Journal
    Applied Mechanics, 79, 1957, pp. 361-364.

19. J. Eftis and H. Liebowitz, On The Modified Westergaard
    Equations For Certain Plane Crack Problems. Journ.
    Fracture Mech., 8, 1972, pp. 383-391.

20. J.L. Swedlow, On Griffith's Theory Of Fracture. Journ.
    Fracture Mechanics, 1, 1965, pp. 210-216.

21. K.Z. Wolf, Zur Bruch Theories von A. Griffith. Zietschrift
    für Angewandte Mathematik und Mechanik, Vol. 3, 2, 1923,
    pp. 107-112.

22. A.K. Head, The Growth Of Fatigue Cracks. Phil. Mag.,
    Vol. 44, 1953, p. 925.

23. N.E. Frost and D.S. Dugdale, The Propagation Of Fatigue
    Cracks in Sheet Specimens. Journ. Mech. Physics Solids,
    1958, p. 52.

24. H.W. Liu, Crack Propagation in Thin Metallic Sheet Under
    Repeated Loading. Journ. Basic Engr., ASME, Series D,
    Vol. 83, 1961, p. 23.

25. P.C. Paris and F. Erdogan, A Critical Analysis of Crack
    Propagation Laws, Journ. Basic Engr., ASME, Series D,
    Vol. 85, 1963, p. 528.

26. F. Erdogan, Crack Propagation Theories. Chapt. 5, Vol.
    II, Fracture, Ed. H. Liebowitz, Academic Press, New York,
    1968, p. 497.

27. J. Schijve, Four Lectures On Fatigue Crack Growth. Engng.
    Fracture Mechanics, Vol. 11, 1979, pp. 167-221.

REFERENCES (con't)

28. S.J. Maddox, The Effect Of Mean Stress On Fatigue Crack
    Propagation. A Literature Review. Journ. Fracture
    Mechanics, Vol. 11, No. 3, 1975, pp. 389-408.

29. R.G. Forman, V.E. Kearney and R.M. Engle, Numerical
    Analysis Of Crack Propagation In Cyclic-Loaded Structures.
    Journ. Basic Engng, Trans. ASME D, 89, 1967, p. 459.

30. A. Hartmann and J. Schijve, The Effects of Environment
    And Load Frequency On The Crack Propagation Law For
    Macro-Fatigue Crack Growth In Aluminum Alloys. Engng
    Fracture Mechanics, Vol. 1, 1970, pp. 615-531.

31. O. Lomacky and H. Vanderveld, Critical Review Of Fracture
    And Fatigue Analysis. NSRDC Report 3655, Washington, DC,
    March 1972.

32. J.C. Radon, P.S. Leevers and L.E. Culver, A Simple Test-
    ing Technique for Fracture Under Biaxial Stress.
    Experimental Mechanics, Vol. 17, 1977, pp. 228-232.

33. L.P. Pook and R. Holmes, Biaxial Fatigue Crack Growth
    Tests. Presented at I. Conf. on Fatigue Testing and
    Design, London, April, 1976.

34. C.D. Hopper and K.J. Miller, Fatigue Crack Propagation
    in Biaxial Stress Fields. J. Strain Analysis, Vol. 12,
    1977, pp. 23-28.

35. J.J. Kibler and R. Roberts, The Effect of Biaxial
    Stresses on Fatigue and Fracture. J. Engng. Industry,
    Transactions of ASME, 1970, pp. 727-734.

36. A.F. Liu and D.F. Dittmer, Effect of Multiaxial Loading
    on Crack Growth. AFFDL-TR-78-175, Vol. 1, 1978.

37. I.M. Daniel, Behavior of Graphite/Epoxy Plates with
    Holes Under Biaxial Loading. Experimental Mechanics,
    Vol. 20, 1980, pp. 1-8.

38. A.F. Liu, D.F. Dittmer and J.R. Yamani, Effect of
    Multiaxial Loading on Crack Growth, Interim Report No.
    3, Contract F33615-76-C-3121, Wright-Patterson Air
    Force Base, Ohio.

39. S.G. Sampath, D. Brock, and S.H. Smith, Specimens for
    Fatigue-Crack-Propagation Tests Under Biaxial Loading.
    Unpublished report.

REFERENCES (con't)

40. P.S. Leevers, J.C. Radon, and L.E. Culver, Crack Growth
    in Plastic Panels Under Biaxial Stress. Polymer, Vol.
    17, 1976, pp. 627-632.

41. J.C. Radon, and P.S. Leevers, Fracture Toughness of
    PMMA Under Biaxial Stress. Fracture 1977, Vol. 3, pp.
    1113-1118, ICF4, Waterloo, Canada.

42. P.S. Leevers, J.C. Radon and L.E. Culver, Fracture
    Trajectories in a Biaxially Stressed Plate. J. Mech.
    Phys. Solids, Vol. 24, 1976, pp. 381-395.

43. N.J.I. Adams, Some Comments on The Effect of Biaxial
    Stress on Fatigue Crack Growth and Fracture. Engng.
    Fracture Mechanics, Vol. 5, 1973, pp. 983-991.

44. C.D. Hopper and K.J. Miller, Fatigue Crack Propagation
    in Biaxial Stress Fields. J. Strain Analysis, Vol. 12,
    1977, pp. 23-28.

45. P.S. Leevers, L.E. Culver and J.C. Radon, Fatigue Crack
    Growth in PMMA and Rigid PVC Under Biaxial Stress. Engng.
    Fracture Mechanics, Vol. 11, 1979, pp. 487-498.

46. A.F. Liu, J.E. Allison, D.F. Dittmer and J.R. Yamane,
    Effect of Biaxial Stresses on Crack Growth. Report to
    Air Force Flight Dynamics Laboratory, Wright-Patterson
    AFB, Dayton, 1978.

47. L.P. Pook and R. Holmes, Biaxial Fatigue Crack Growth
    Rates. Proc. Conf. Fatigue Testing and Design, London,
    1976.

48. J. Eftis and D.L. Jones, Influence of Load Biaxiality
    on The Fracture Load of Center Cracked Sheets. (Submitted
    for publication).

49. G.R. Irwin, Analysis of Stresses And Strains Near The End
    of a Crack Traversing a Plate. Trans. ASME, Journ. Applied
    Mech., 79, 1957, pp. 361-364.

50. G.R. Irwin, Fracture Mechanics. In Structural Mechanics,
    Eds. J.N. Goodier and N.J. Hoff, Pergamon Press, New York,
    1960.

51. H.M. Westergaard, Bearing Pressures and Cracks, Trans.
    ASME, Journ. Applied Mech., 6, 1939.

52. A.F. Liu and D.F. Dittmer, Effect of Multiaxial Loading on
    Crack Growth, Vol. 1, Final Report, AFFDL-TR-78-175, Wright-
    Patterson Air Force Base, Dayton, 1978.

TABLE I   Comparison of Predicted and Measured Values for
           the Angle of Initial Crack Extension for Angle-
           Cracked Specimens

BIAXIALITY RATIO	θ_0(predicted)[1] (degrees)	θ_0(measured)[2] (degrees)
k = 0	-52	-48
k = 0.25	-46	-44
k = 0.5	-41	-27
k = 1.0	- 0	- 3

1. Determined from Fig. 19 for $\alpha=45^o$. Estimated accuracy
    ±2 degrees except for k=0.25, which was obtained by
    interpolation.

2. Determined by averaging the measured values of each
    pair of specimens having the same values of k. Estimated
    accuracy ±3 degrees.

TABLE II   Effect of Biaxial Loads on the Fatigue Crack
Growth Rates of 7075-T6 Aluminum

Biaxiality Ratio	$\frac{da}{dN}$(in/cycle)	
	$\Delta K = 7\text{ksi}\sqrt{\text{in}}$	$\Delta K = 10\text{ksi}\sqrt{\text{in}}$
k = 0	$3\text{x}10^{-5}$	$9\text{x}10^{-5}$
k = 0.5	$3\text{x}10^{-6}$	$6.5\text{x}10^{-6}$
k = 1.0	$3\text{x}10^{-6}$	$9\text{x}10^{-6}$
k = 1.5	$3.5\text{x}10^{-6}$	$3\text{x}10^{-5}$

TABLE III   Effect of Biaxial Loads on the Fatigue Crack
Growth Rates fo 2024-T3 Aluminum

Biaxiality Ratio	$\frac{da}{dN}$(in/cycle)	
	$\Delta K = 10ksi\sqrt{in}$	$\Delta K = 40ksi\sqrt{in}$
k = 0	1.9×10^{-6}	1.3×10^{-4}
k = 0.5	1.5×10^{-6}	1.0×10^{-4}
k = 1.0	1.4×10^{-6}	1.1×10^{-4}
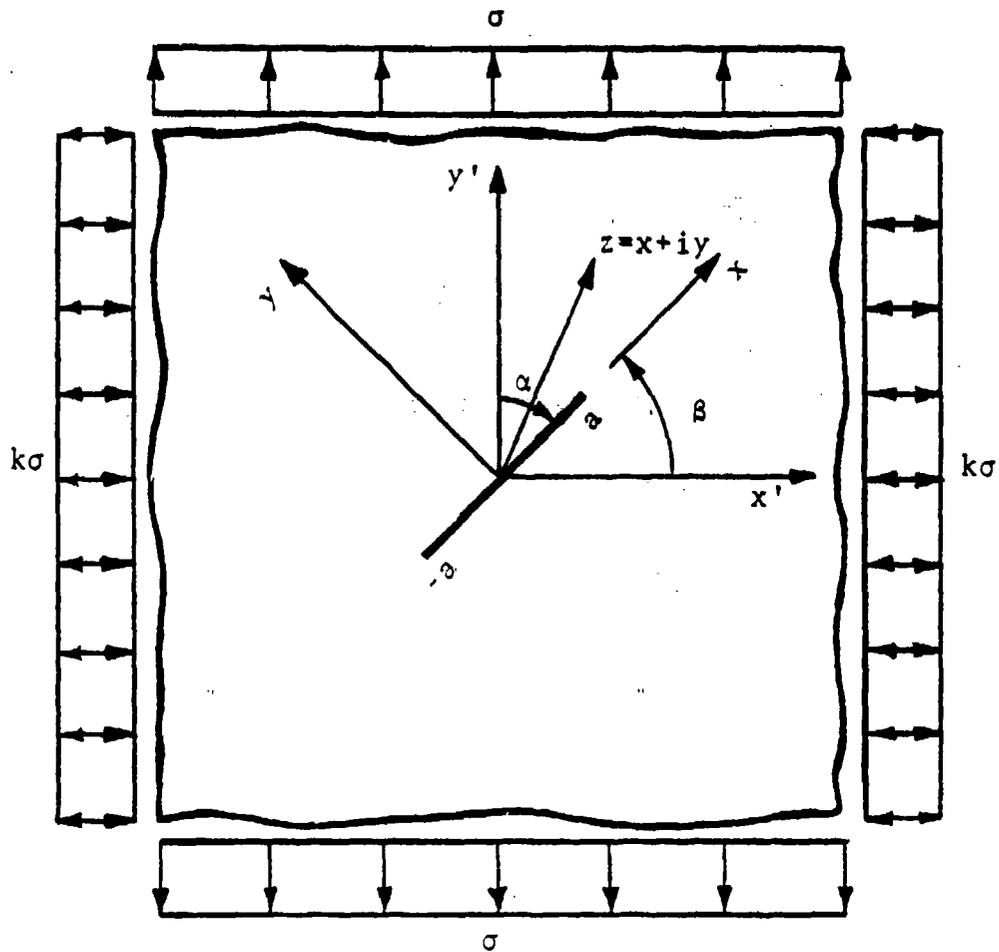
Fig. 1. Inclined interior crack geometry.
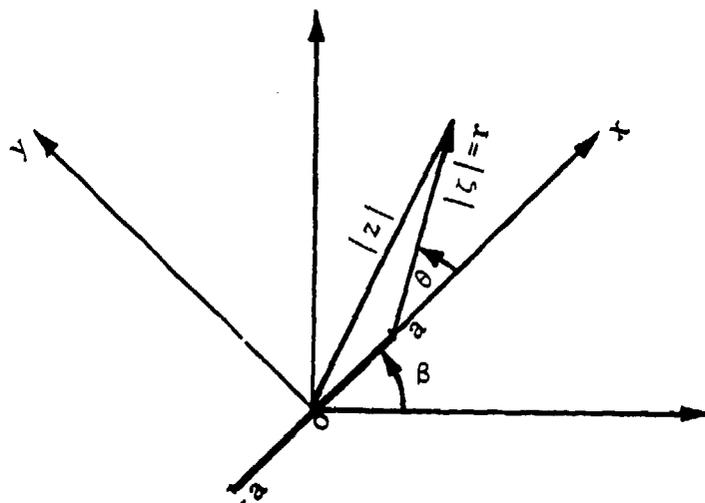
Fig. 2. Polar coordinate system at the crack tip.
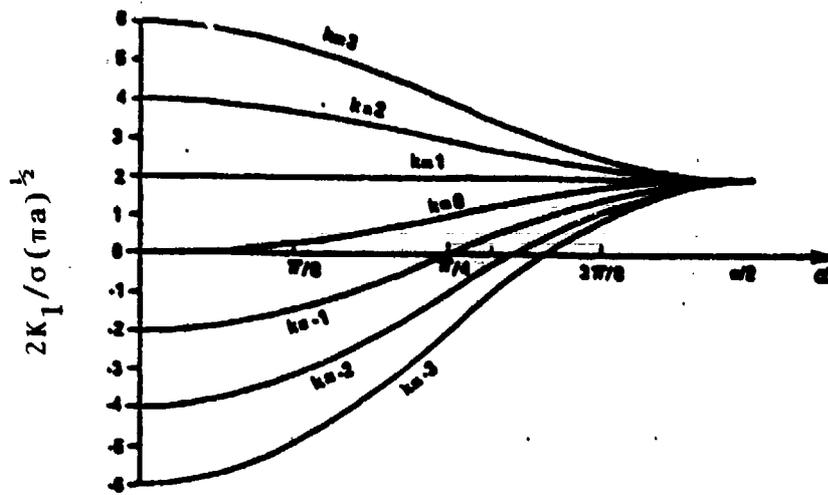
Fig. 3. Stress intensity factor K_1 for the inclined crack geometry.
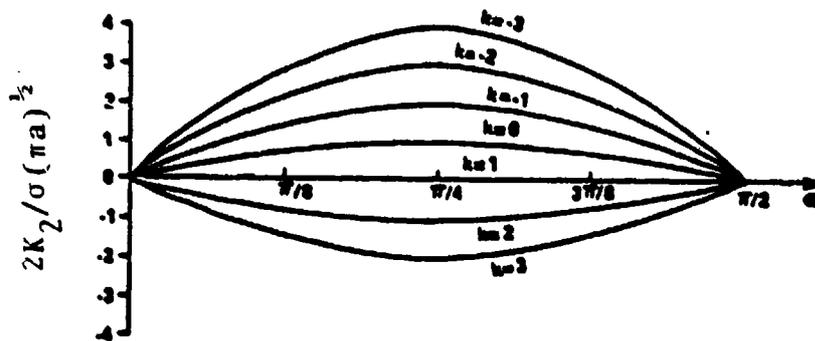
Fig. 4. Stress intensity factor K_2 for the inclined crack geometry.
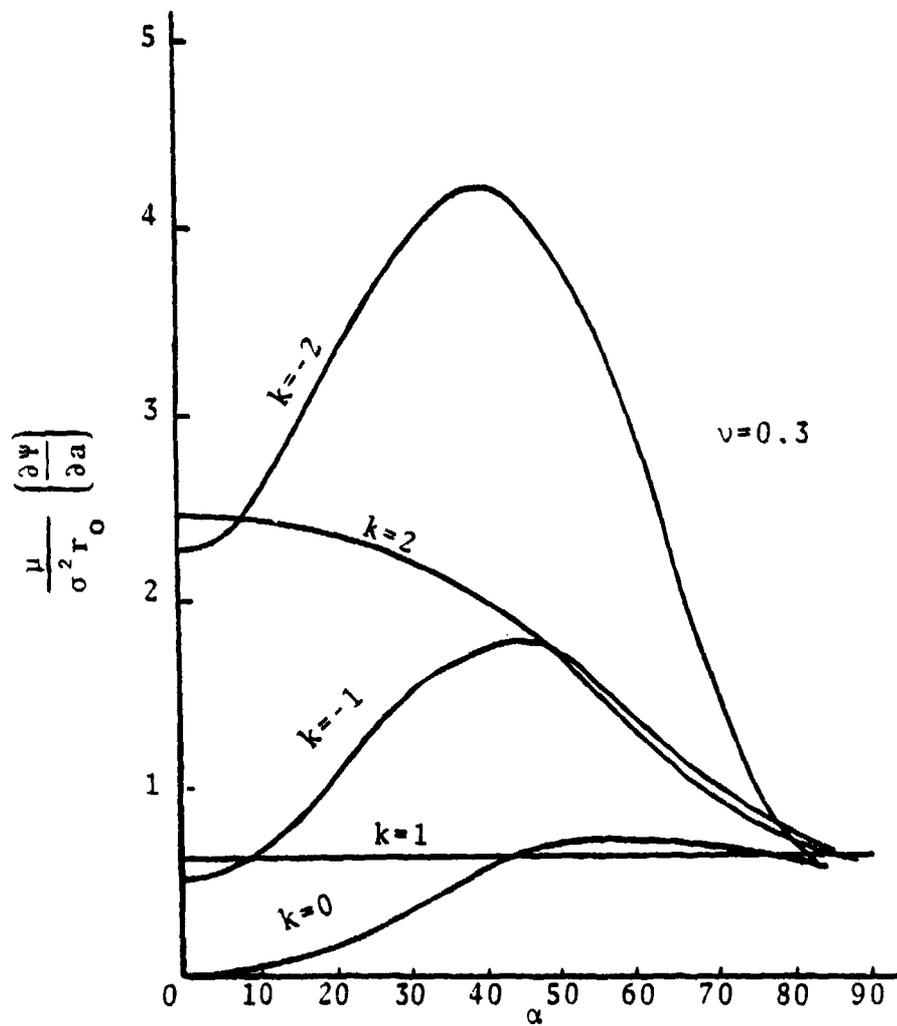
Fig. 5. Local elastic strain energy rate.
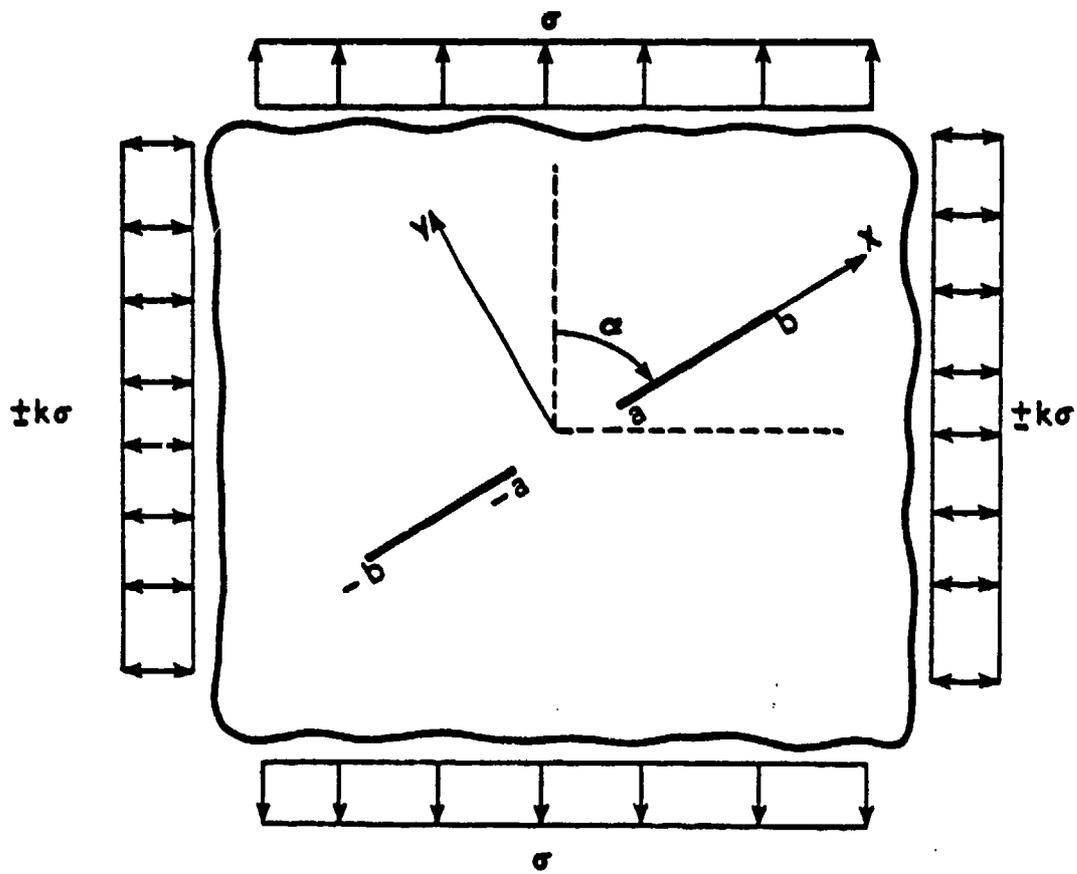
Fig. 6. Double interior crack geometry.
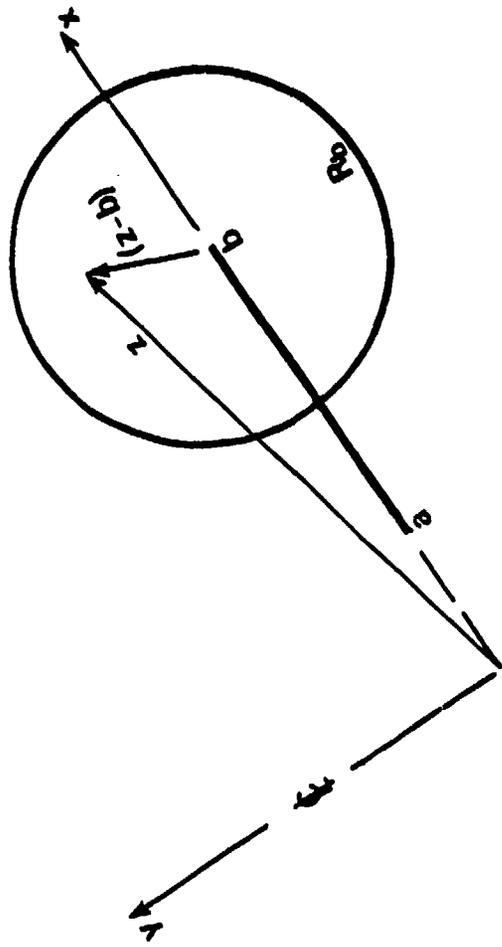
Fig. 7. Region R_b enclosing the end of the cut at $z = b$.
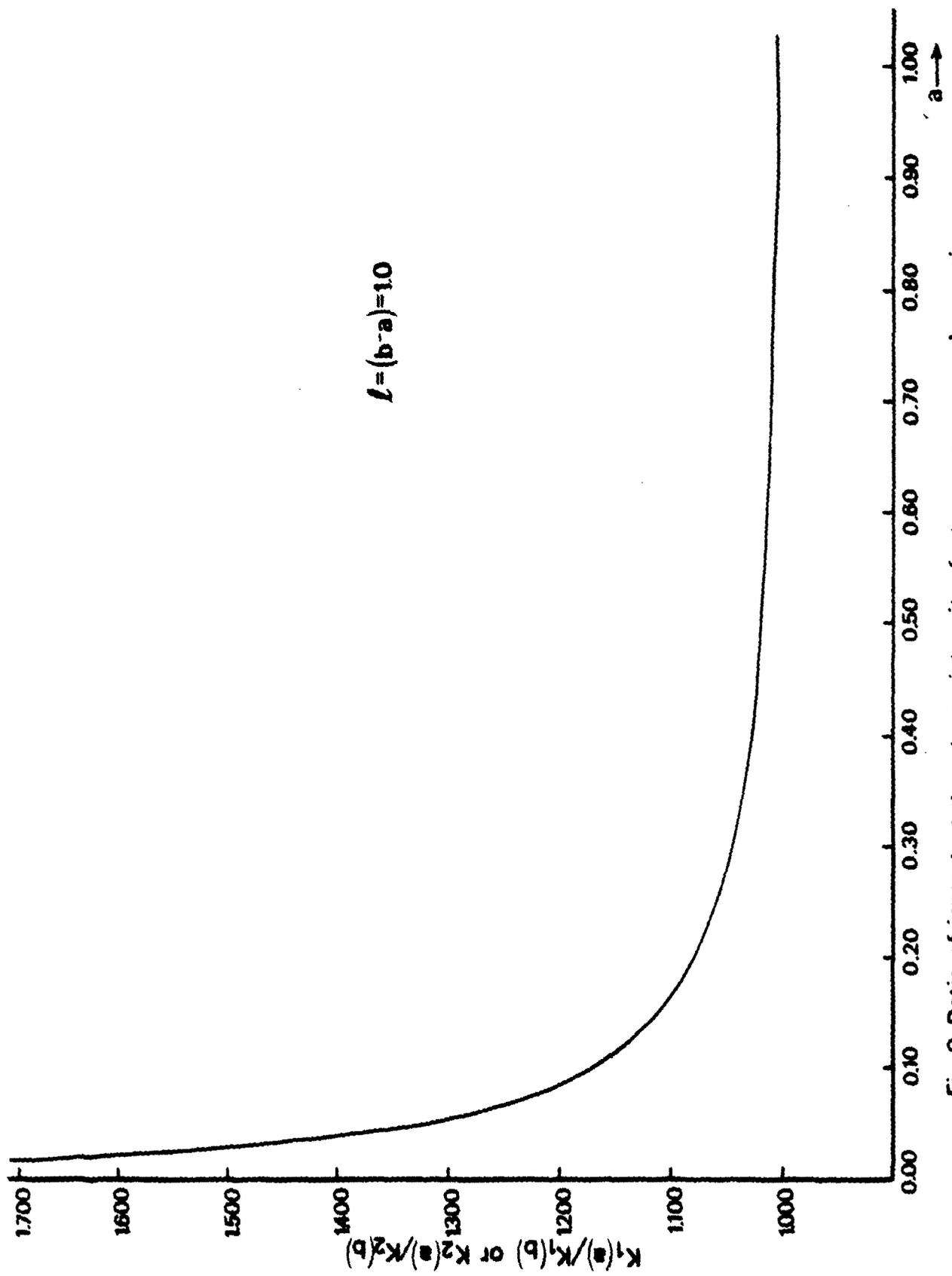
Fig. 8. Ratio of inner to outer stress intensity factors versus crack spacing.

$\ell = (b-a) = 1.0$

$K_1(a)/K_1(b)$ or $K_2(a)/K_2(b)$

$a \longrightarrow$
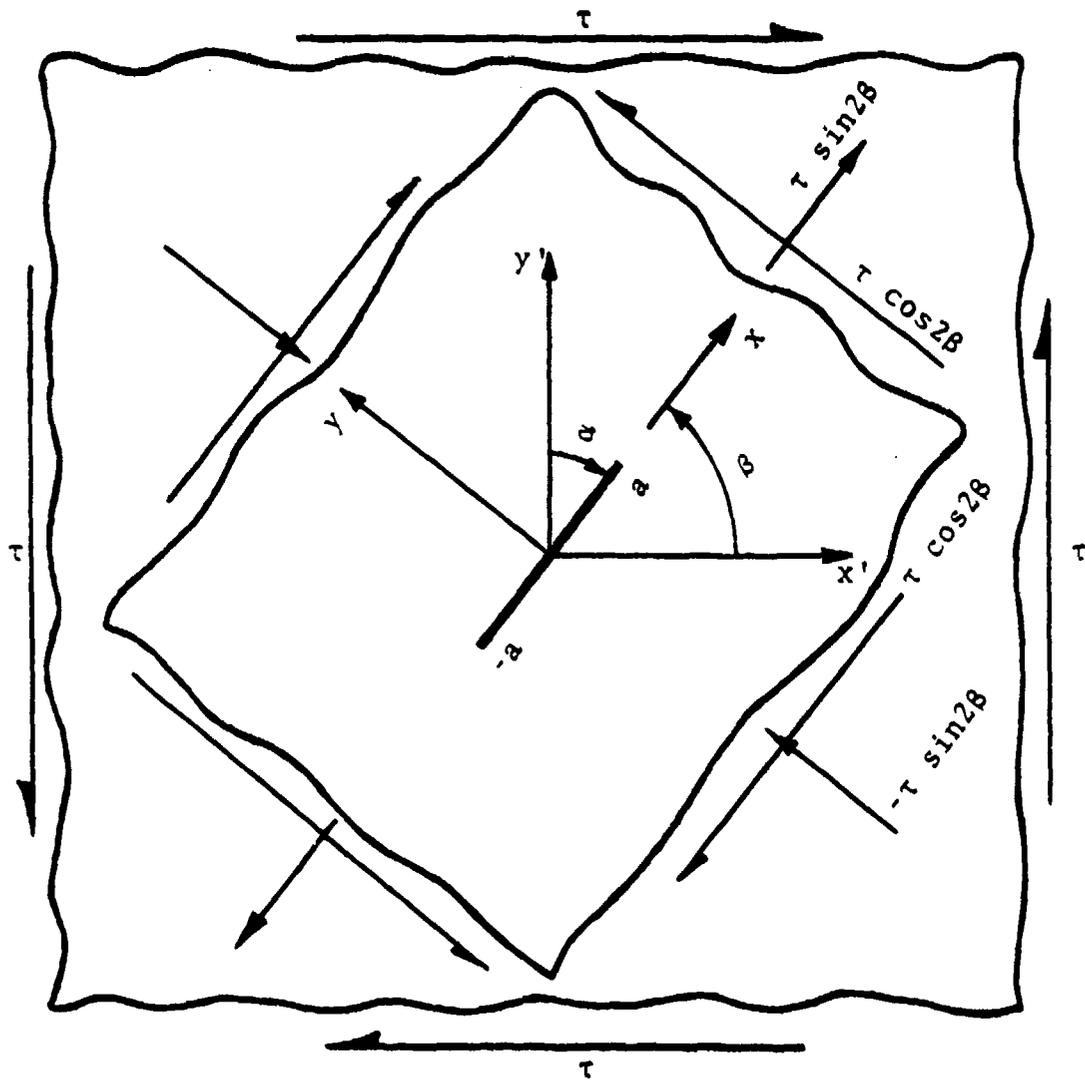
Fig. 9. Cracked shear panel.
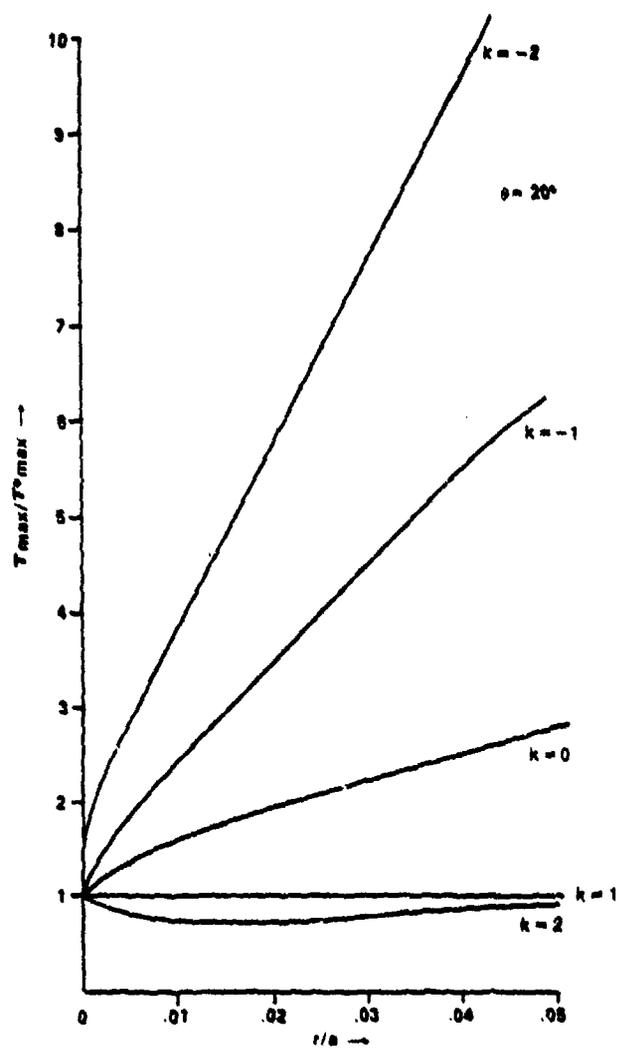
Fig. 10. Error in maximum shear stress calculation, horizontally oriented crack.
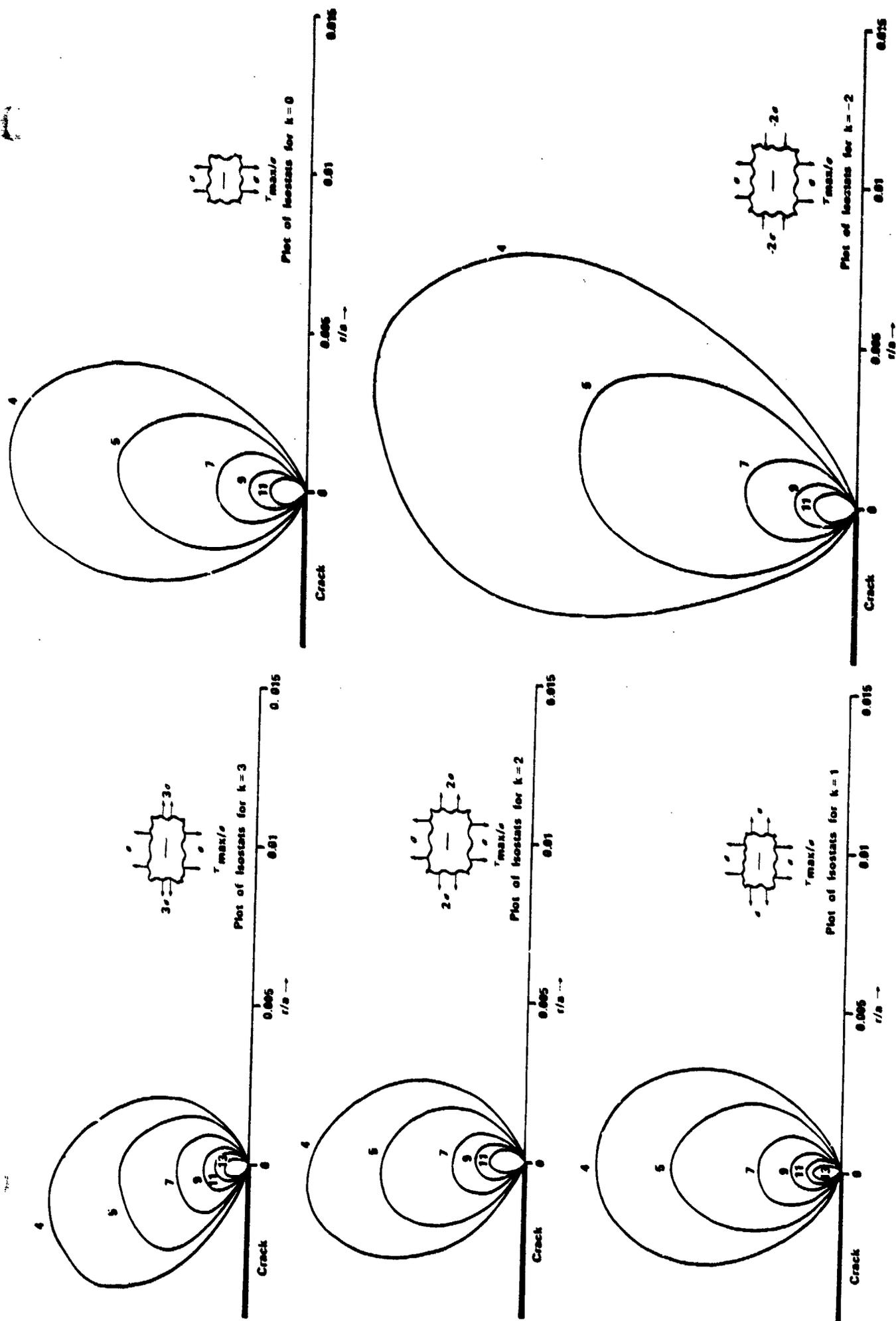
Fig. 11. Maximum shear stress contours, horizontal crack.
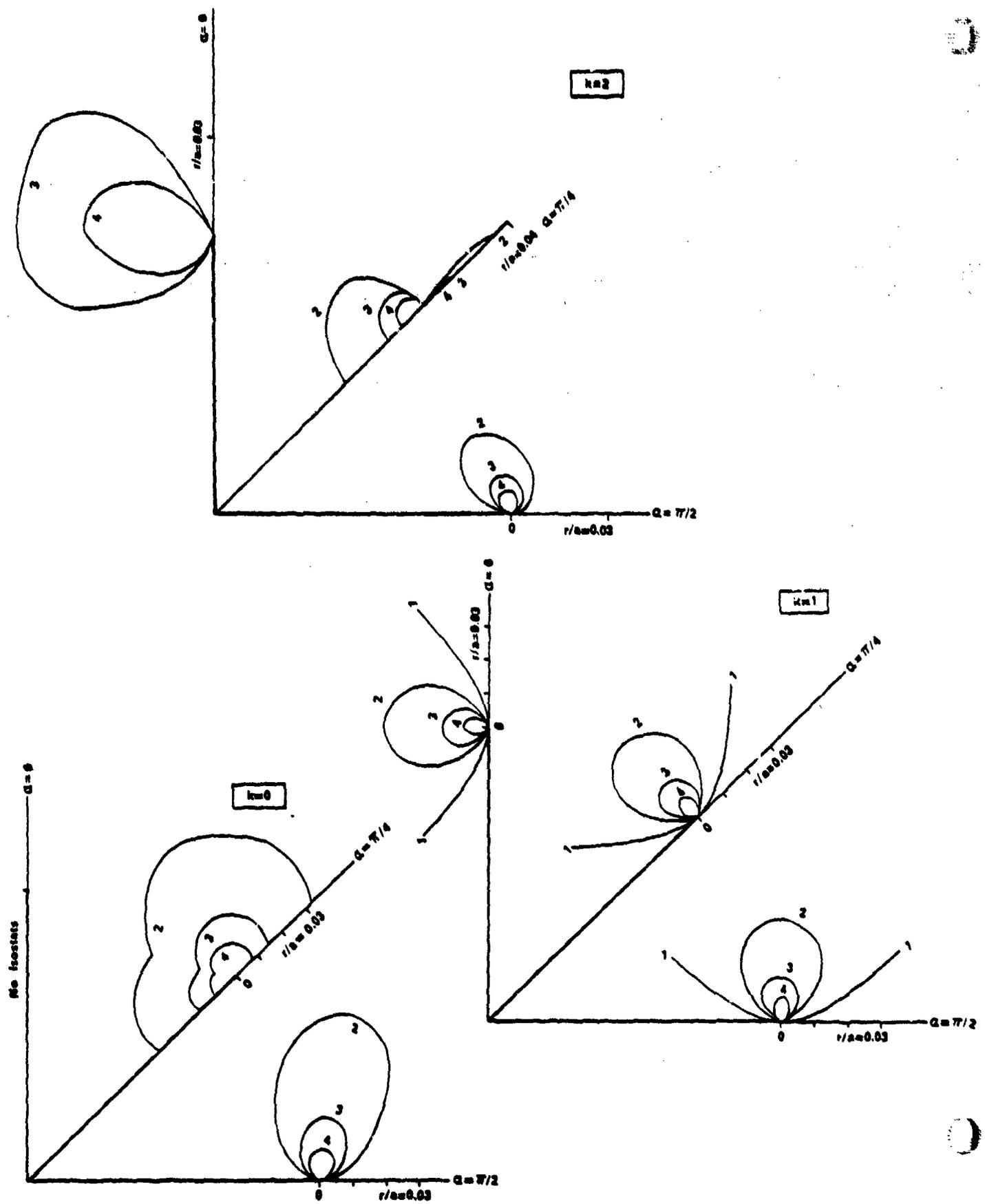
Fig. 12. Maximum shear stress contours, inclined crack.

Fig. 13. Maximum shear stress contours, inclined crack.

$\alpha = \pi/4, \ k = -1$

τ_m/σ

12.6

15.8

21.0

0

.001

.002

$(b-a)=1$

τ_m/σ

12.6

15.8

21.0

.001

.002

.003

$a = 0.10000$
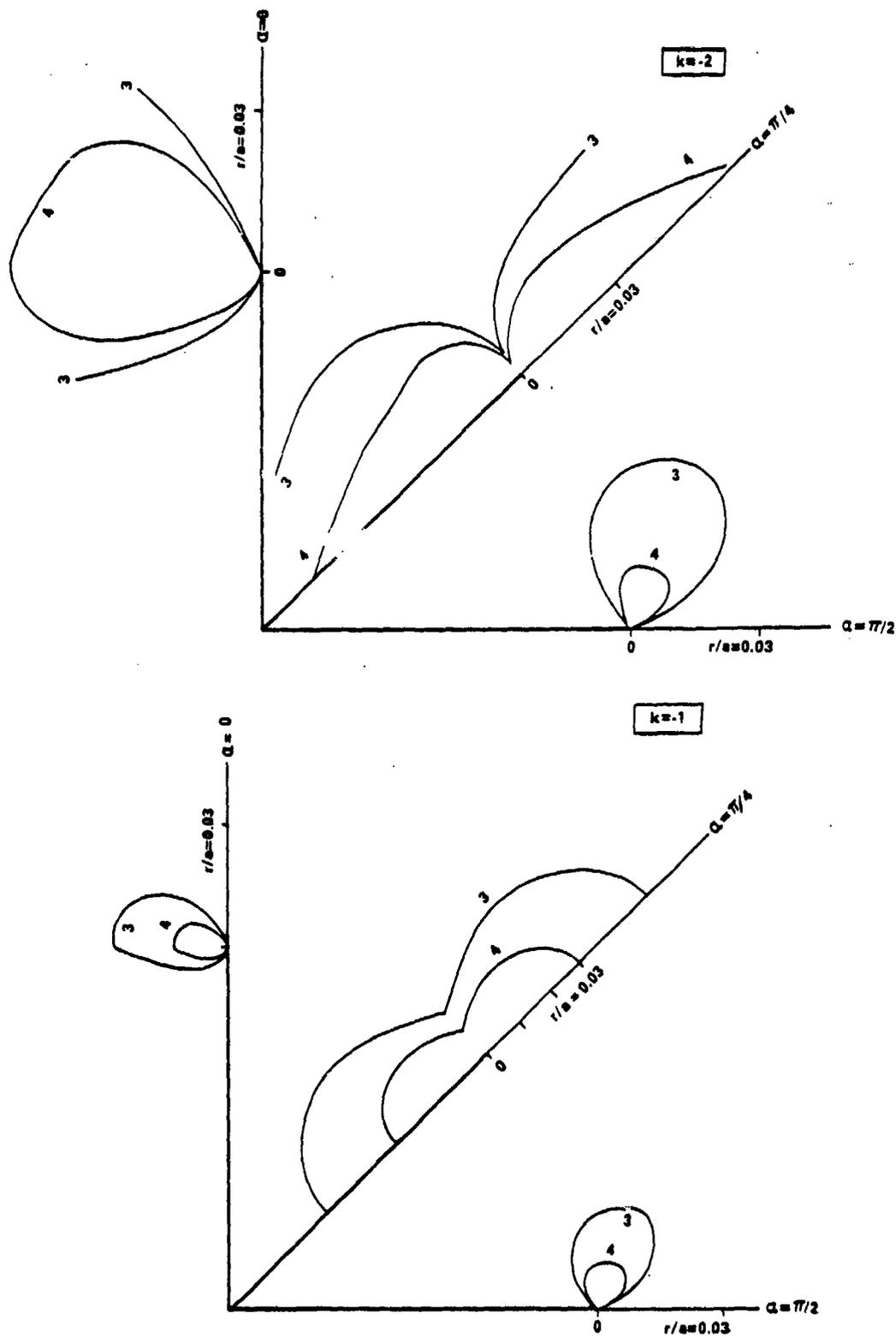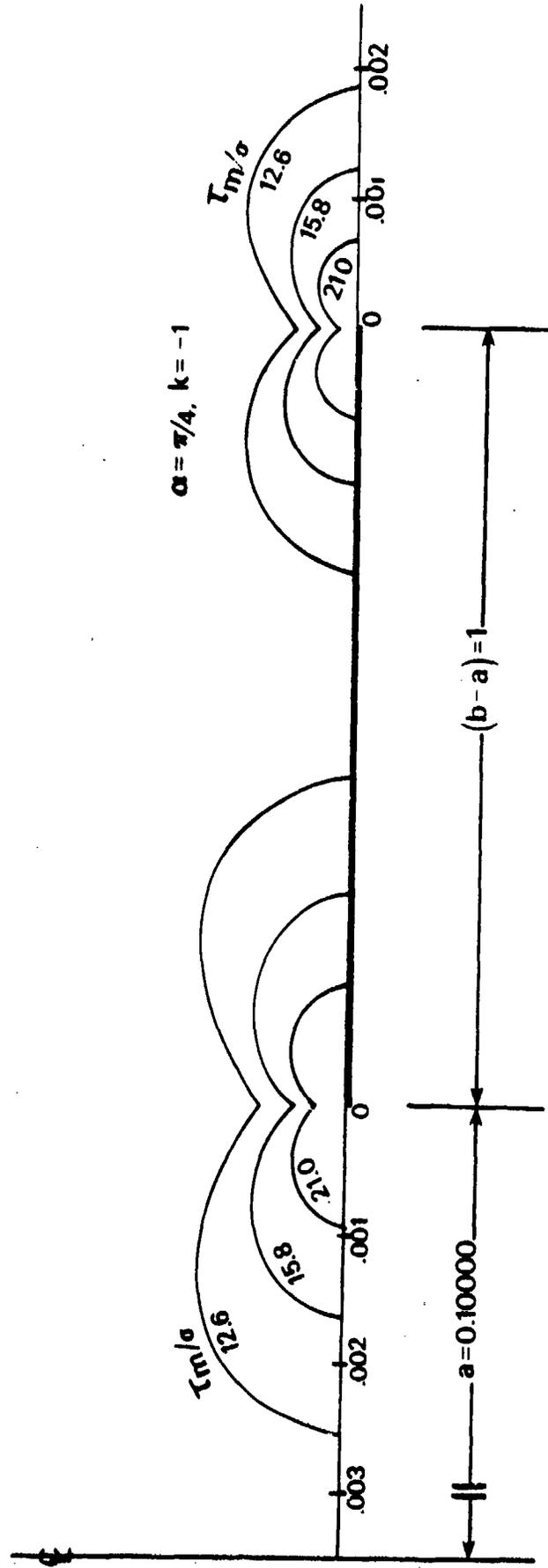
Fig. 14. Maximum shear stress contours for $k=1$, $\alpha \ \pi/4$.
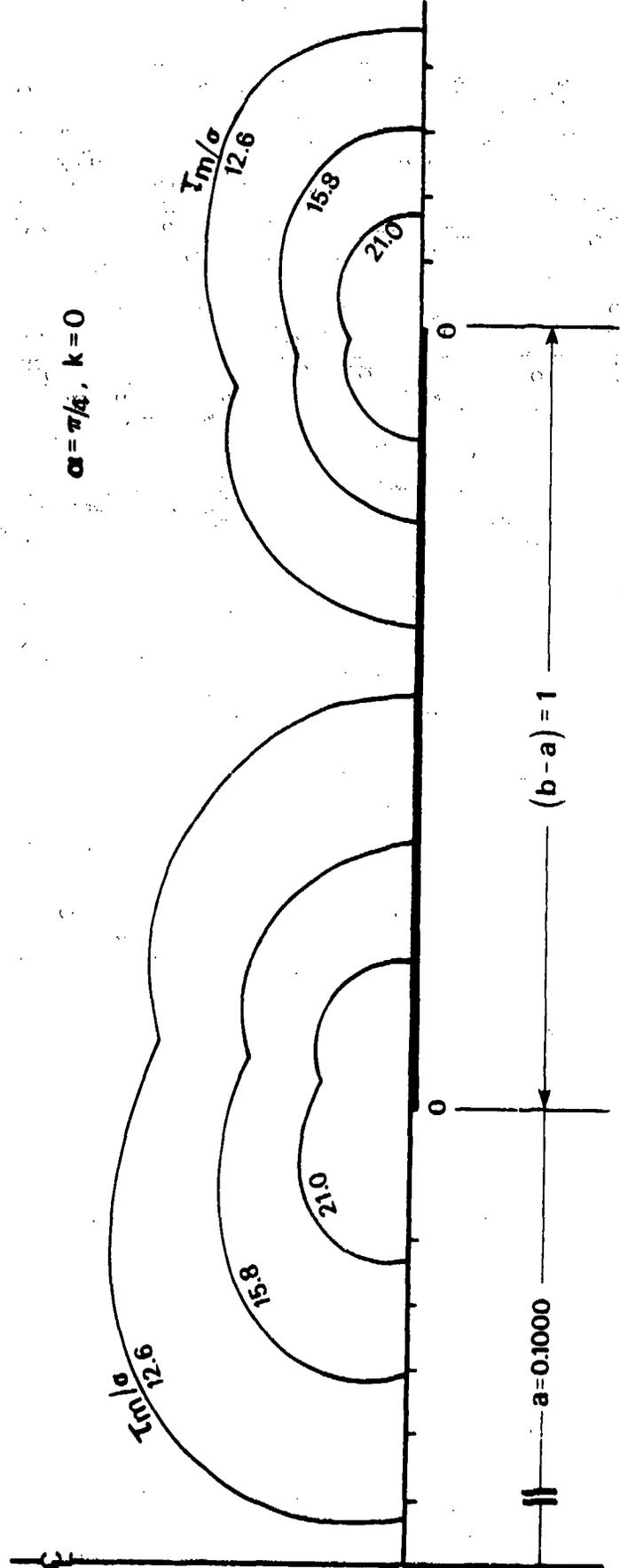
Fig.15. Maximum shear stress contours for $k=0$, $\alpha = \pi/4$.
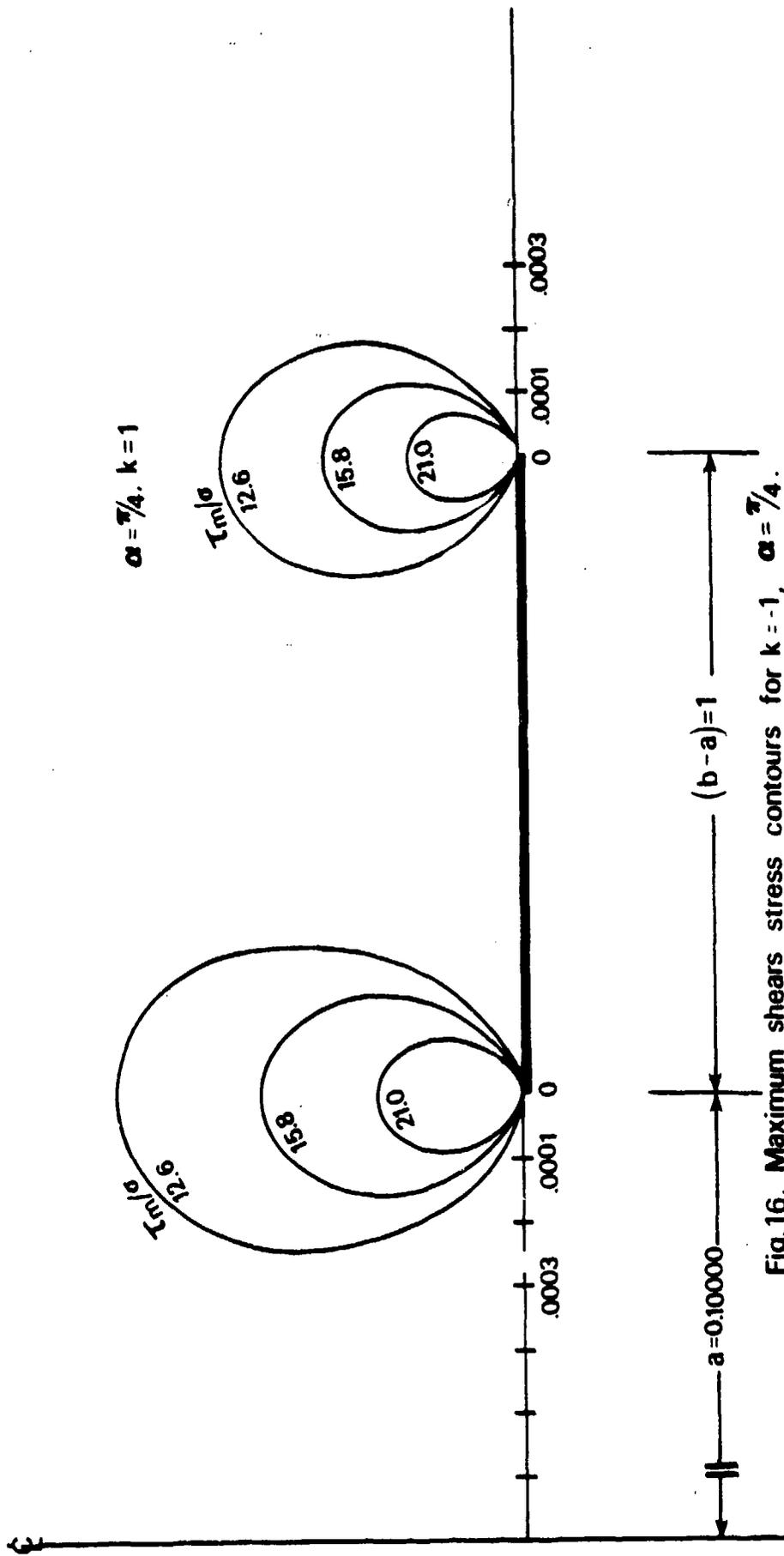
Fig. 16. Maximum shears stress contours for $k = -1$, $\alpha = \pi/4$.
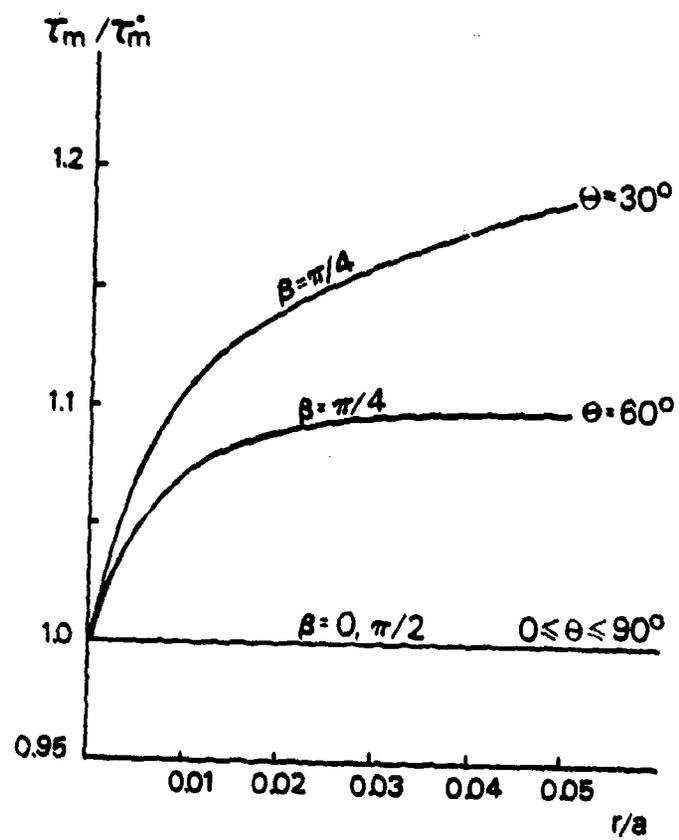
Fig. 17. Error in maximum shear stress
calculation, shear panel.
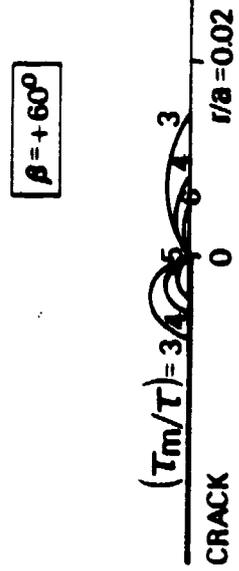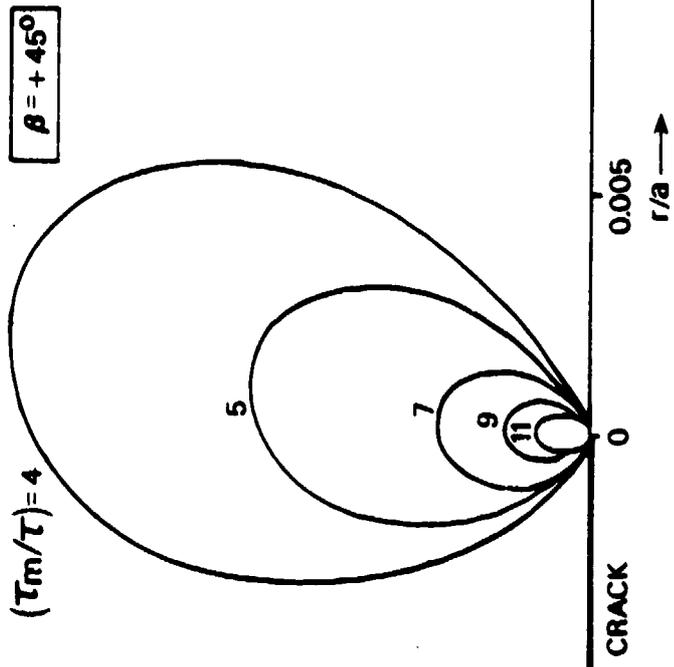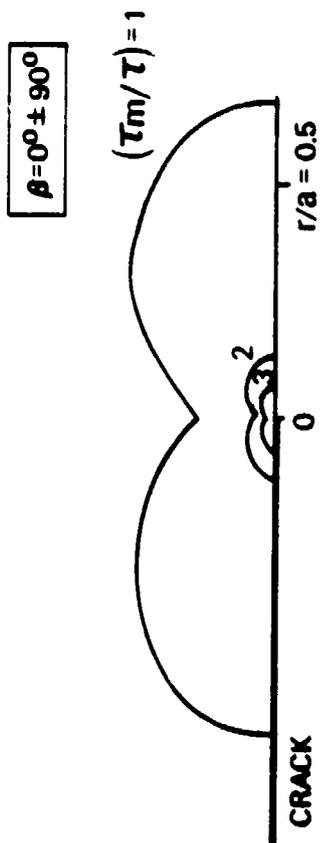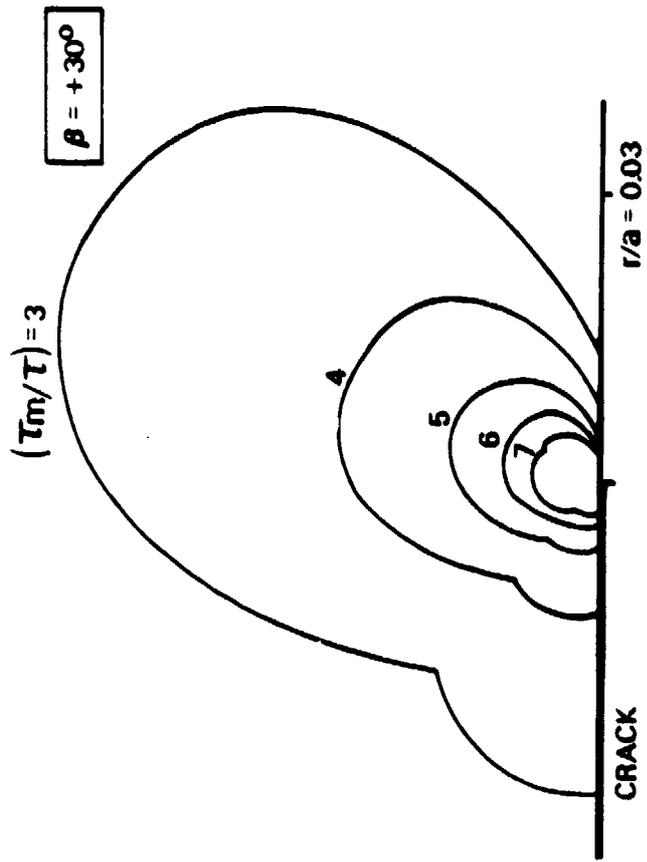
Fig. 18. Maximum shear stress contours, shear panel.
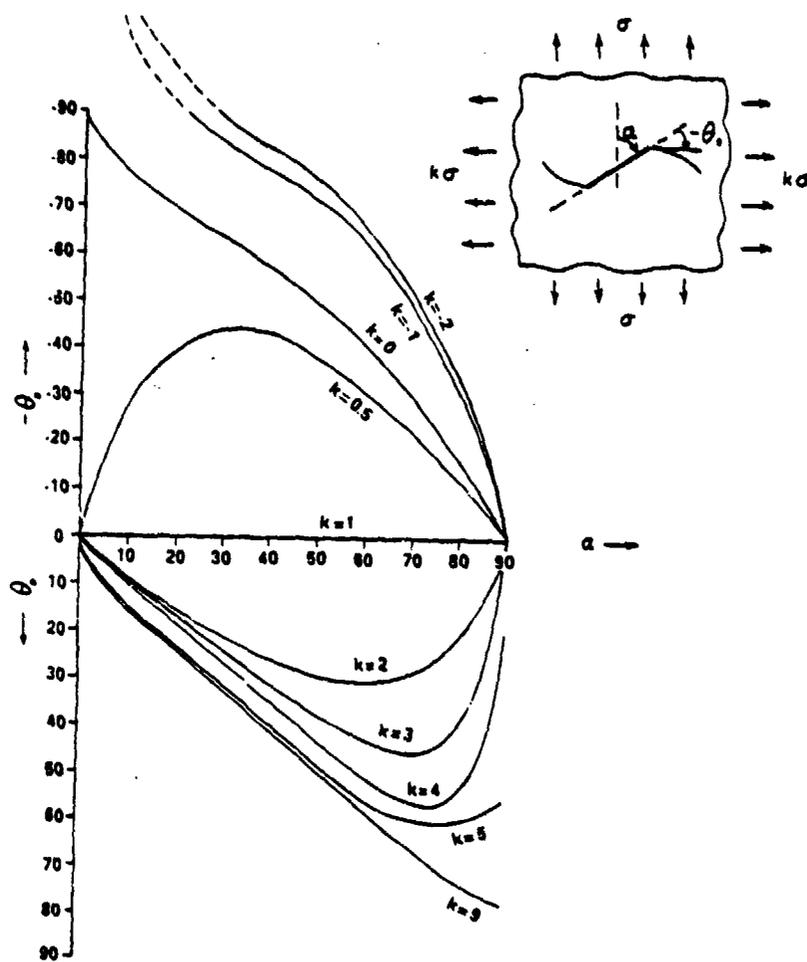
Fig. 19. Angle of initial crack extension, inclined crack.
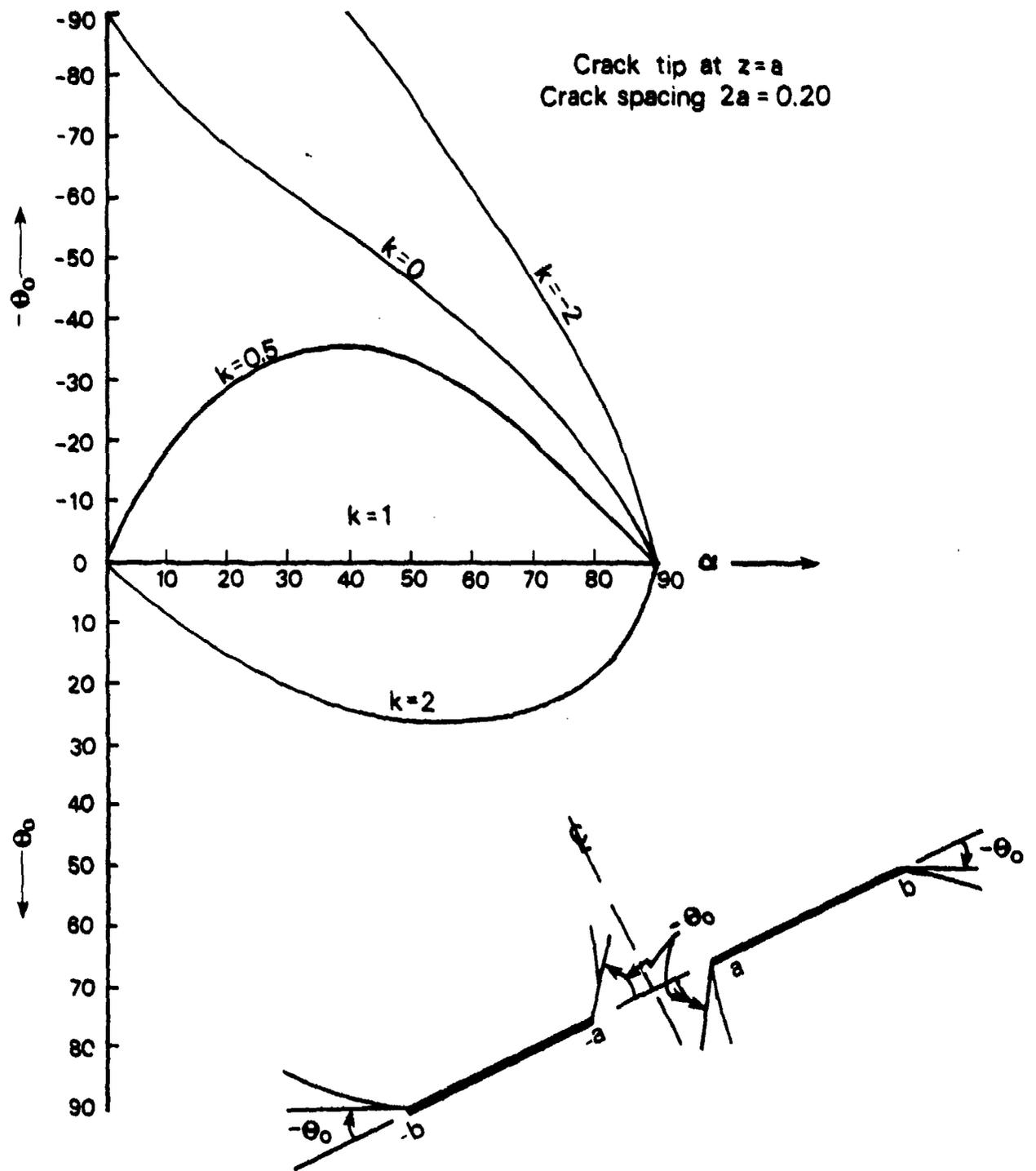
Fig. 20. Angle of initial crack extension at the inner crack ends.
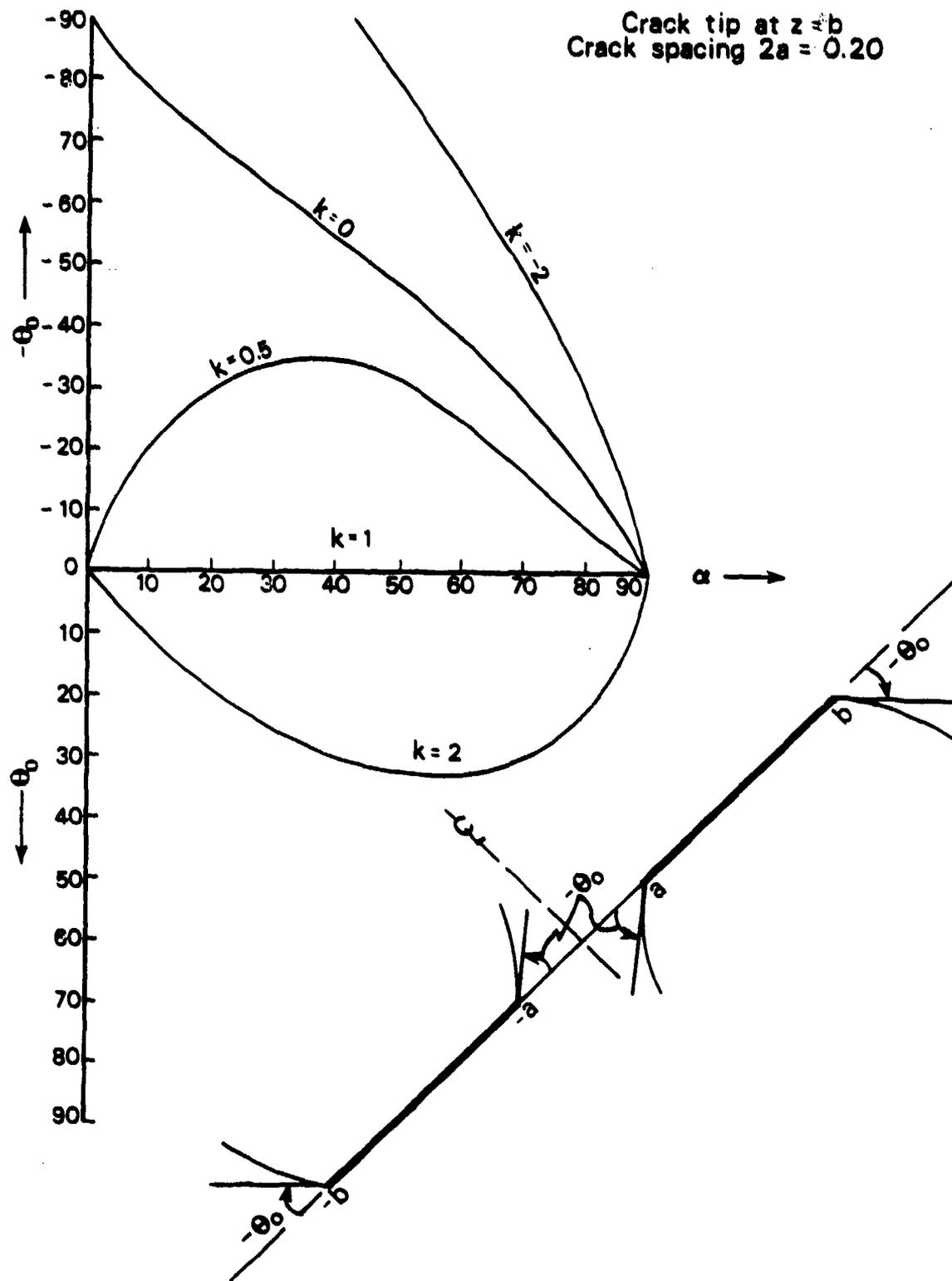
Fig. 21. Angle of initial crack extension at the outer crack ends.
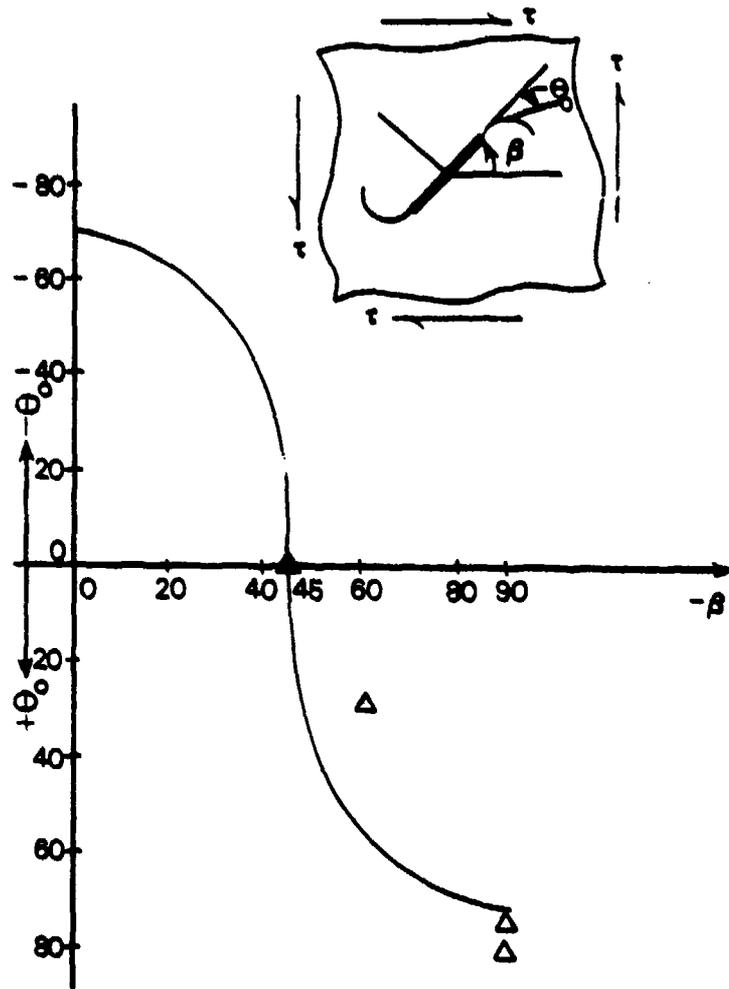
Fig. 22. Angle of initial crack extension, shear panel.
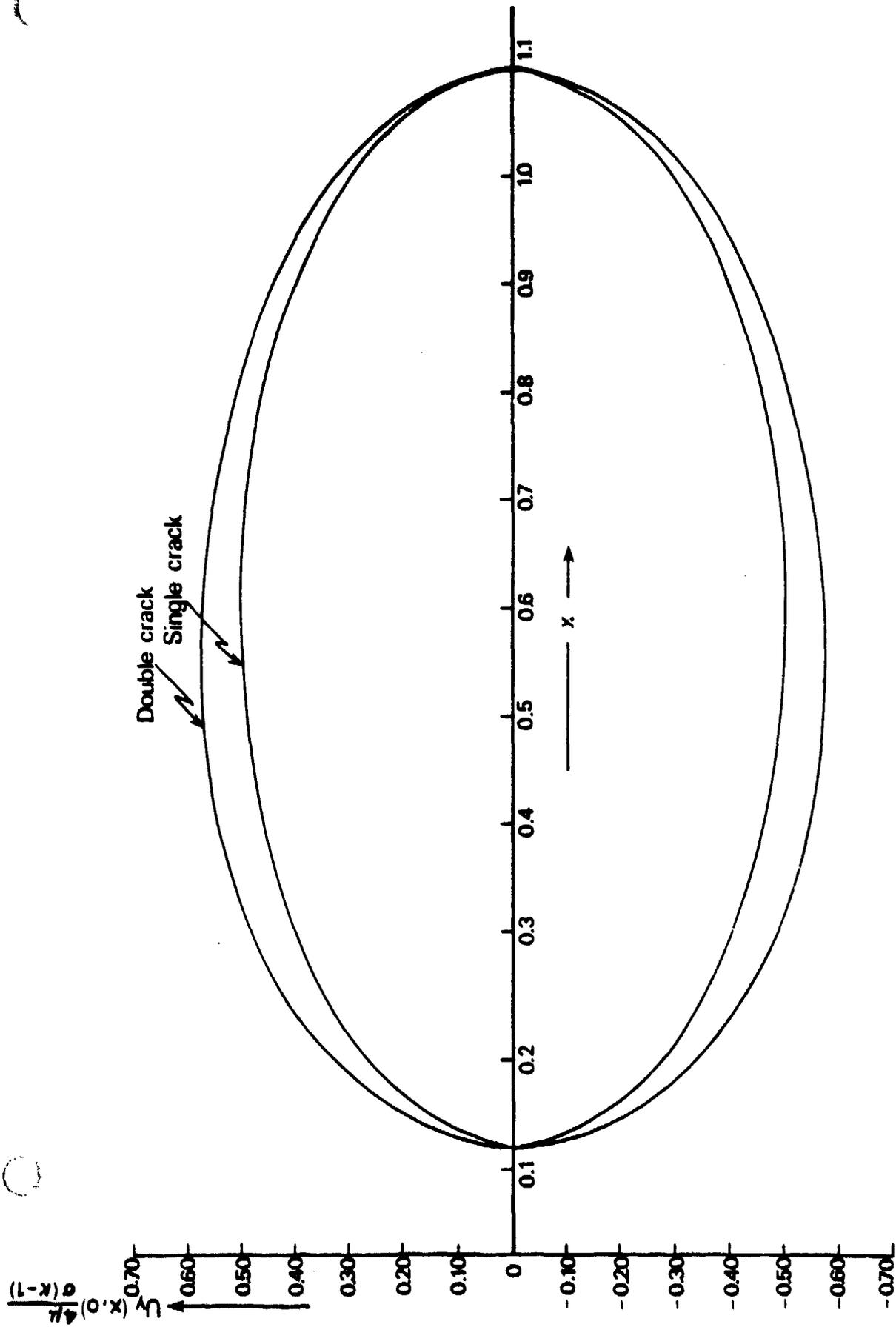
Fig. 23. Vertical component of displacement of crack border, $\alpha = \pi/2$.
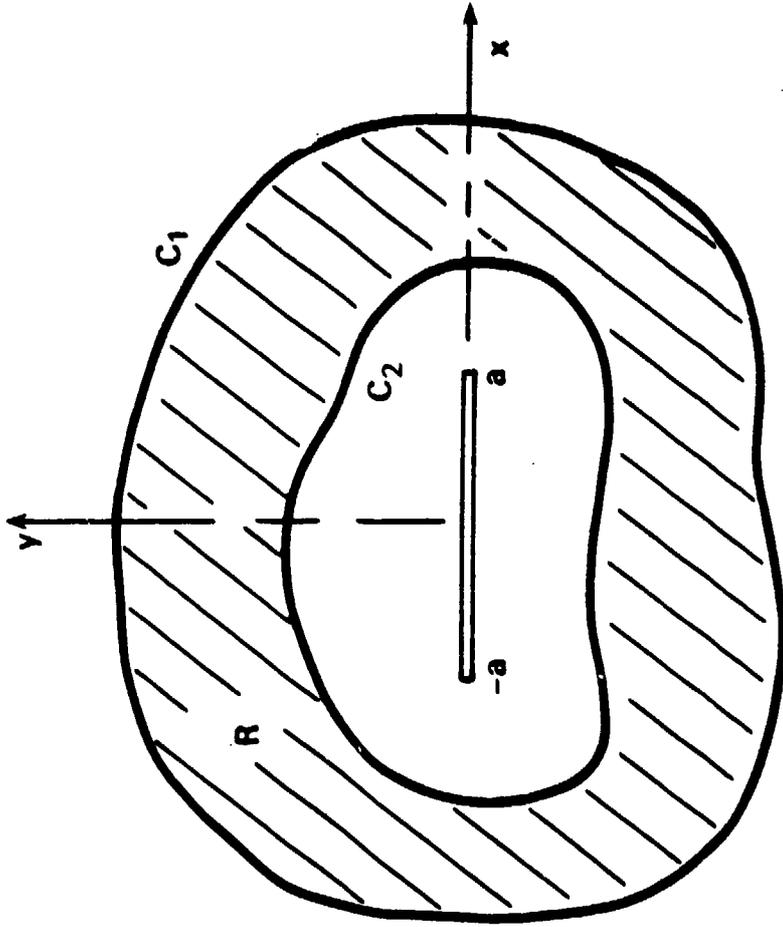
Fig. 24. Bound region enclosing the crack.
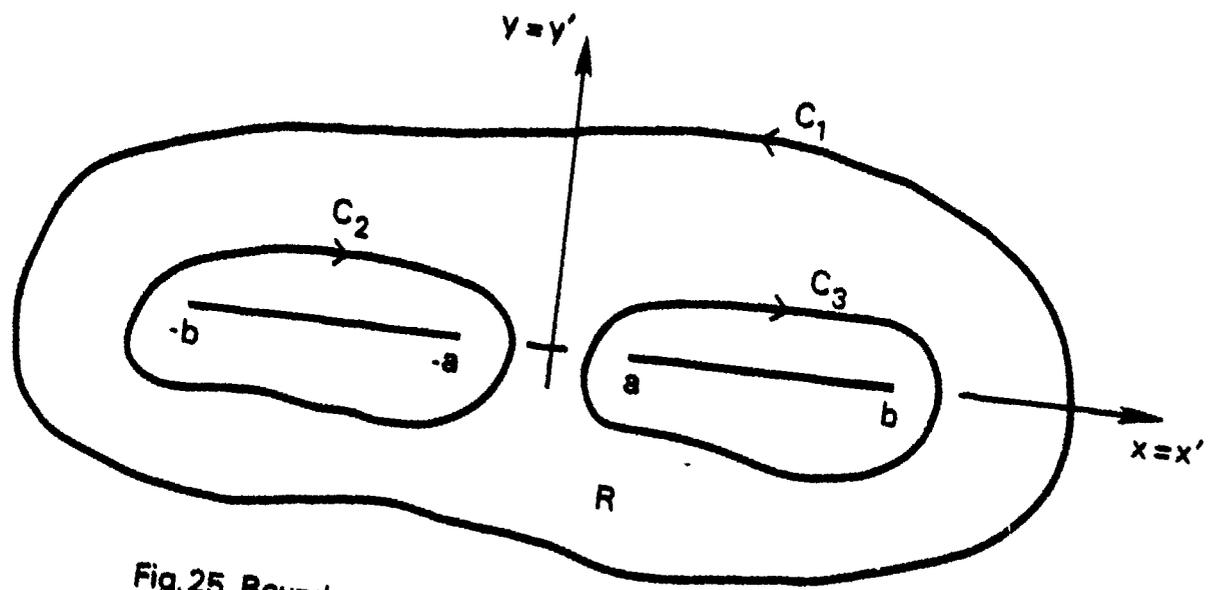
Fig. 25. Bound region enclosing the collinear cracks.
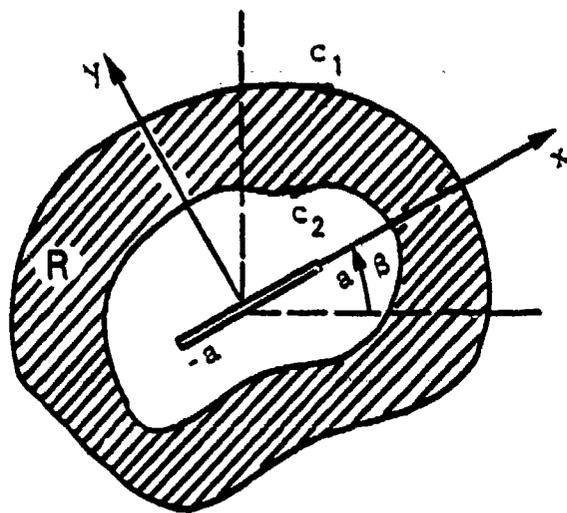
Fig. 26. Bound region enclosing the crack.
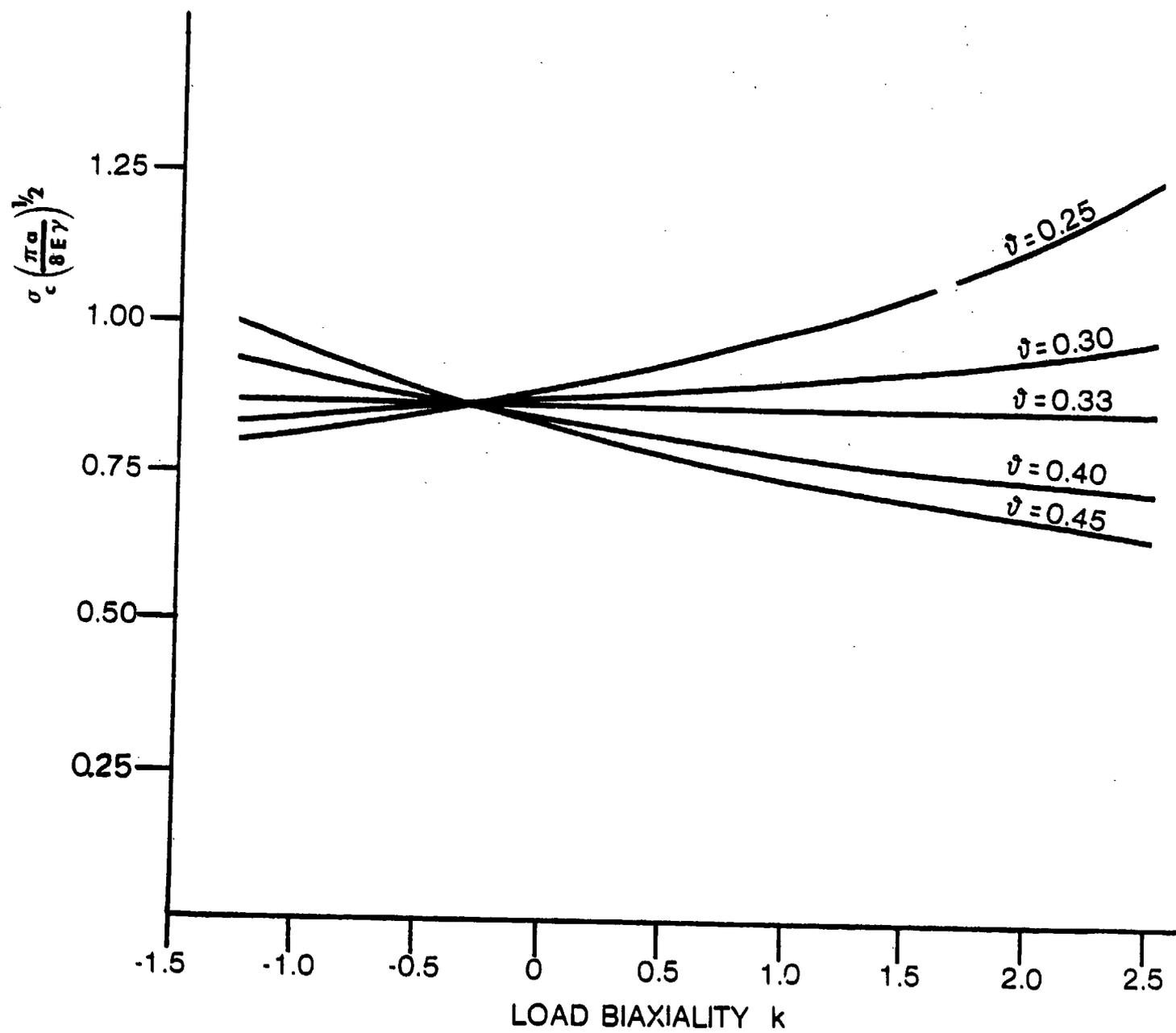
Fig. 27. Critical stress variation with load biaxiality and Poisson ratio
(plane stress)
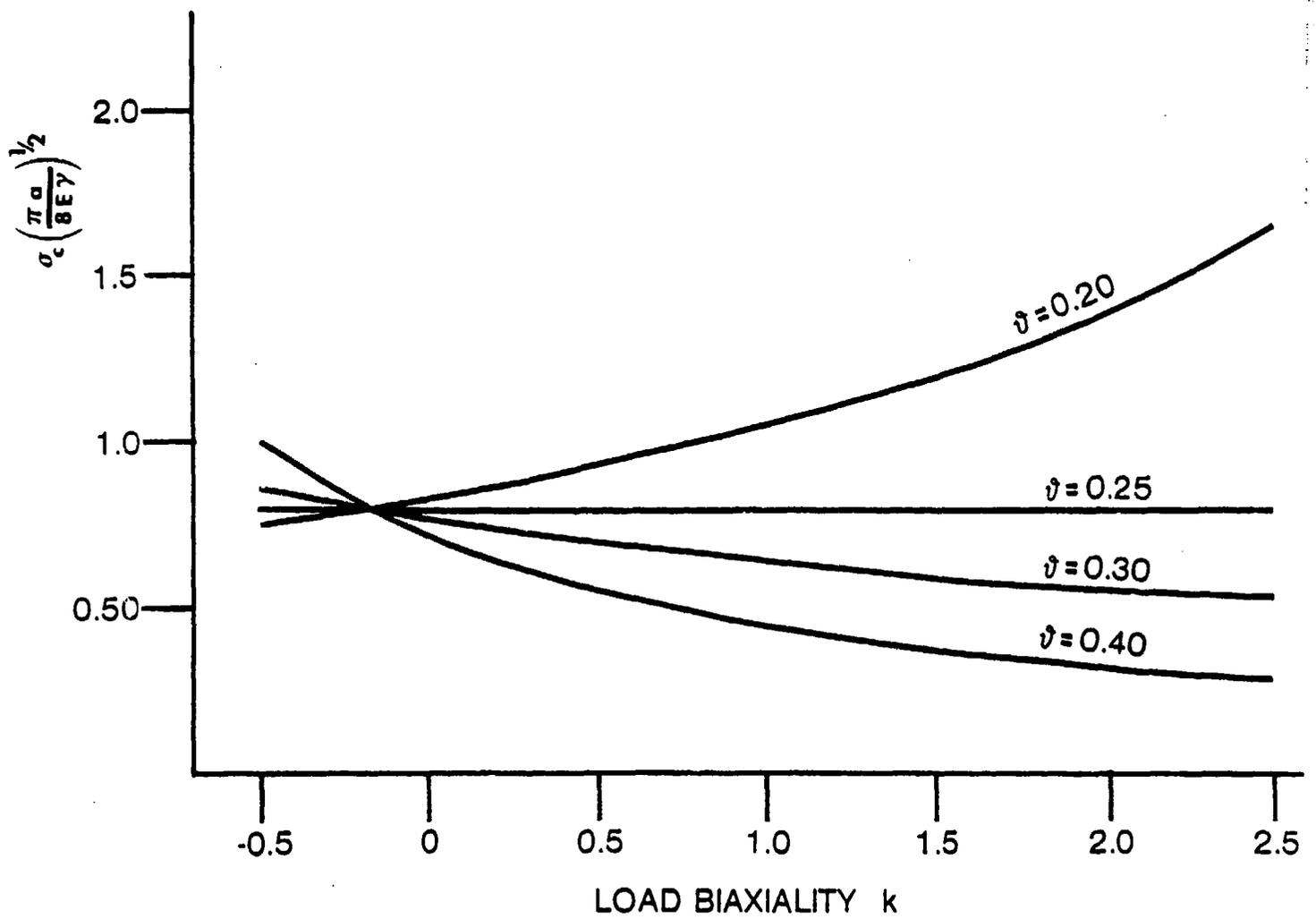
Fig.28. Critical stress variation with load biaxiality and Poisson ratio
(plane strain)
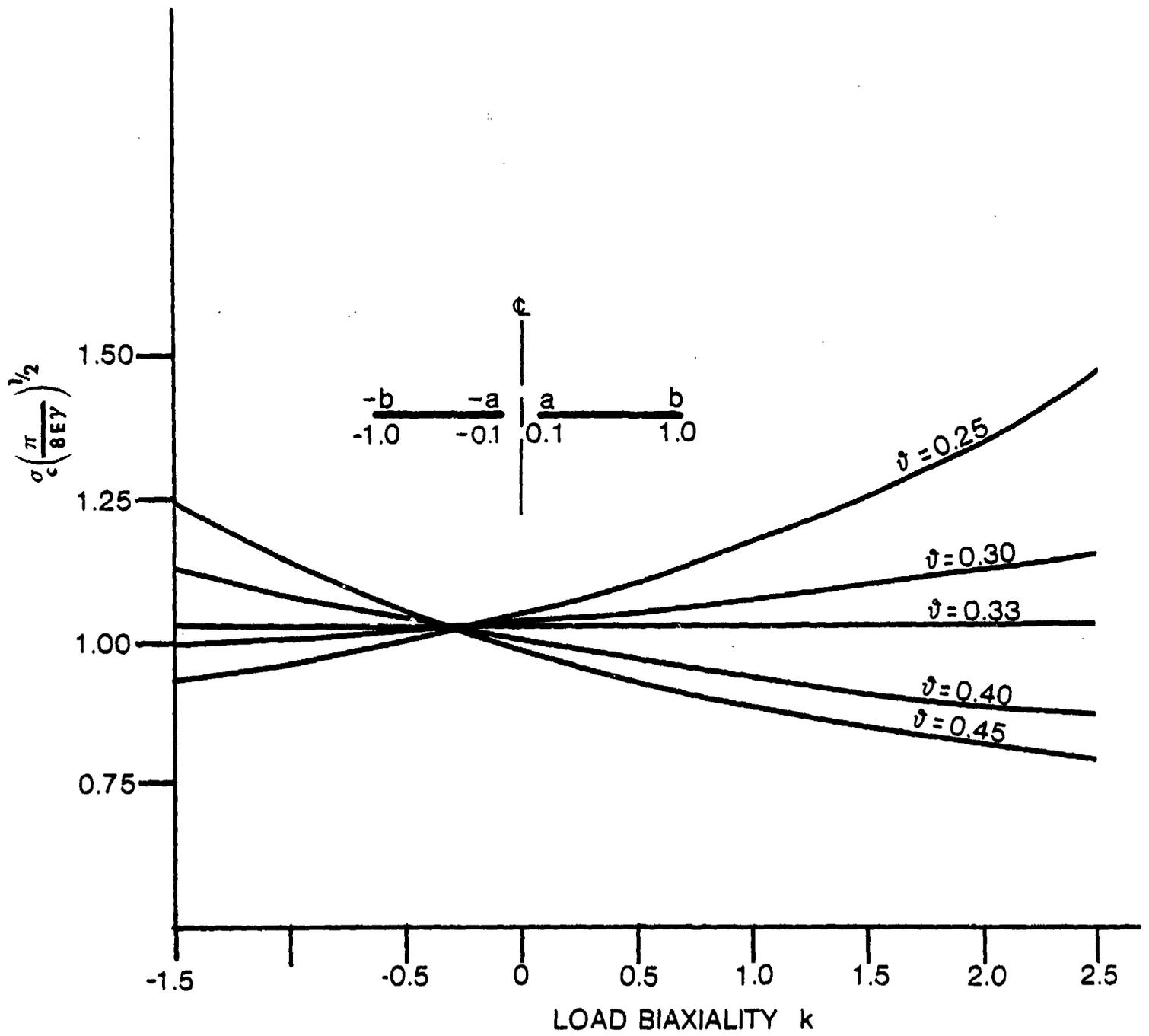
Fig. 29. Critical stress variation with load biaxiality and Poisson ratio (plane stress)
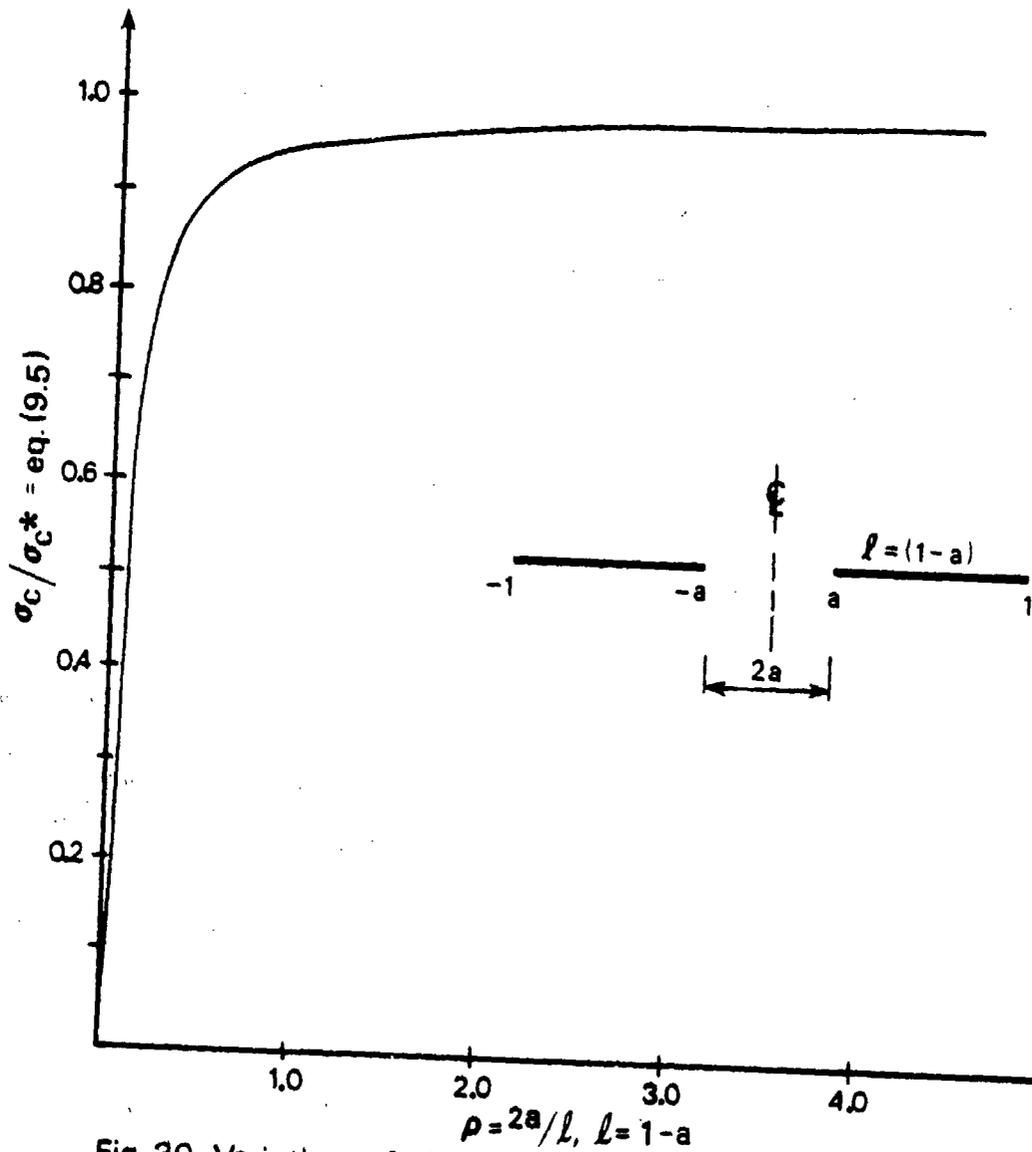
Fig. 30. Variation of the ratio of double crack to single crack breaking loads with double crack spacing.
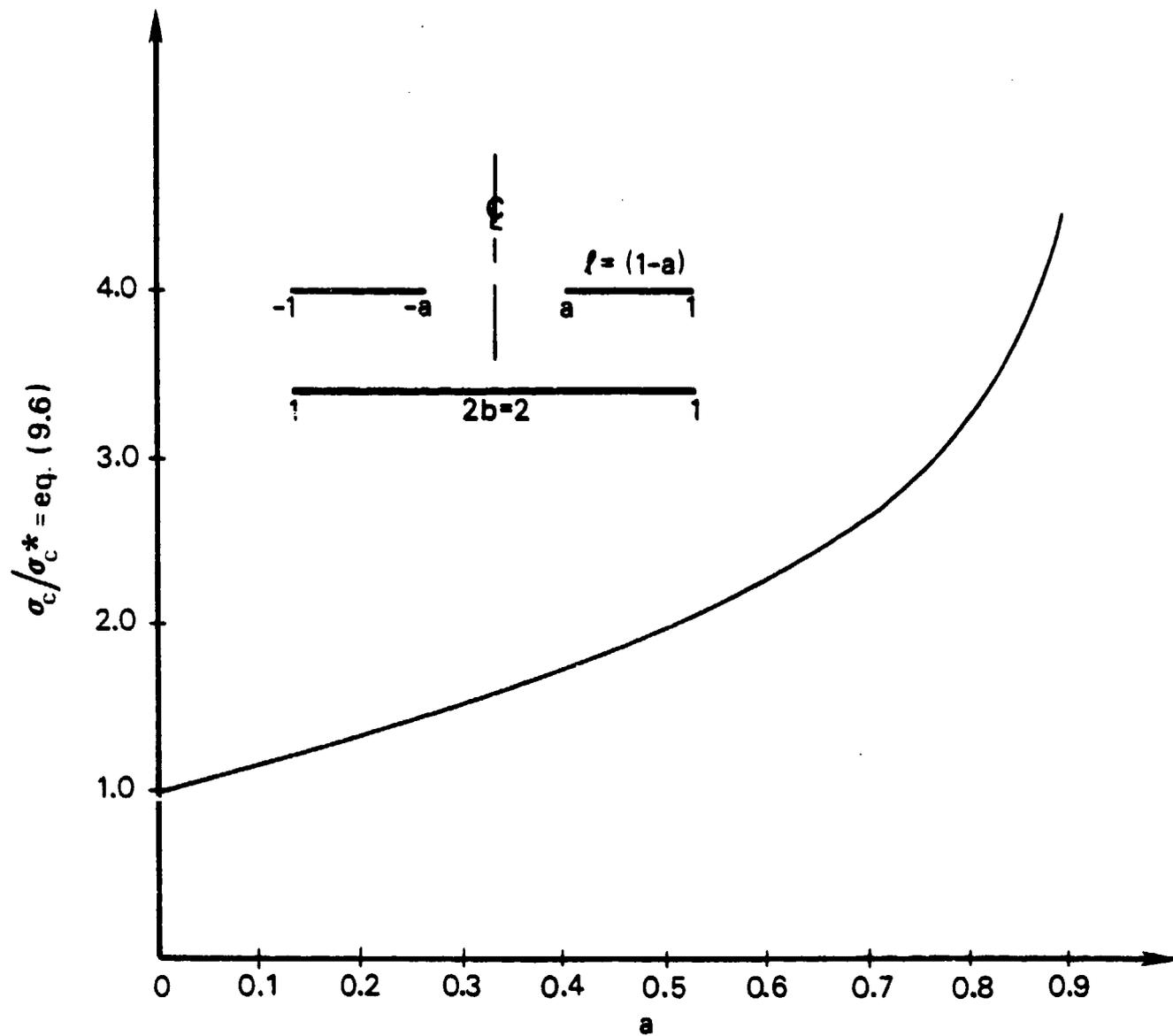
Fig. 31. Variation of the ratio of double to single crack breaking loads with double crack size.
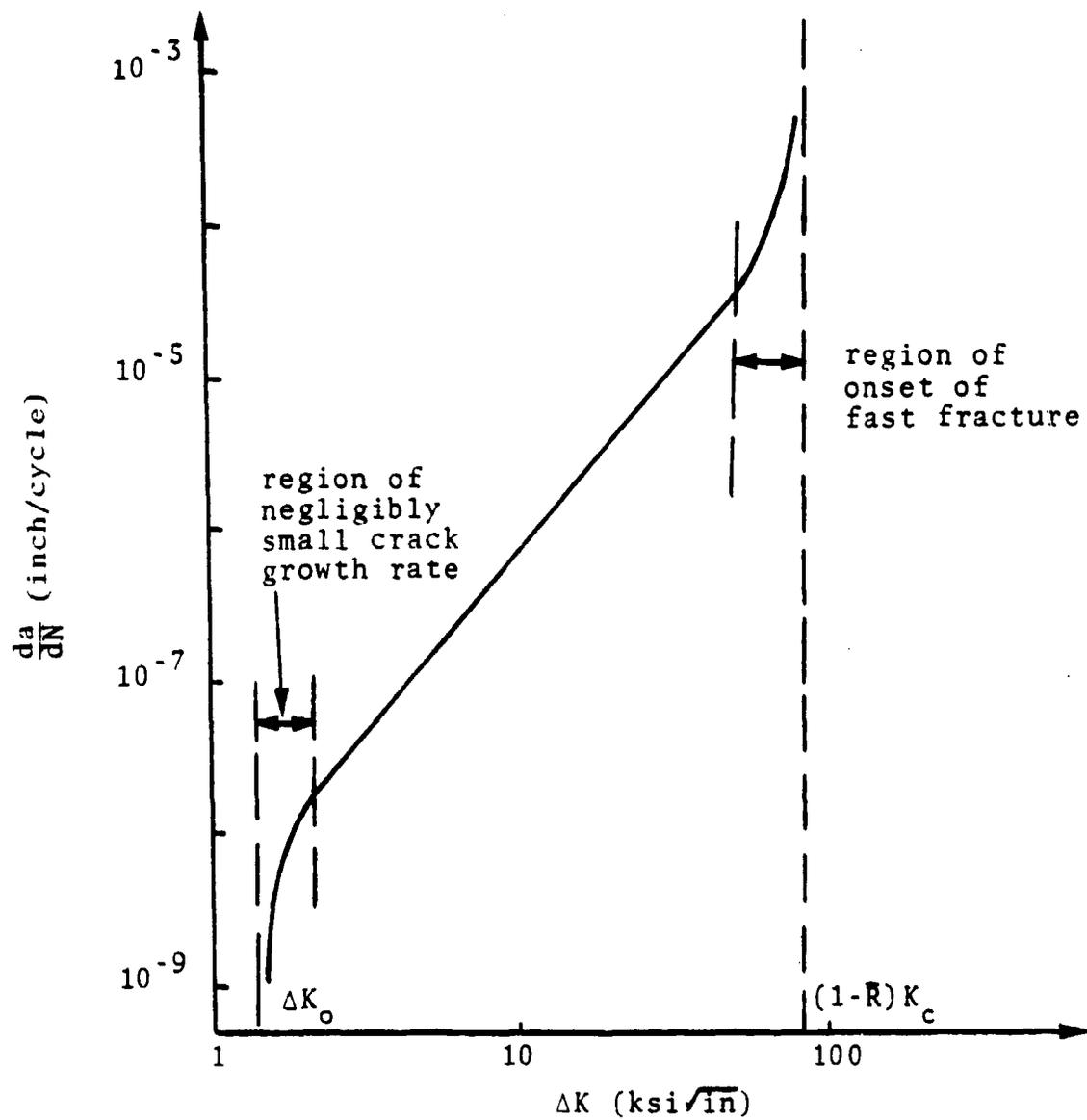
Fig. 32. Illustration of fatigue crack growth
rate versus ΔK.

Figure 33. Biaxial specimen design.
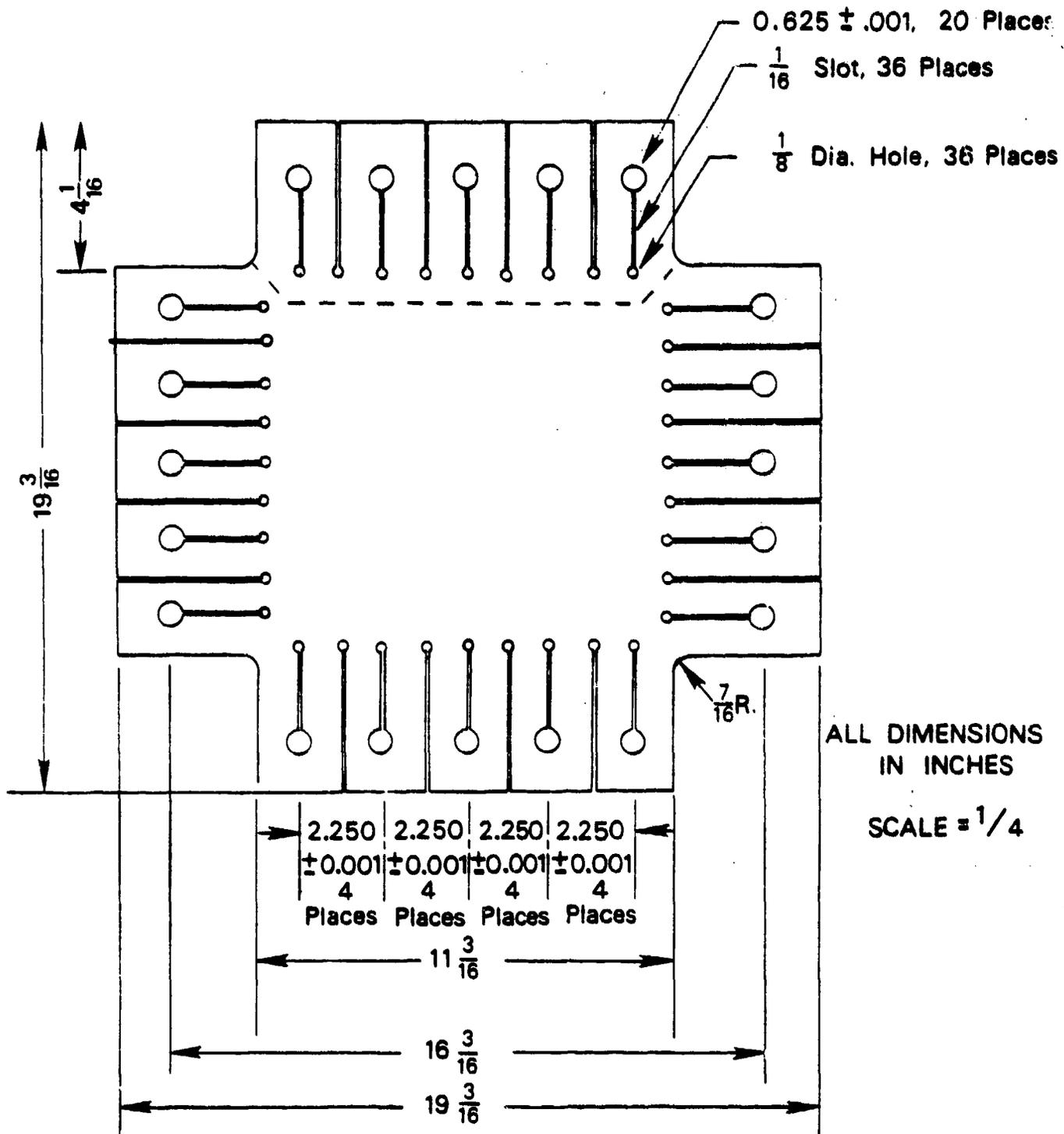
Figure 34. Alternate biaxial specimen design.
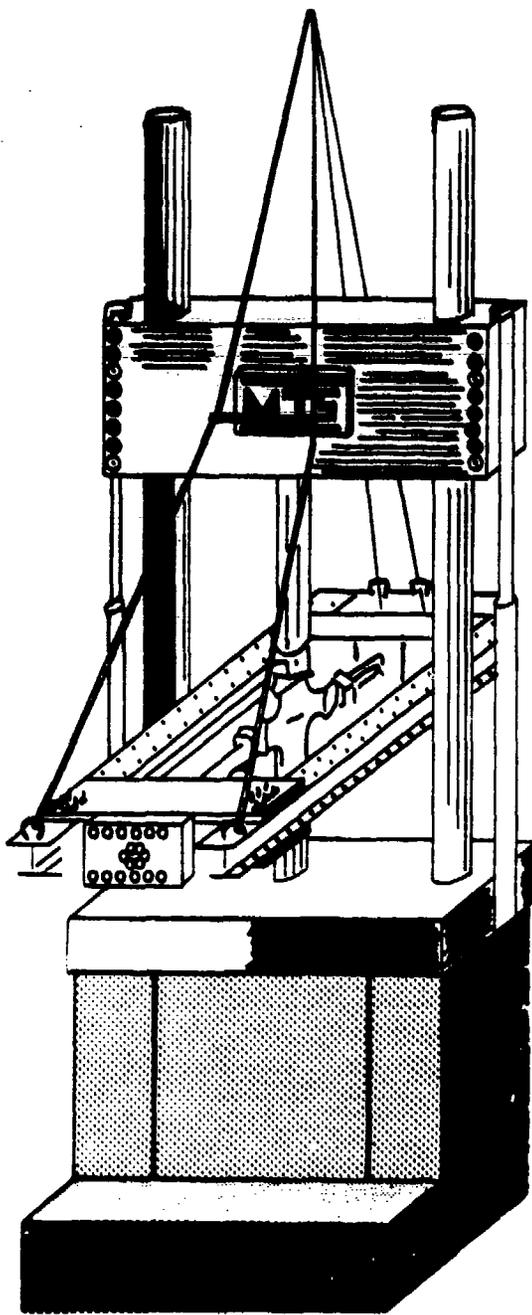
Figure 35. Biaxial test system.
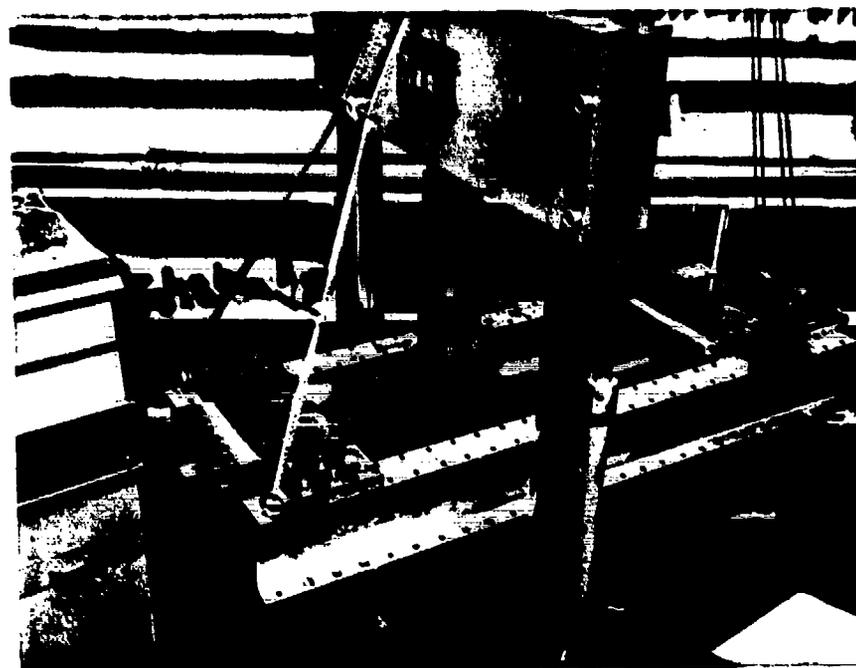
Fig. 36. Photographs of biaxial test system.
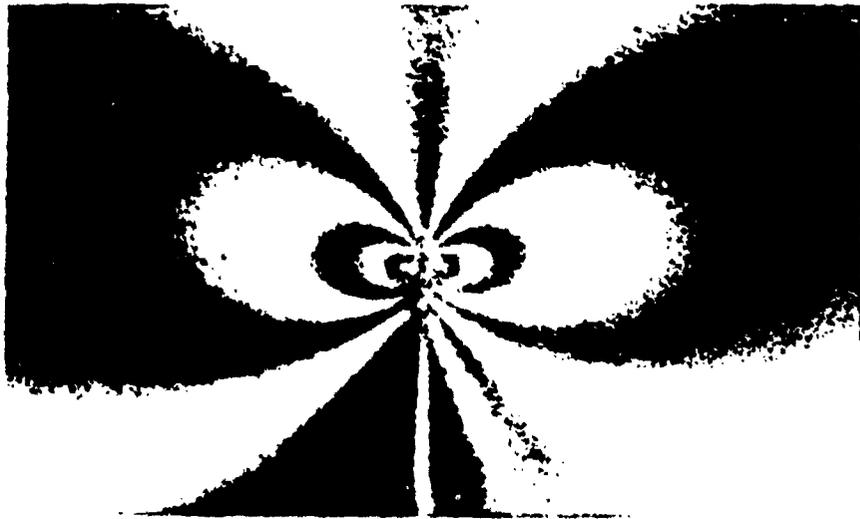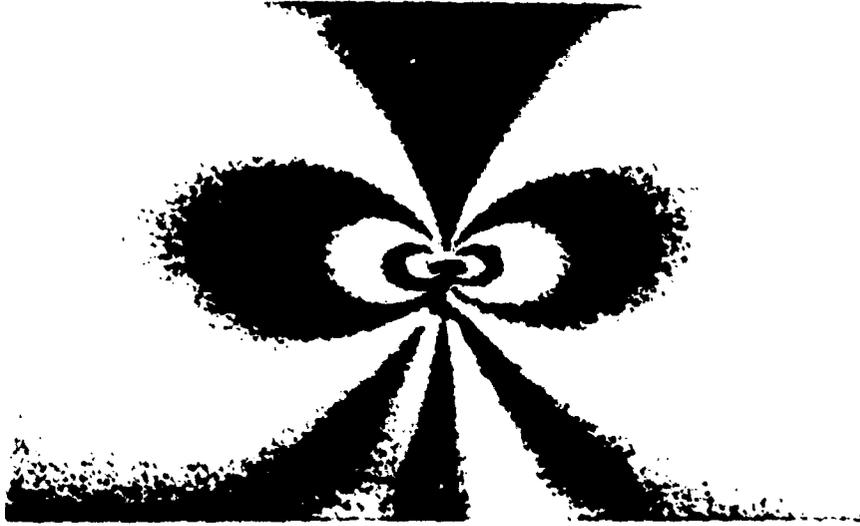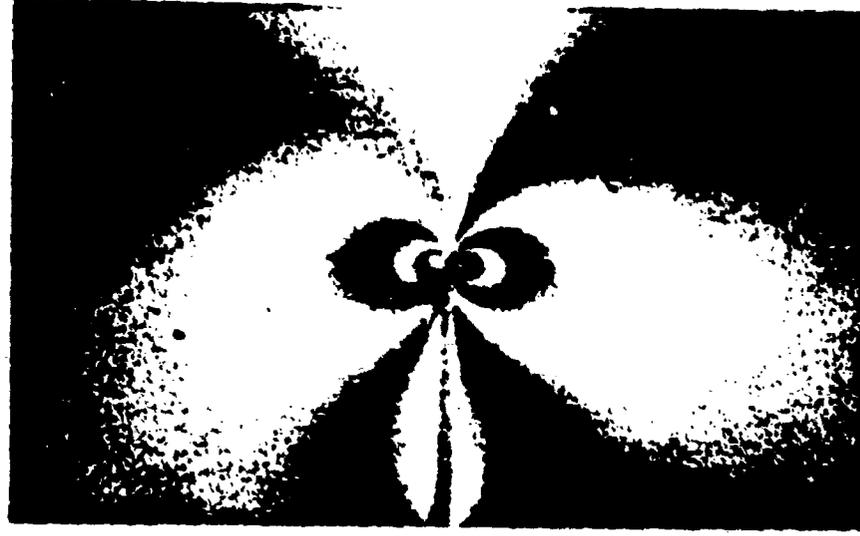
(a) k = 0   (b) k = 0.5   (c) k = 1.0

Fig. 37. Variation of the shear stress isochromatics as a function of applied load biaxiality.
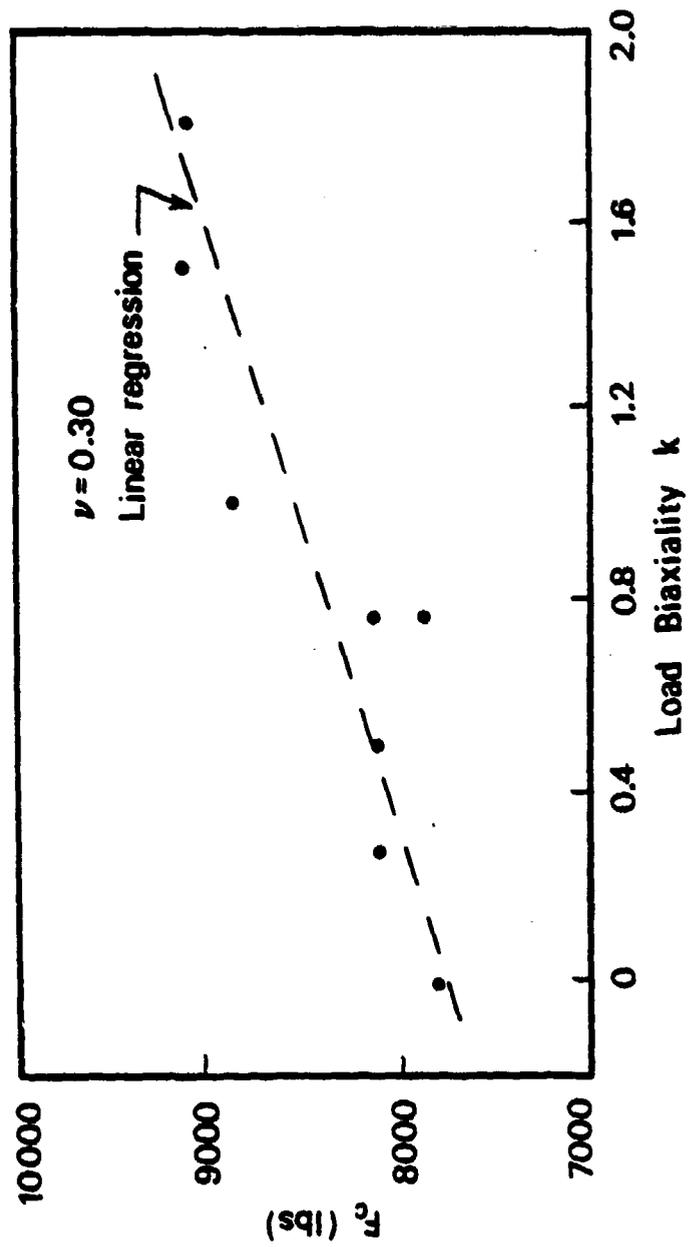
Fig. 38. Fracture load for Aluminum Alloy 7075-T6 sheets. Crack parallel to rolling direction.
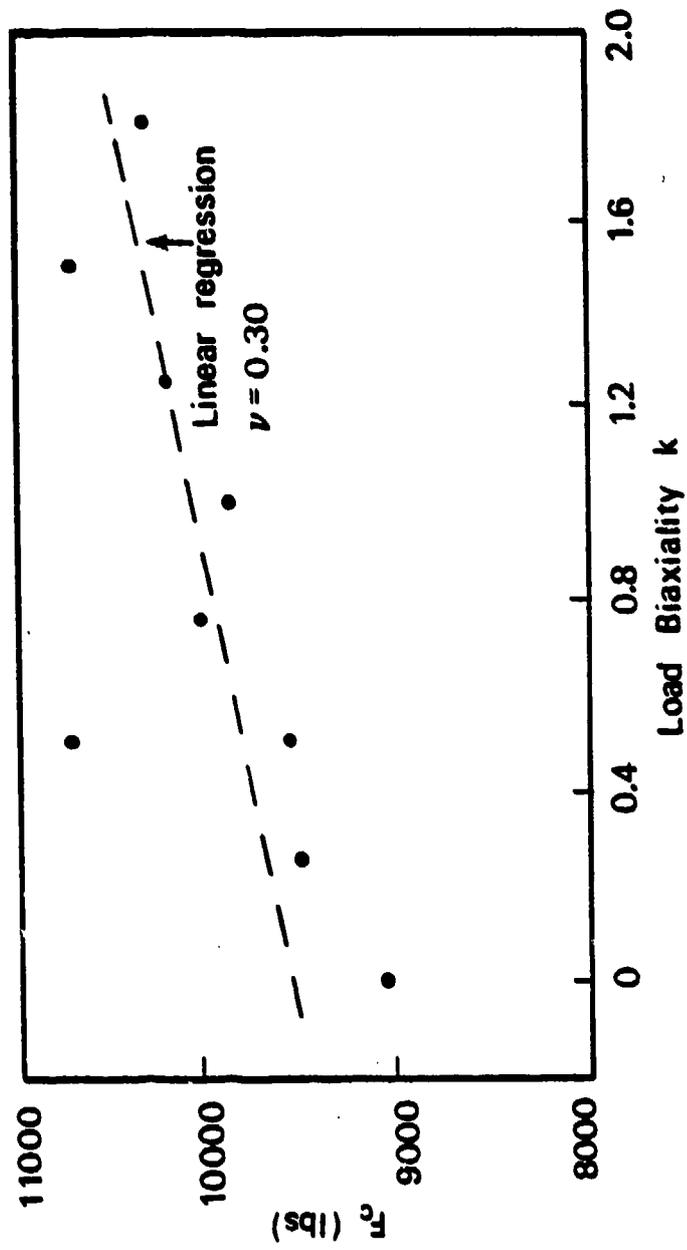
Fig. 39. Fracture load for Aluminum Alloy 7075-T6 sheets. Crack perpendicular to roll direction.
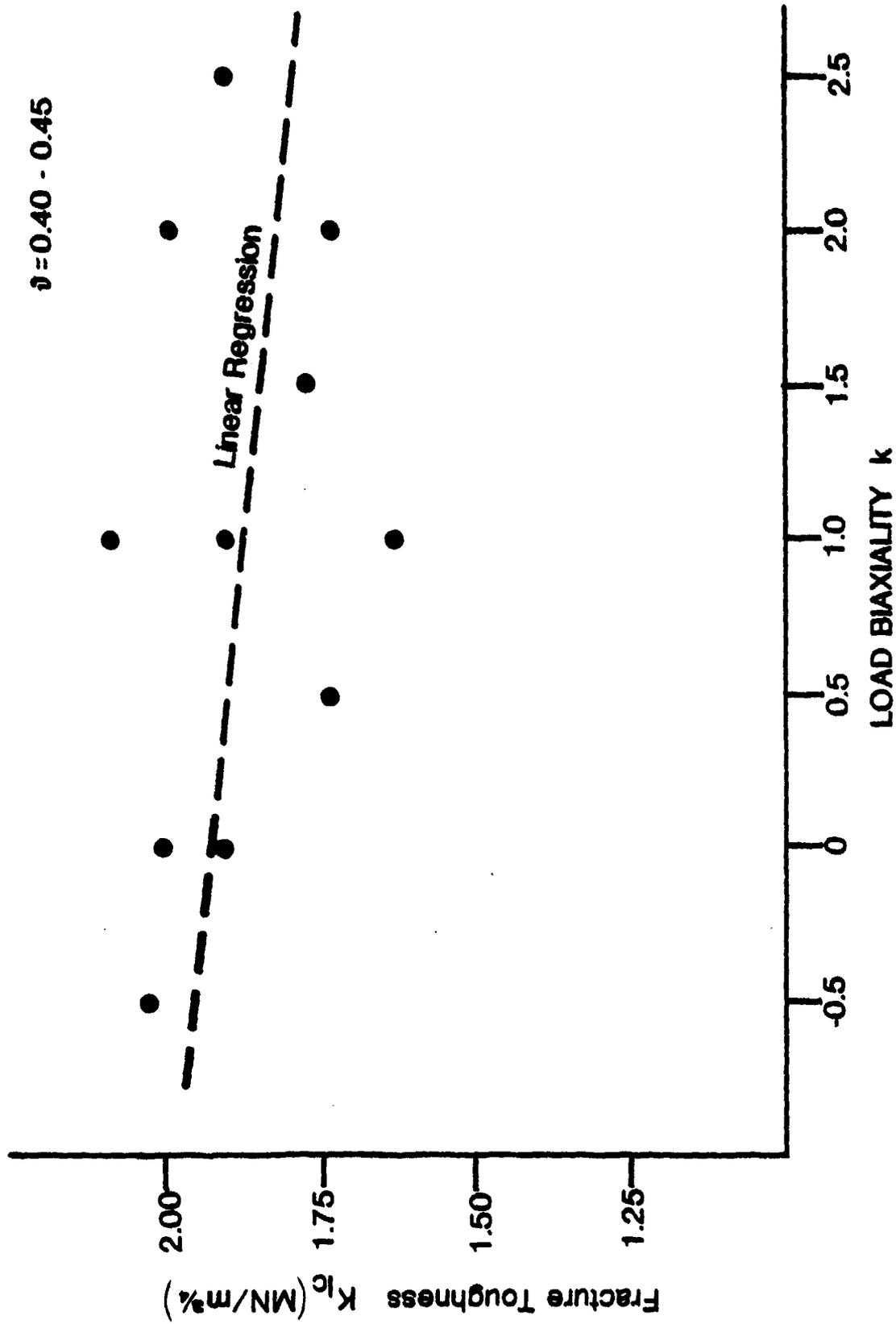
Fig. 40. Fracture toughness (fracture load) for plastic sheets (George Washington University tests).
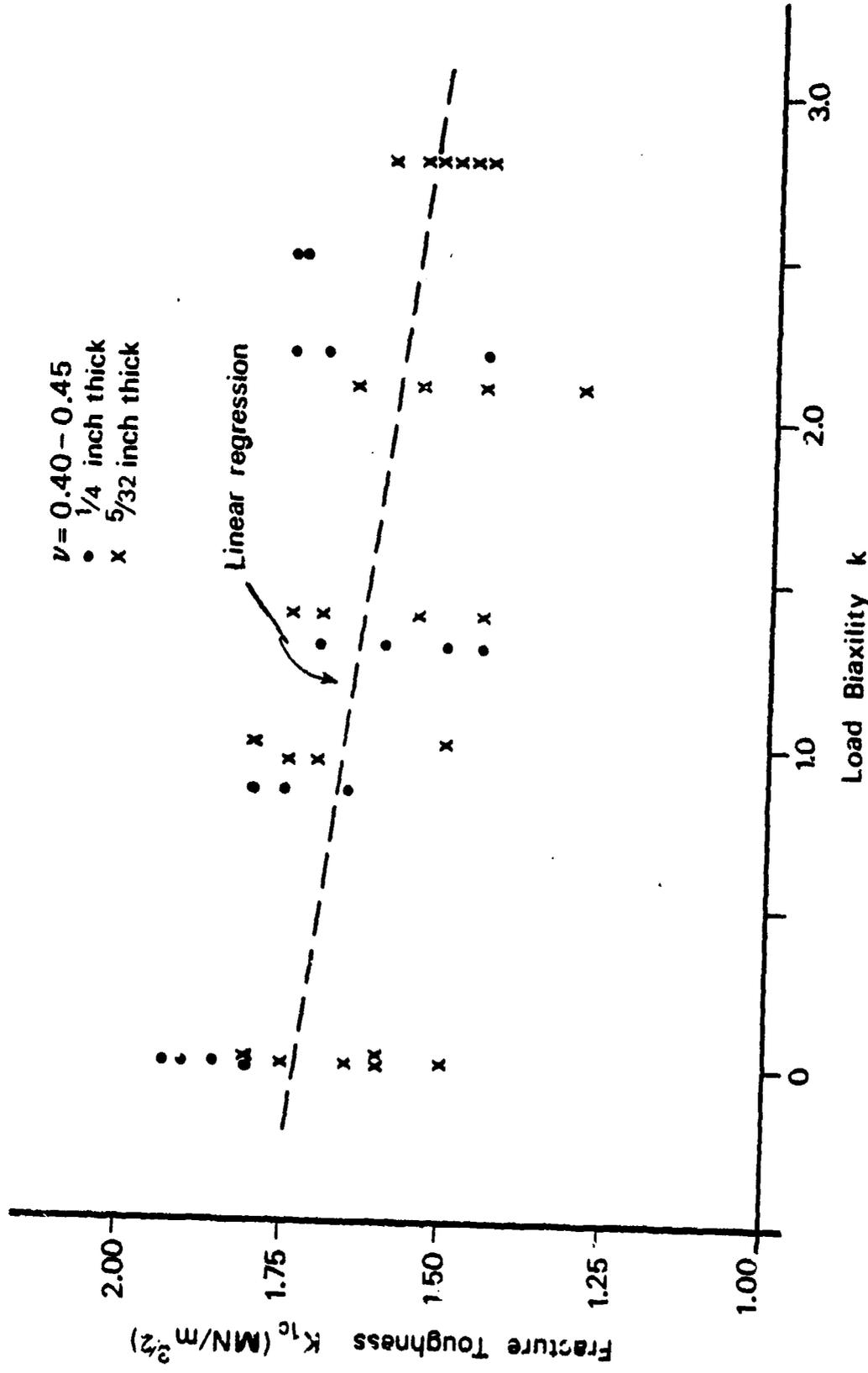
Fig. 41. Fracture toughness (fracture load) for Polymethylmethacrylate (PMMA) sheets (Imperial College of Technology tests).
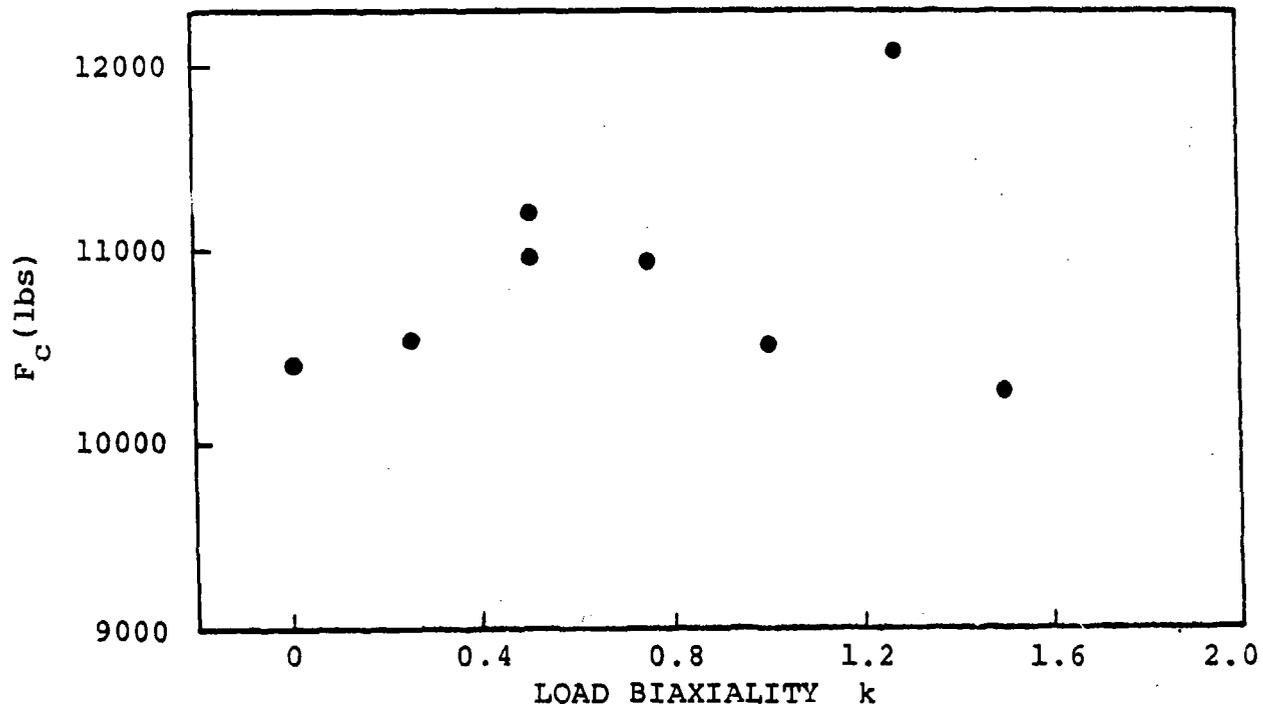
Fig. 42. Critical fracture load for 2024-T3 sheets as a function of load biaxiality. Crack parallel to the rolling direction.
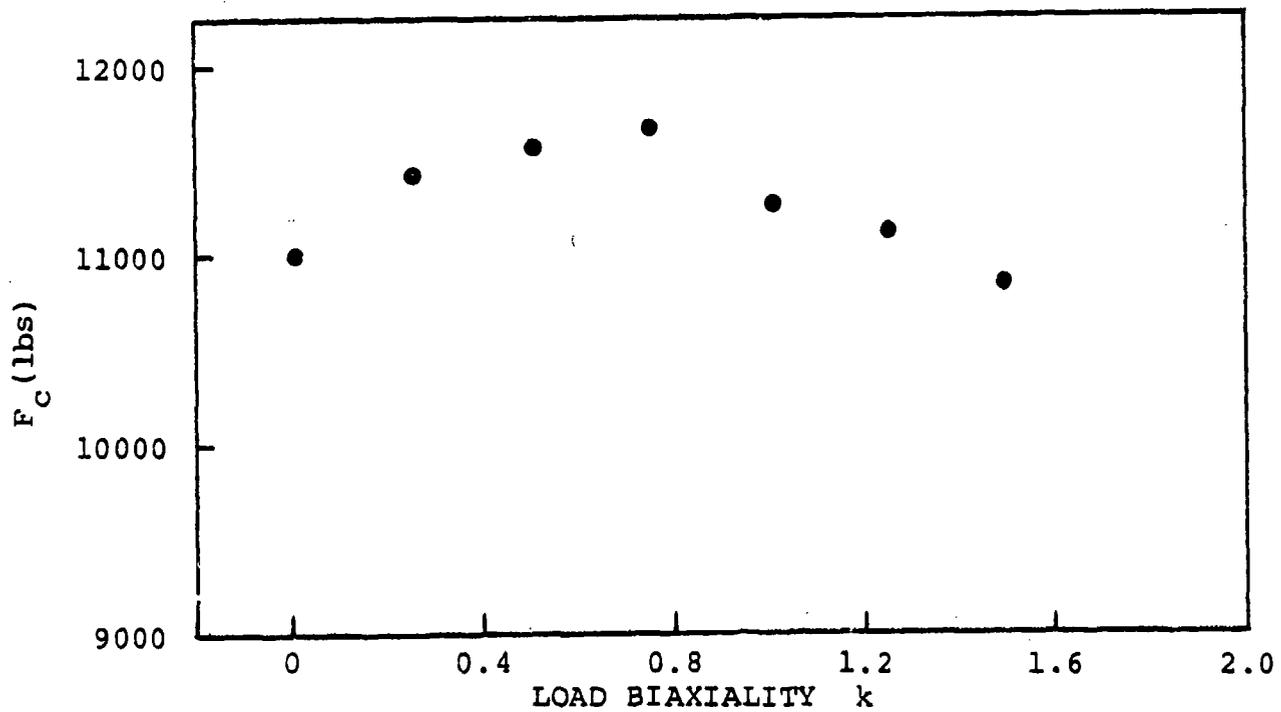
Fig. 43. Critical fracture load for 2024-T3 sheets as a function of load biaxiality. Crack perpendicular to rolling direction.
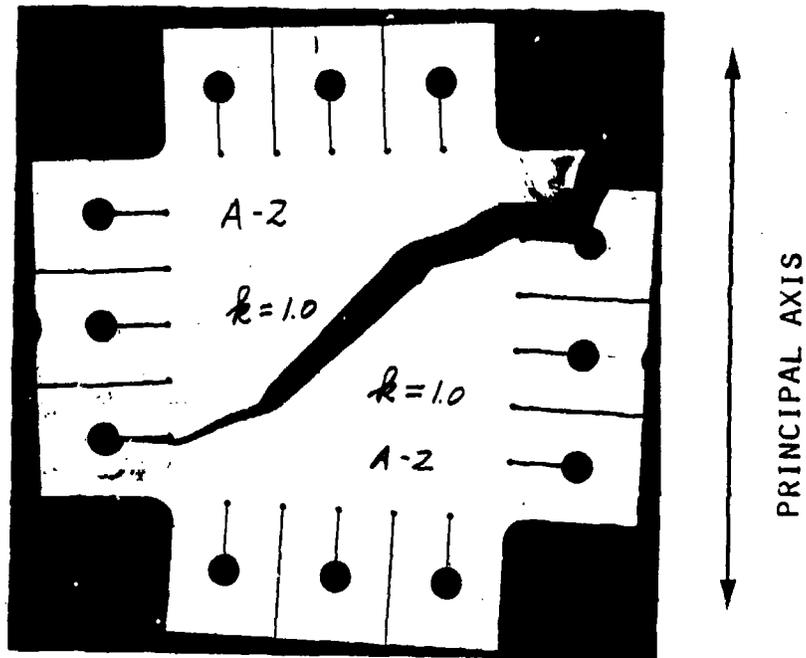
(a) Principal axis perpendicular to rolling direction.
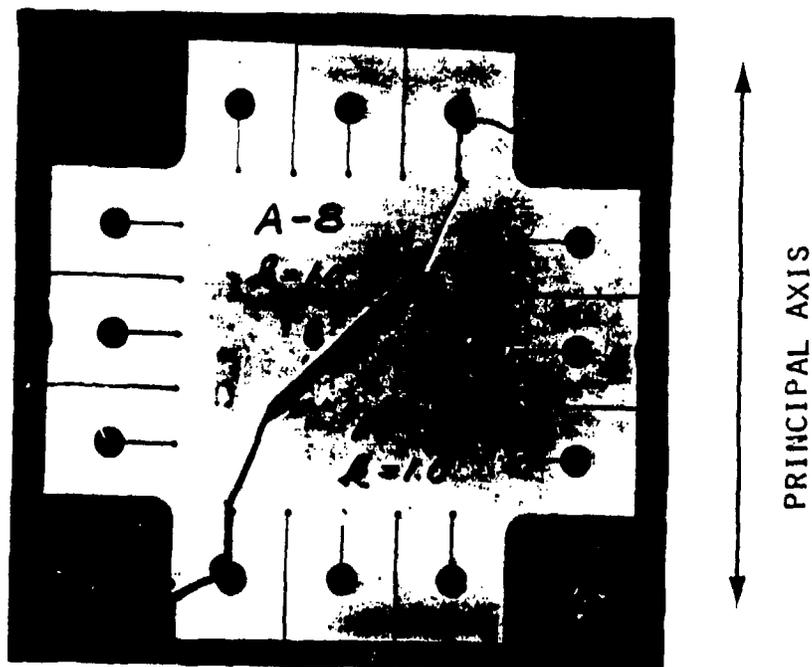
(b) Principal axis parallel to rolling direction.

Fig. 44. Photographs of fractured angle-crack specimens
made of 7075-T6 aluminum, 0.063" thick, k = 1.0.
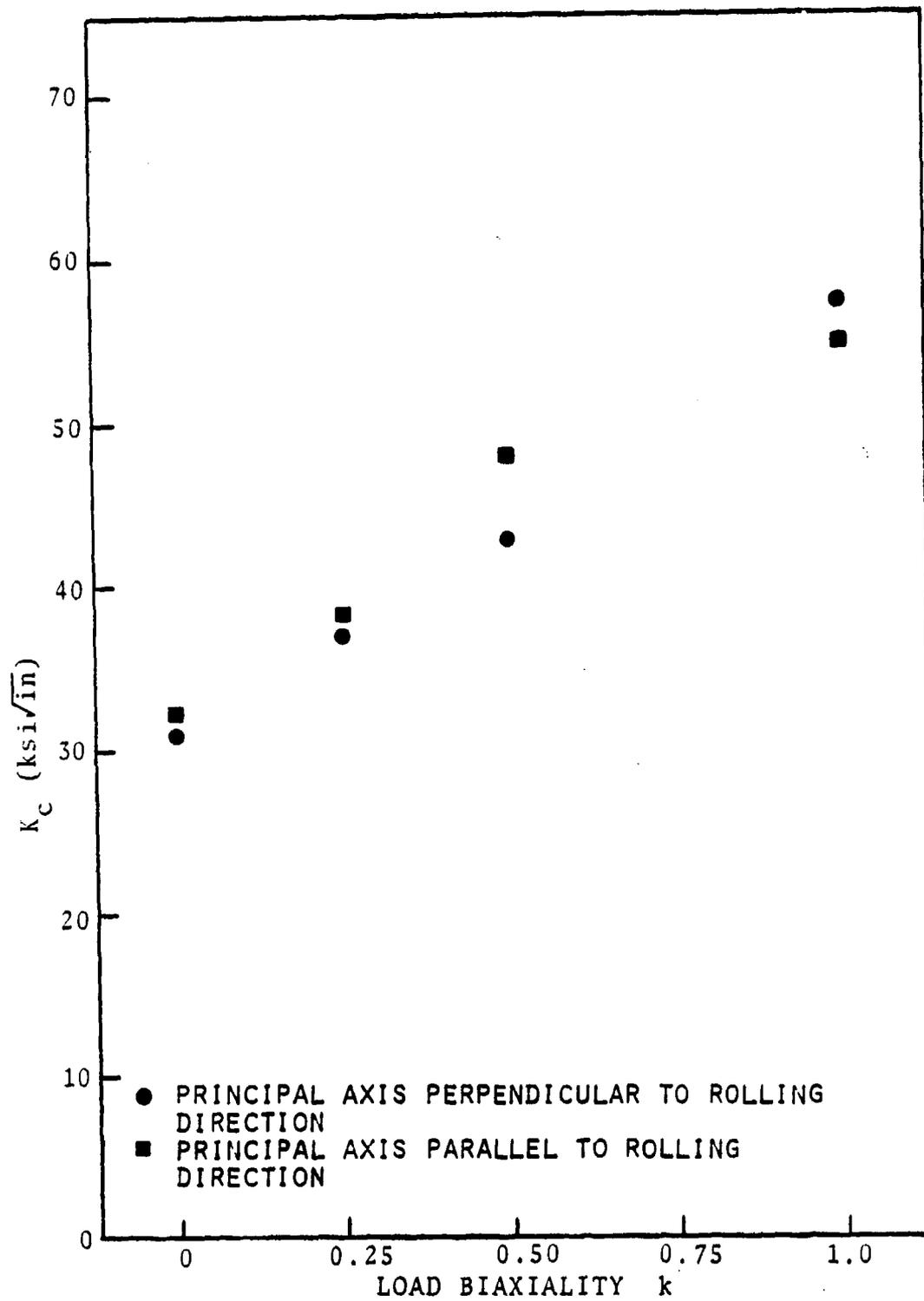
Fig. 45. Fracture toughness as a function of load biaxiality
          for angle-cracked specimens.
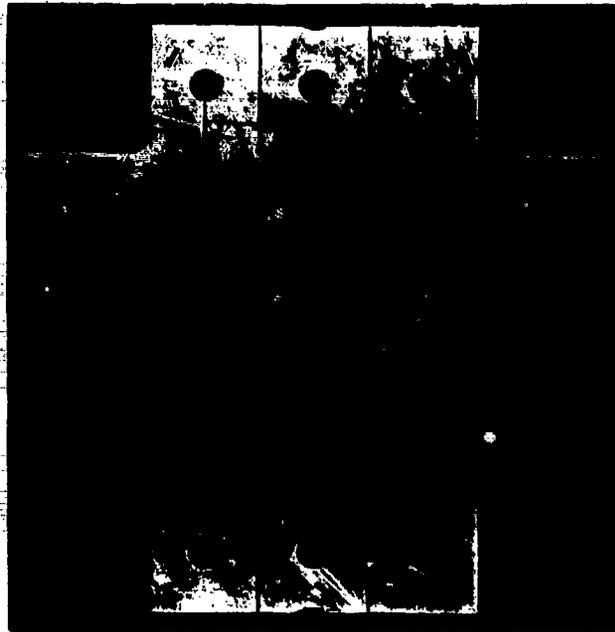
(a) k = 0
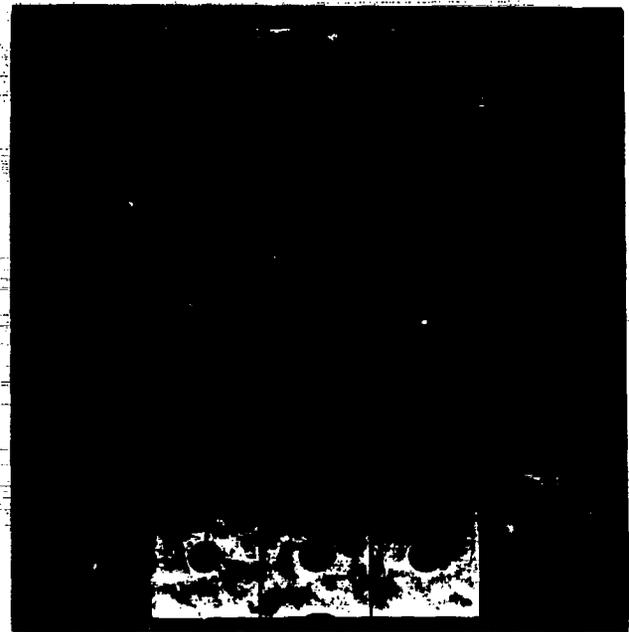
(b) k = 1.5
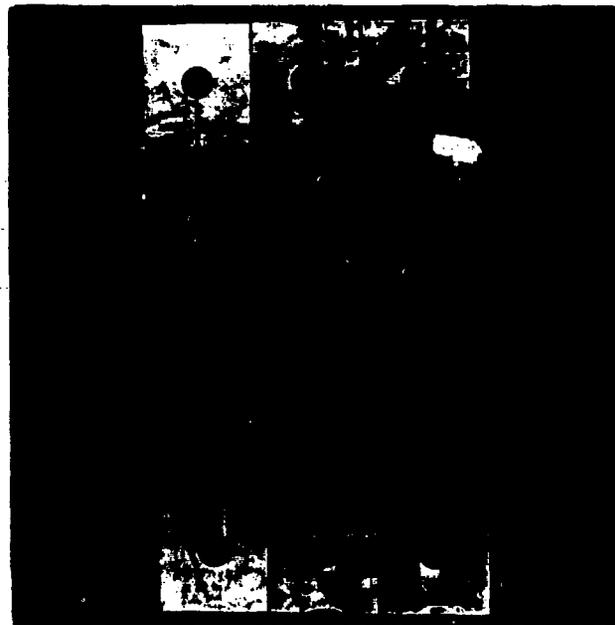
(c) k = 1.8

Fig. 46. Fracture paths of three biaxial test specimens
of 7075-T6. Crack perpendicular to the roll
direction.

(a) k = 0
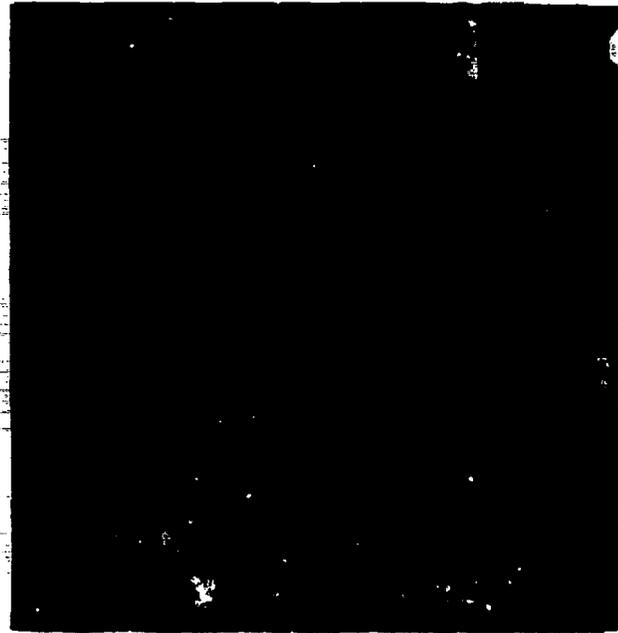
(b) k = 1.0

(c) k = 2.0

Fig. 47.   Photographs of fractured plexiglass specimens
           showing variations in the angle of initial crack
           extension.
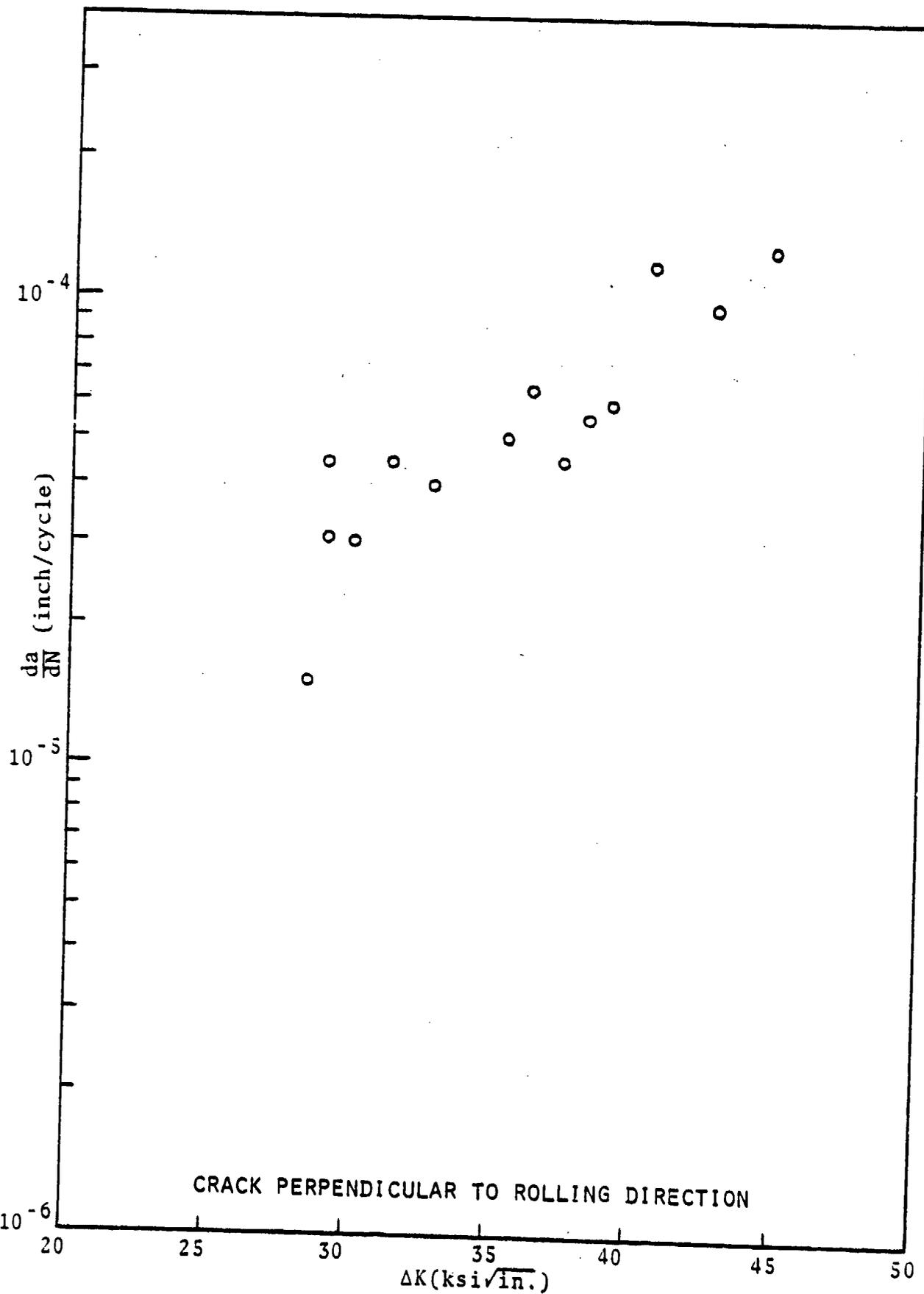
Fig. 48. Fatigue crack growth rate versus ΔK for 2024-T3, k = 0.
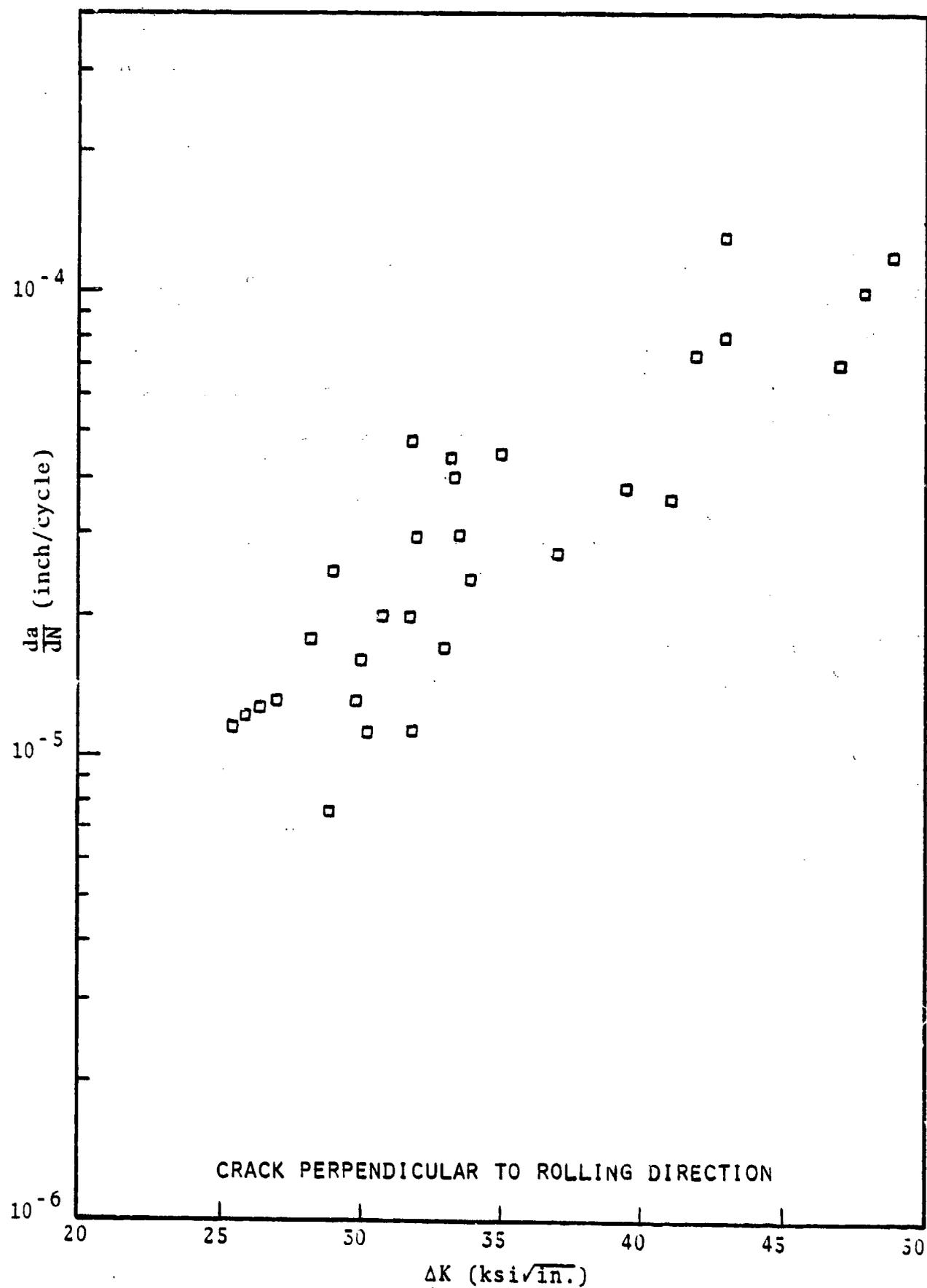
Fig. 49. Fatigue crack growth rate versus ΔK for 2024-T3, k = 1.0.
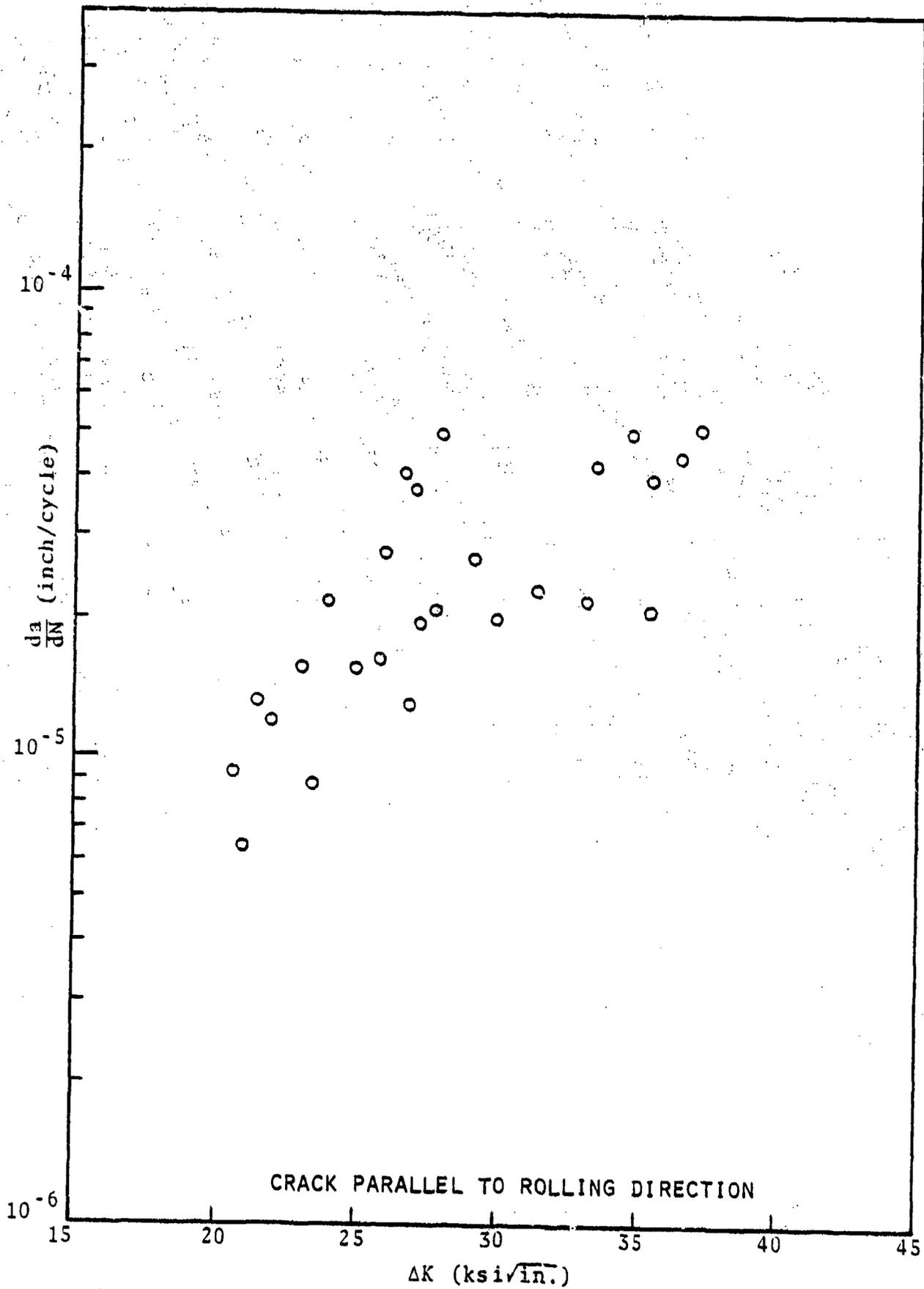
Fig. 50. Fatigue crack growth rate versus ΔK for 2024-T3, $k = 0$.
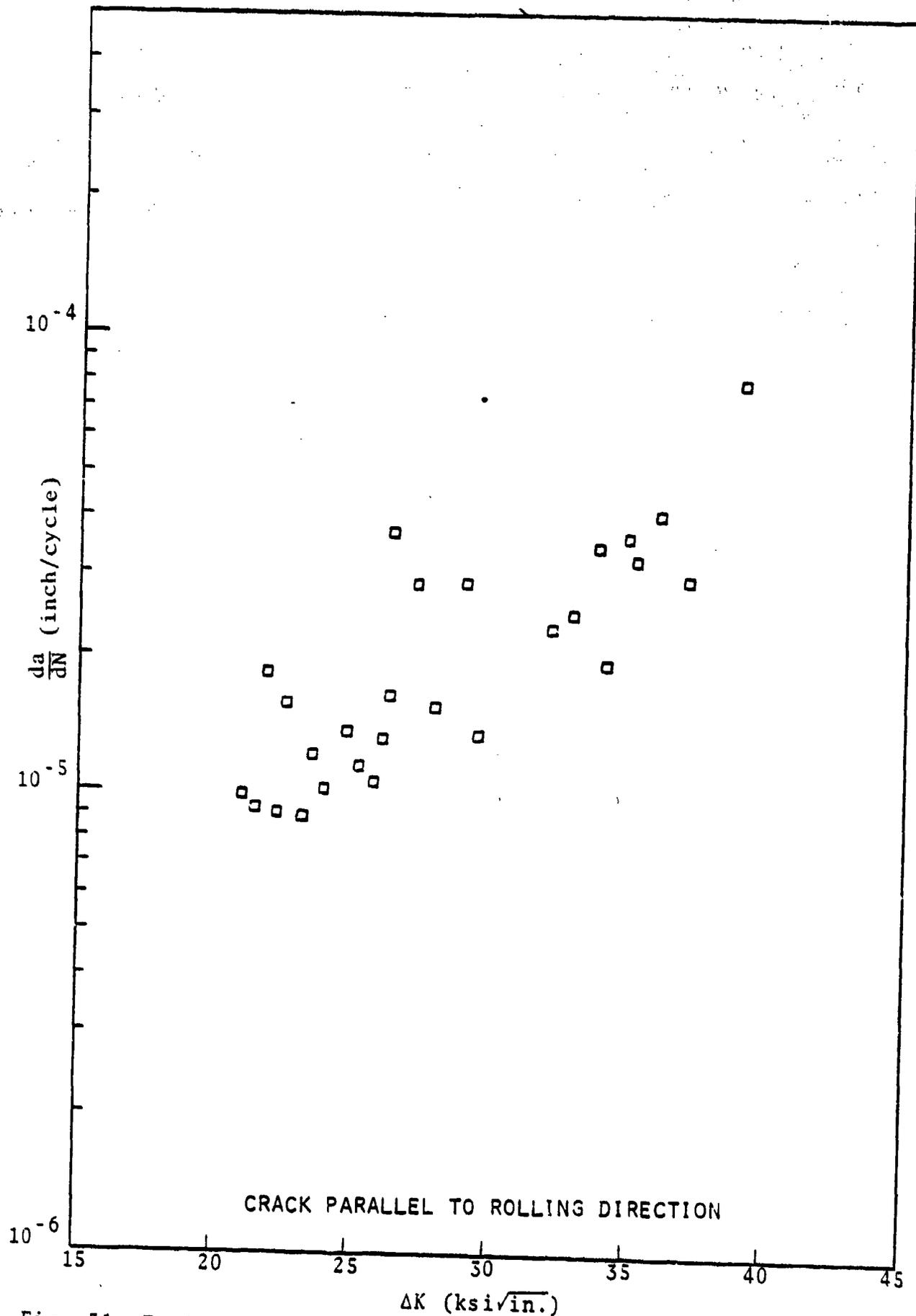
Fig. 51. Fatigue crack growth rate versus ΔK for 2024-T3, k = 1.0.
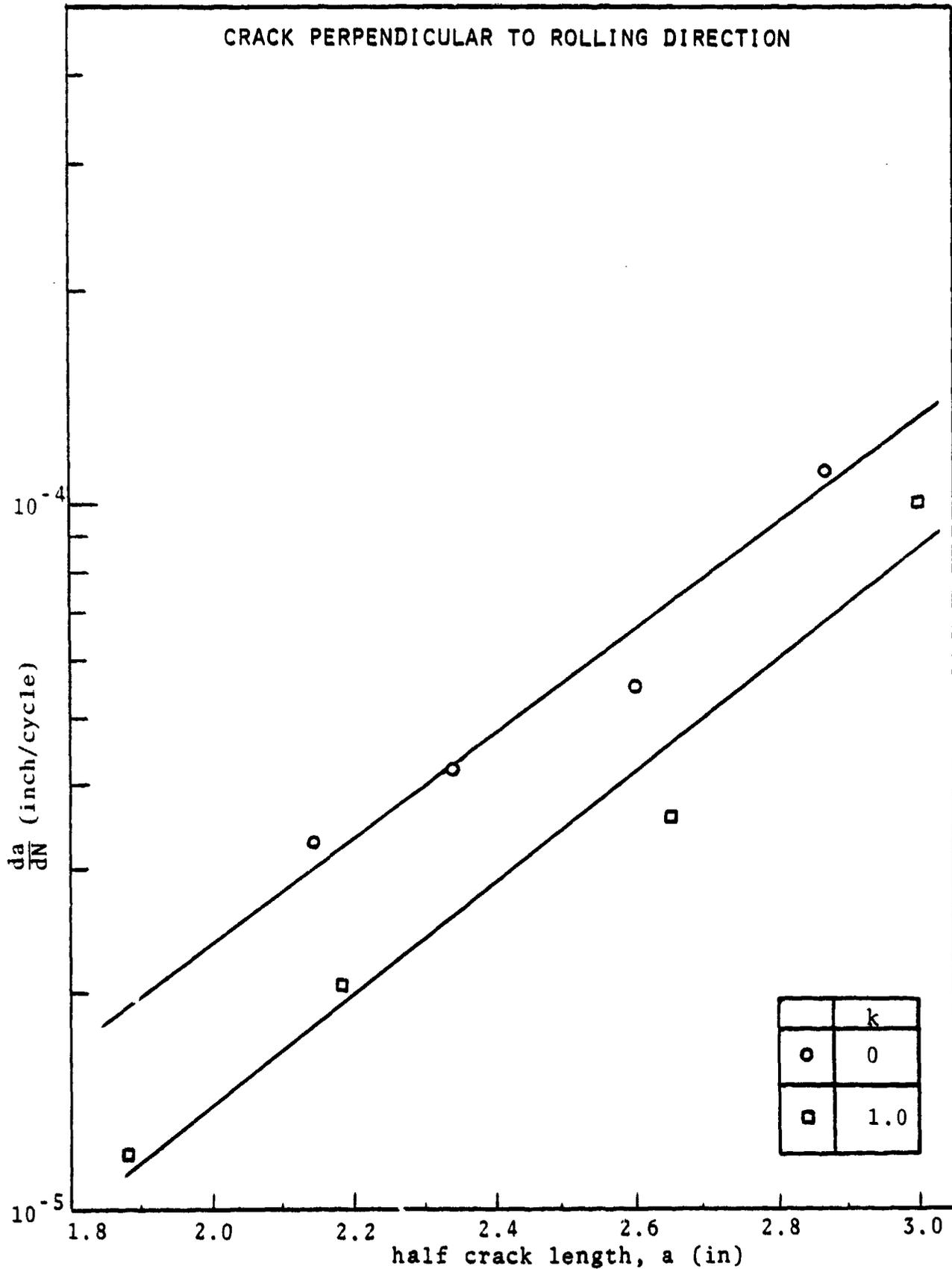
Fig. 52. Fatigue crack growth rate versus a, for 2024-T3.
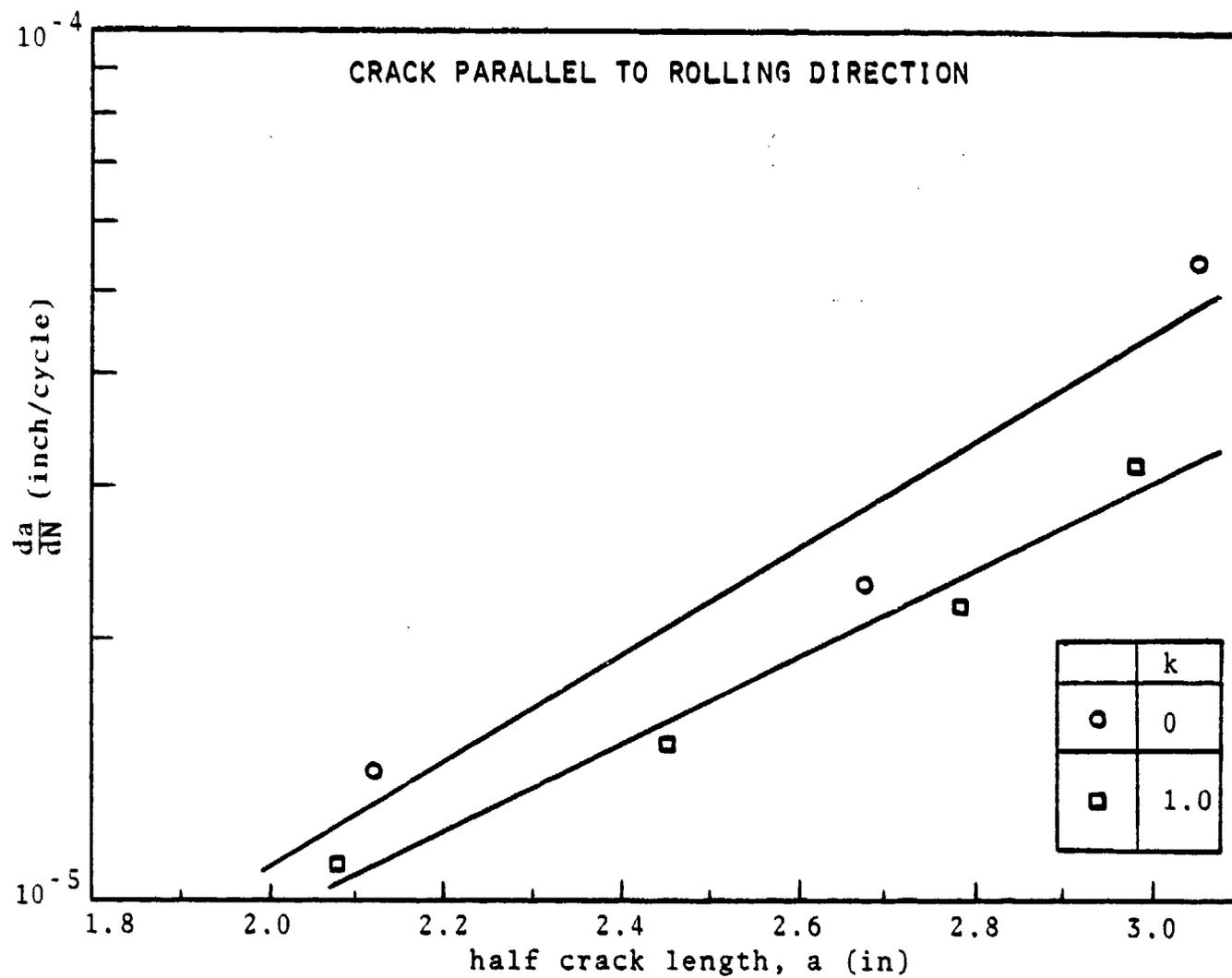
Fig. 53. Fatigue crack growth rate versus a for 2024-T3.
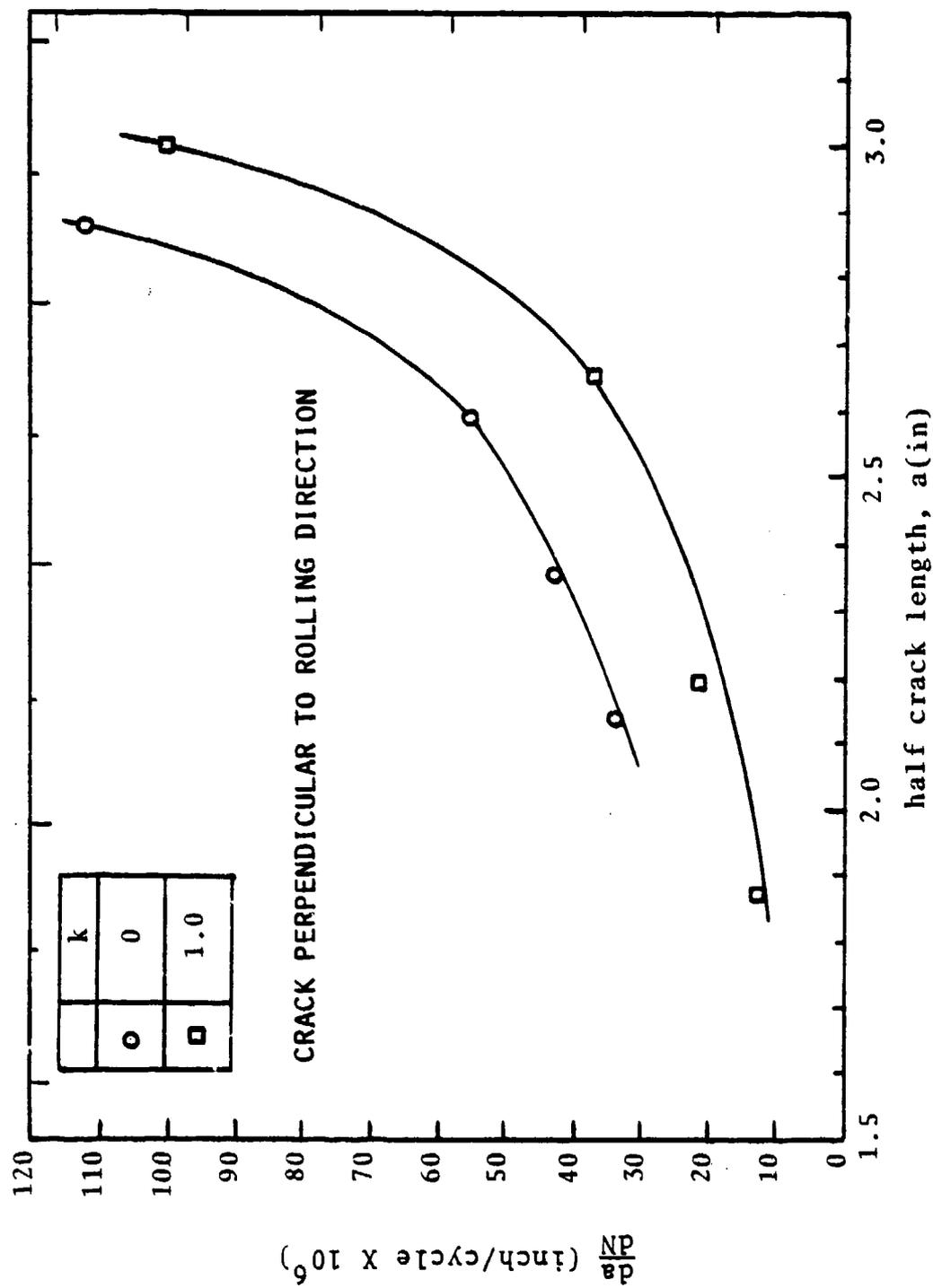
Fig. 54. Fatigue crack growth rate (linear scale) versus a, for 2024-T3.
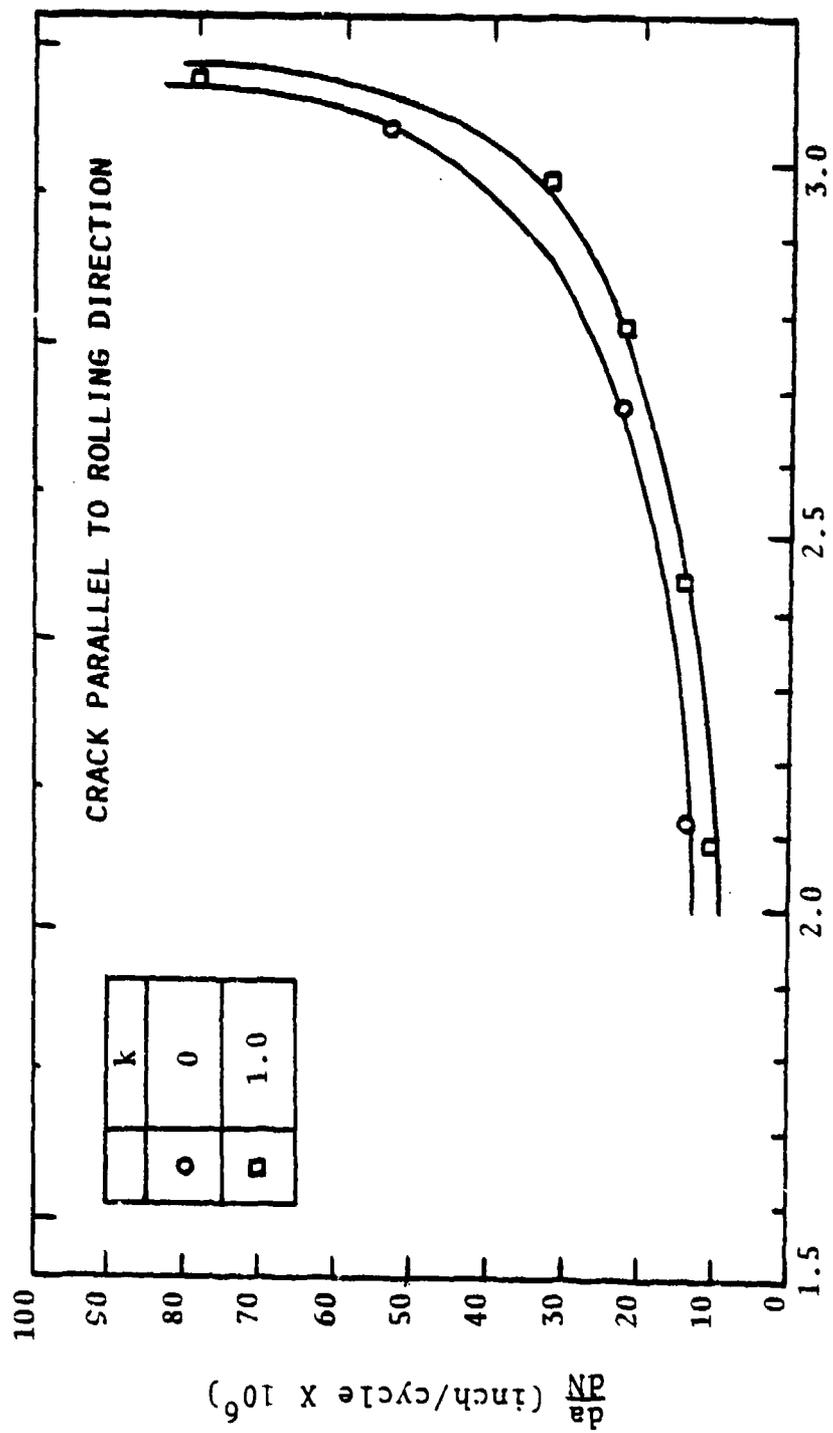
Fig. 55. Fatigue crack growth rate (linear scale) versus a, for 2024-T3.
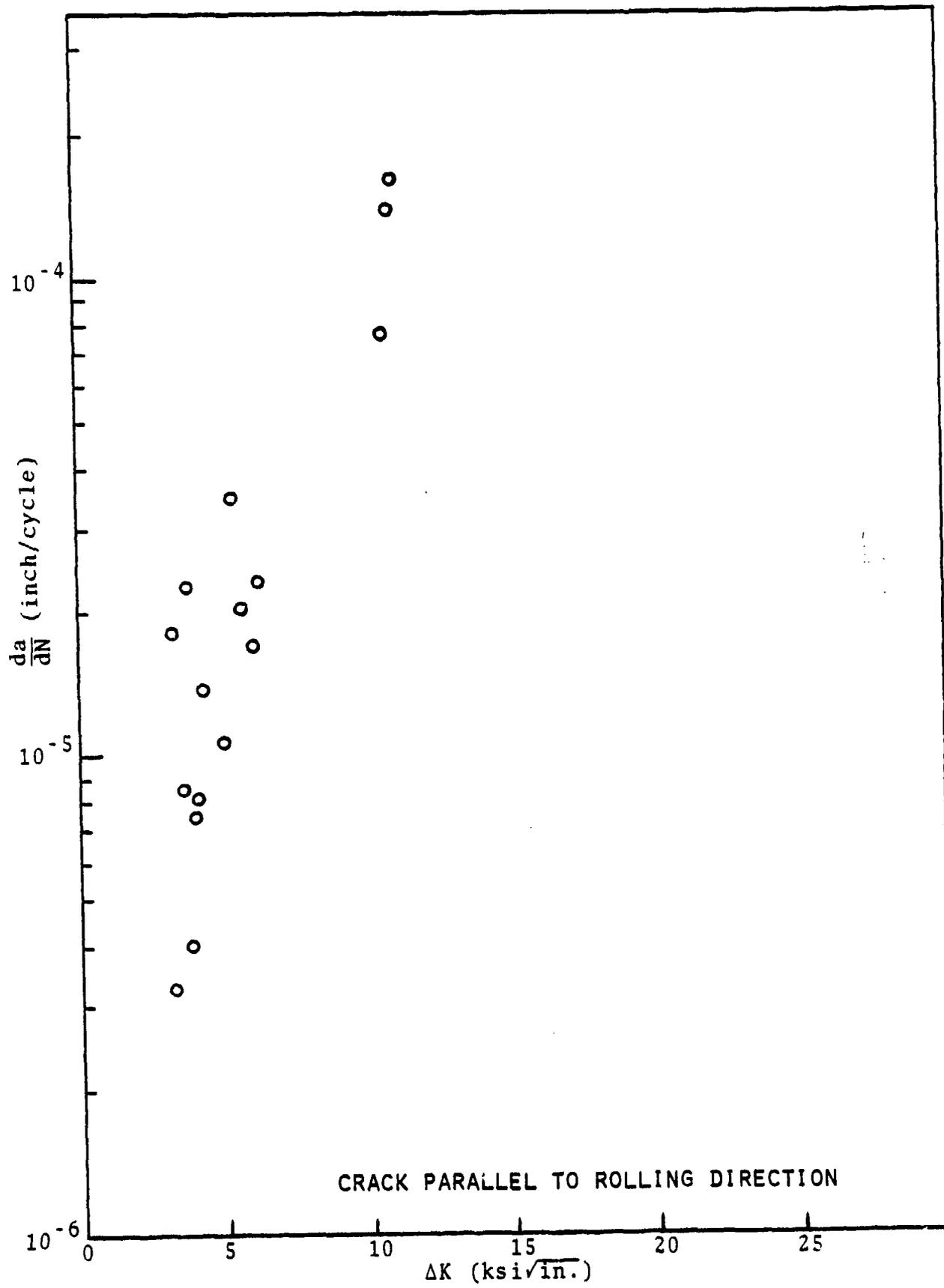
Fig. 56. Fatigue crack growth rate data for 7075-T6, k=0.
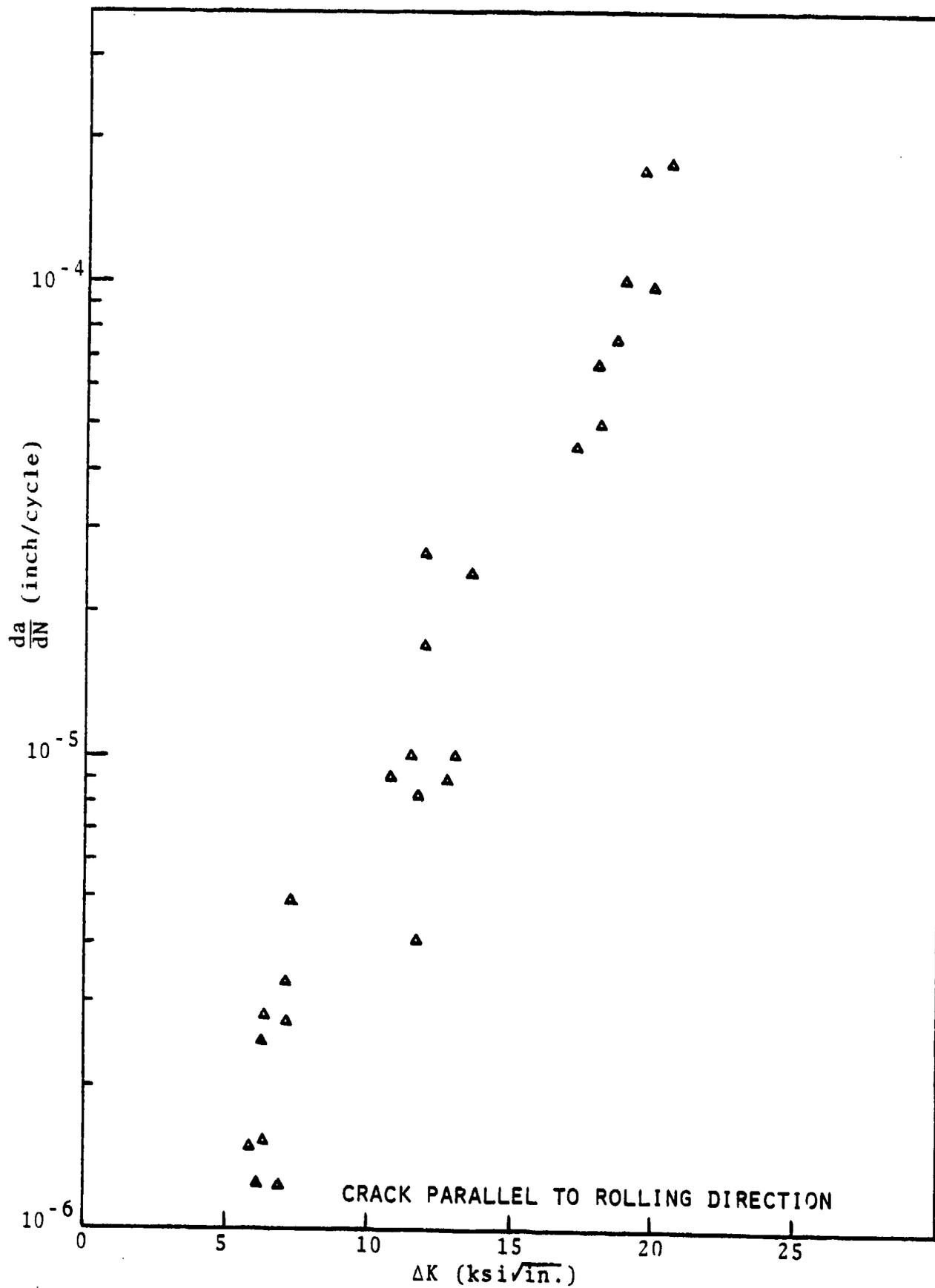
Fig. 57. Fatigue crack growth rate data for 7075-T6, k=0.5.
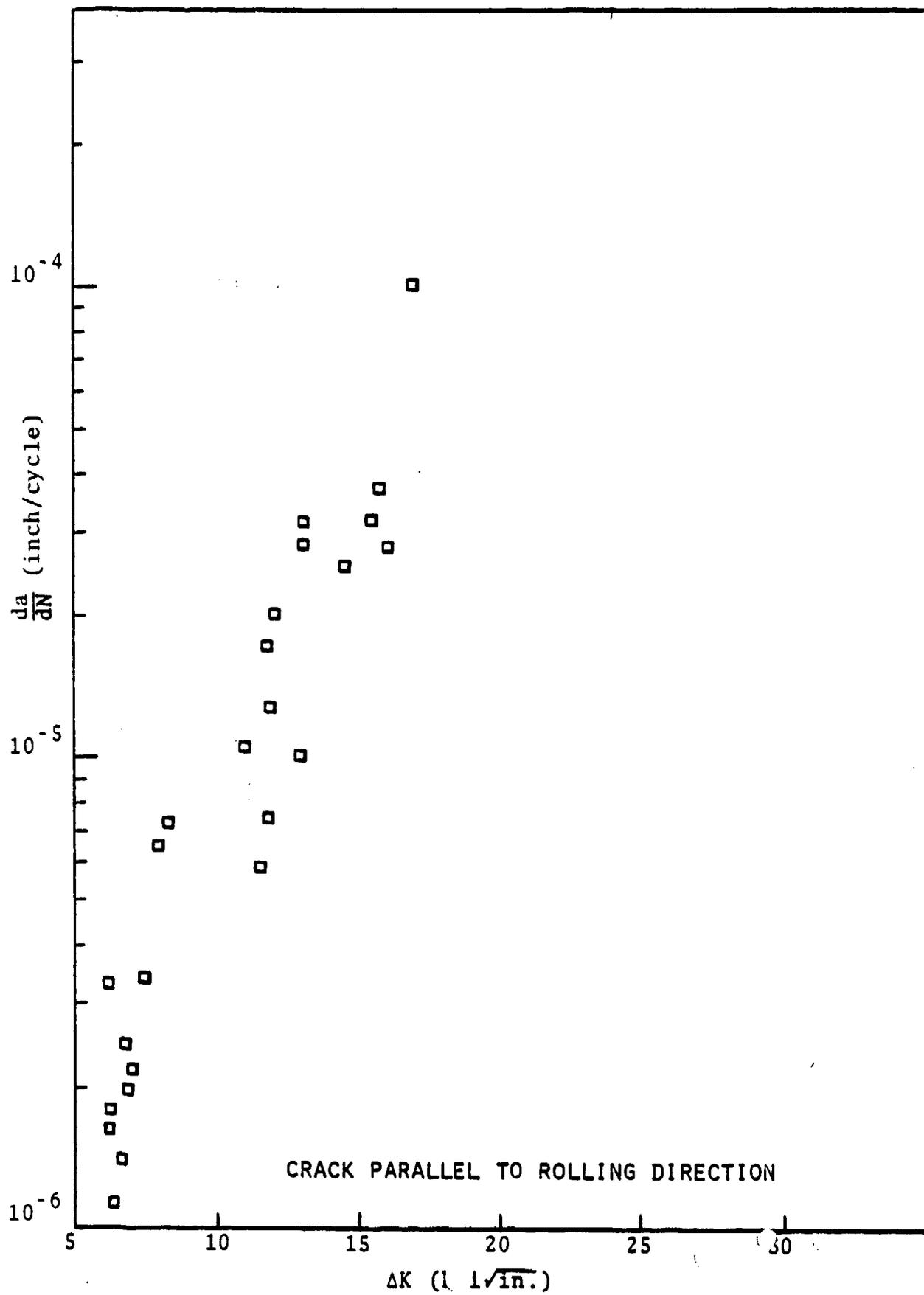
Fig. 58. Fatigue crack growth rate data for 7075-T6, k=1.0.
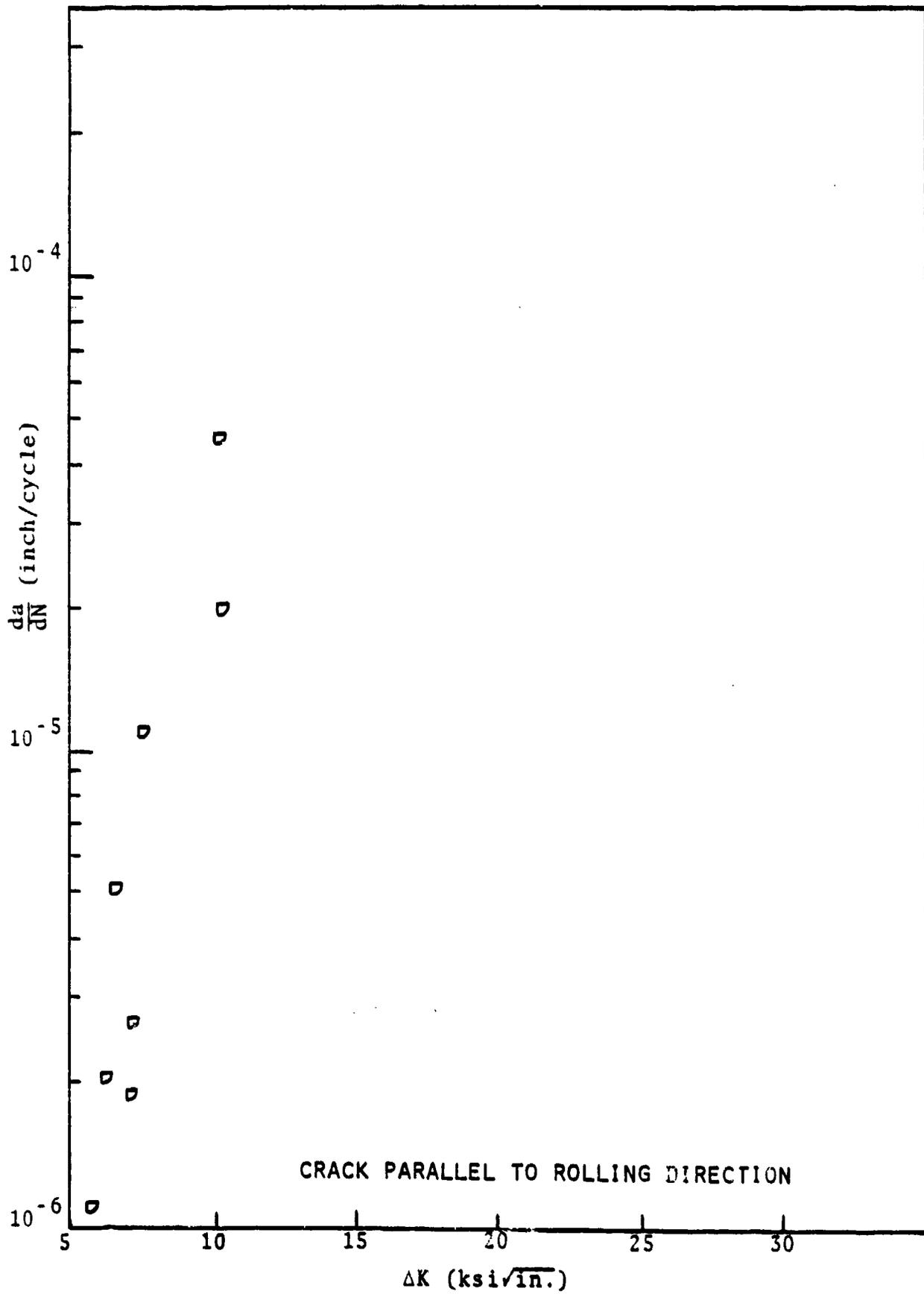
Fig. 59. Fatigue crack growth rate data for 7075-T6, k = 1.5.
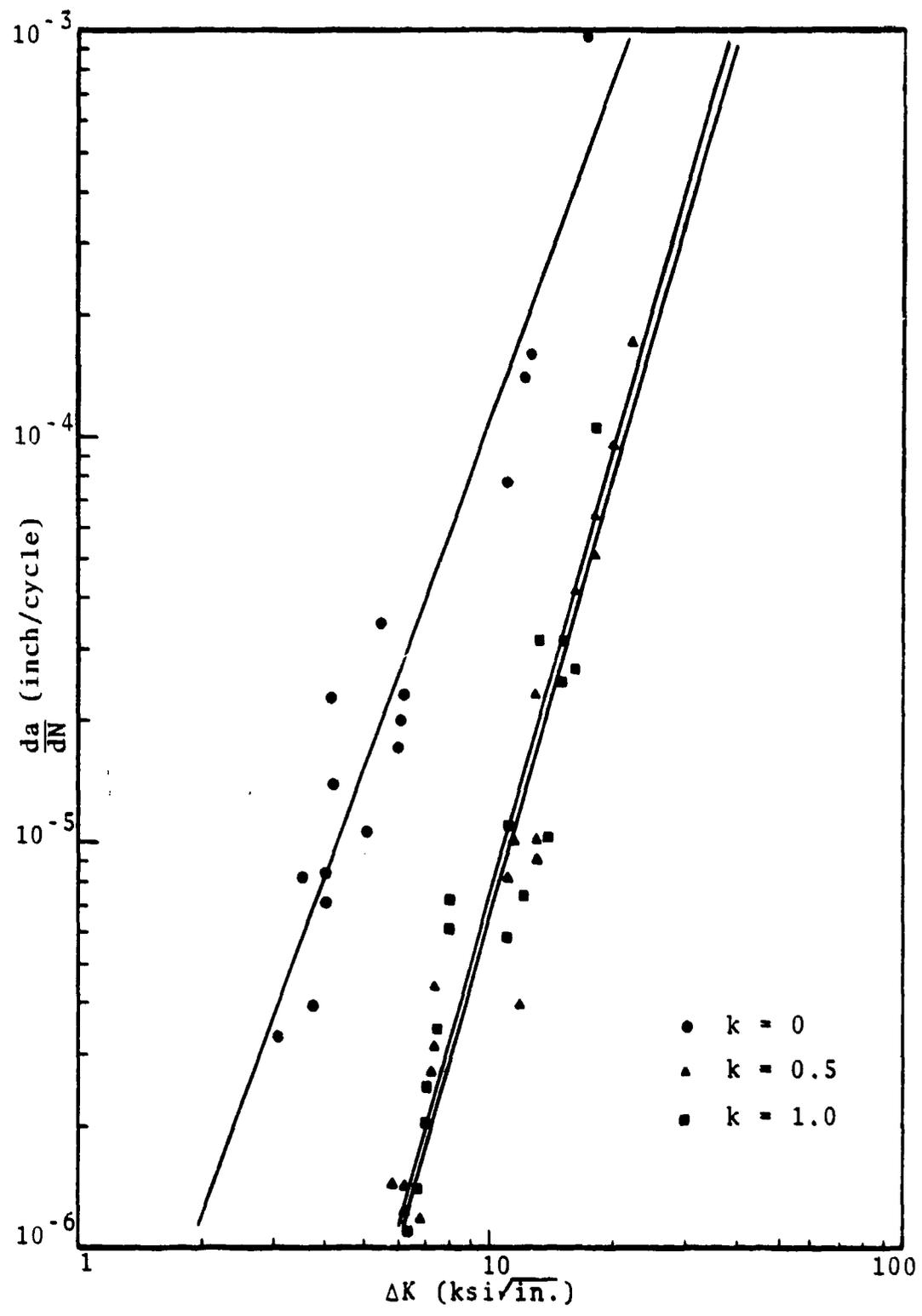
Fig. 60. Fatigue crack growth rate versus ΔK(logarithmic
scale) for 7075-T6.   Crack parallel to rolling
direction
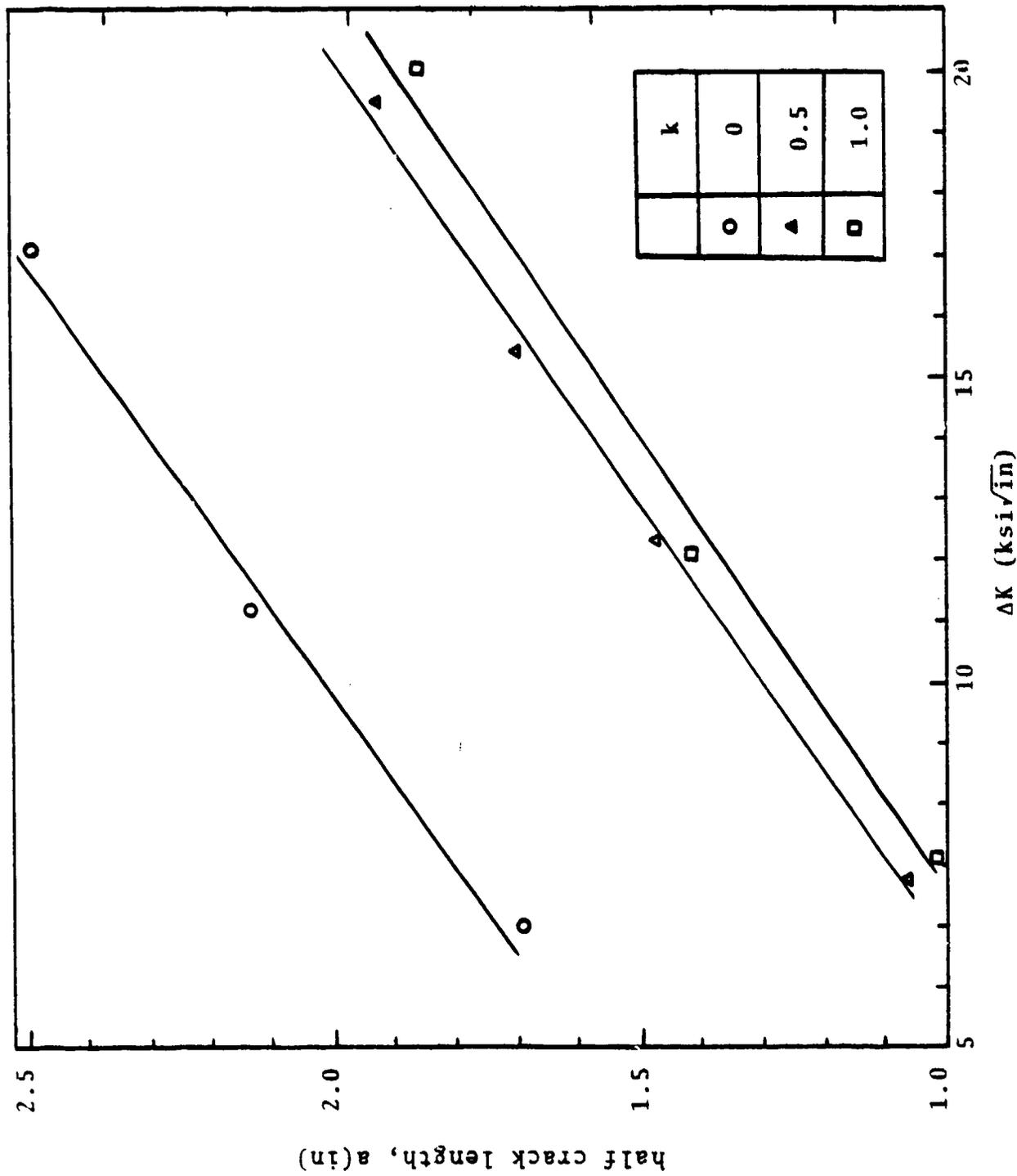
Fig. 61. Half crack length (linear scale) versus ΔK (linear scale) for 7075-T6.

Fig. 62. Fatigue crack growth rate ver. is ΔK for 2024-T3, k=0.

Fig. 63. Fatigue crack growth rate versus ΔK for 2024-T3, k=0.5.

Fig. 64. Fatigue crack growth rate versus ΔK for 2024-T3, k = 1.0.
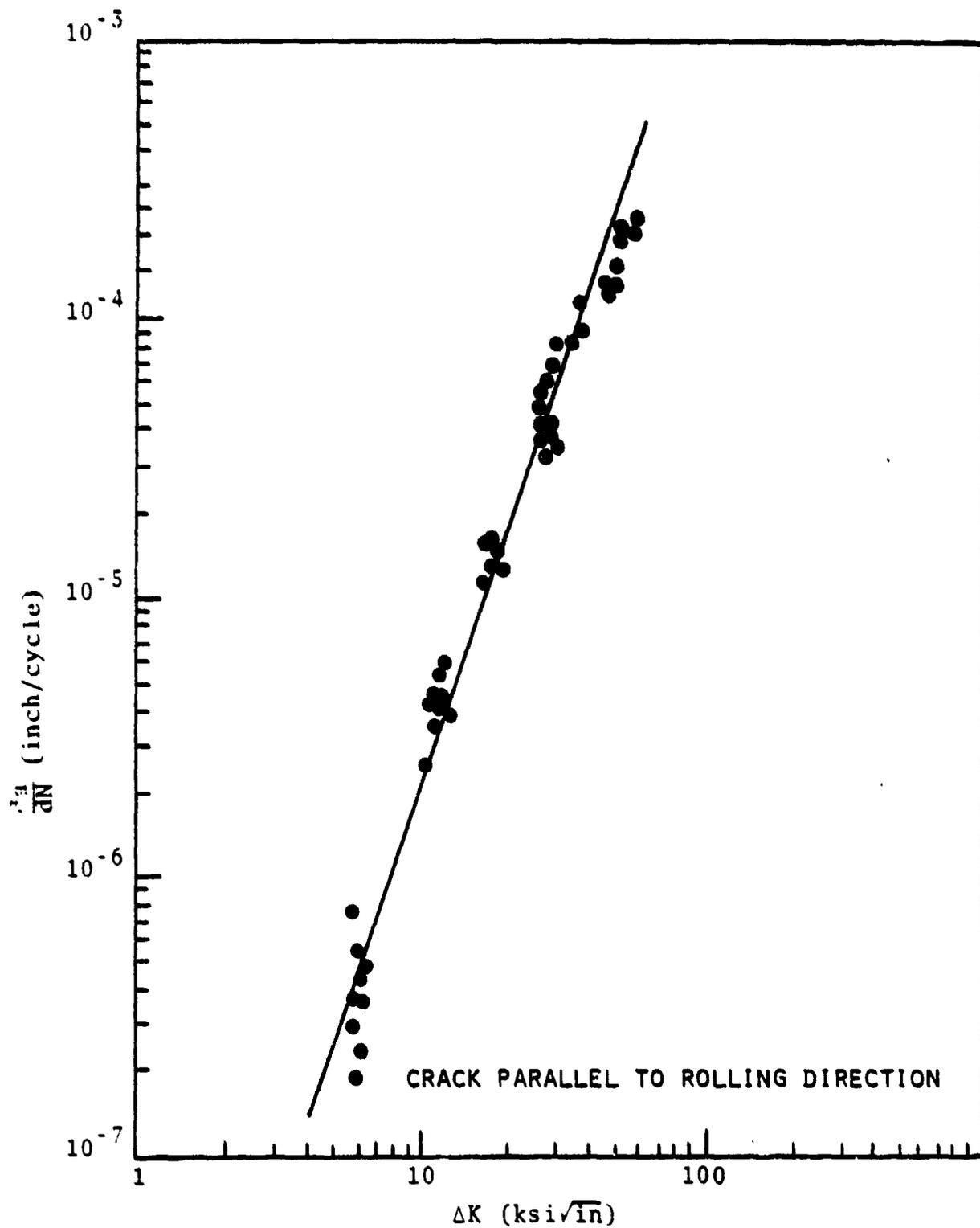
Fig. 65. Fatigue crack growth rate versus ΔK (logarithmic scale) for 2024-T3, k = 0.
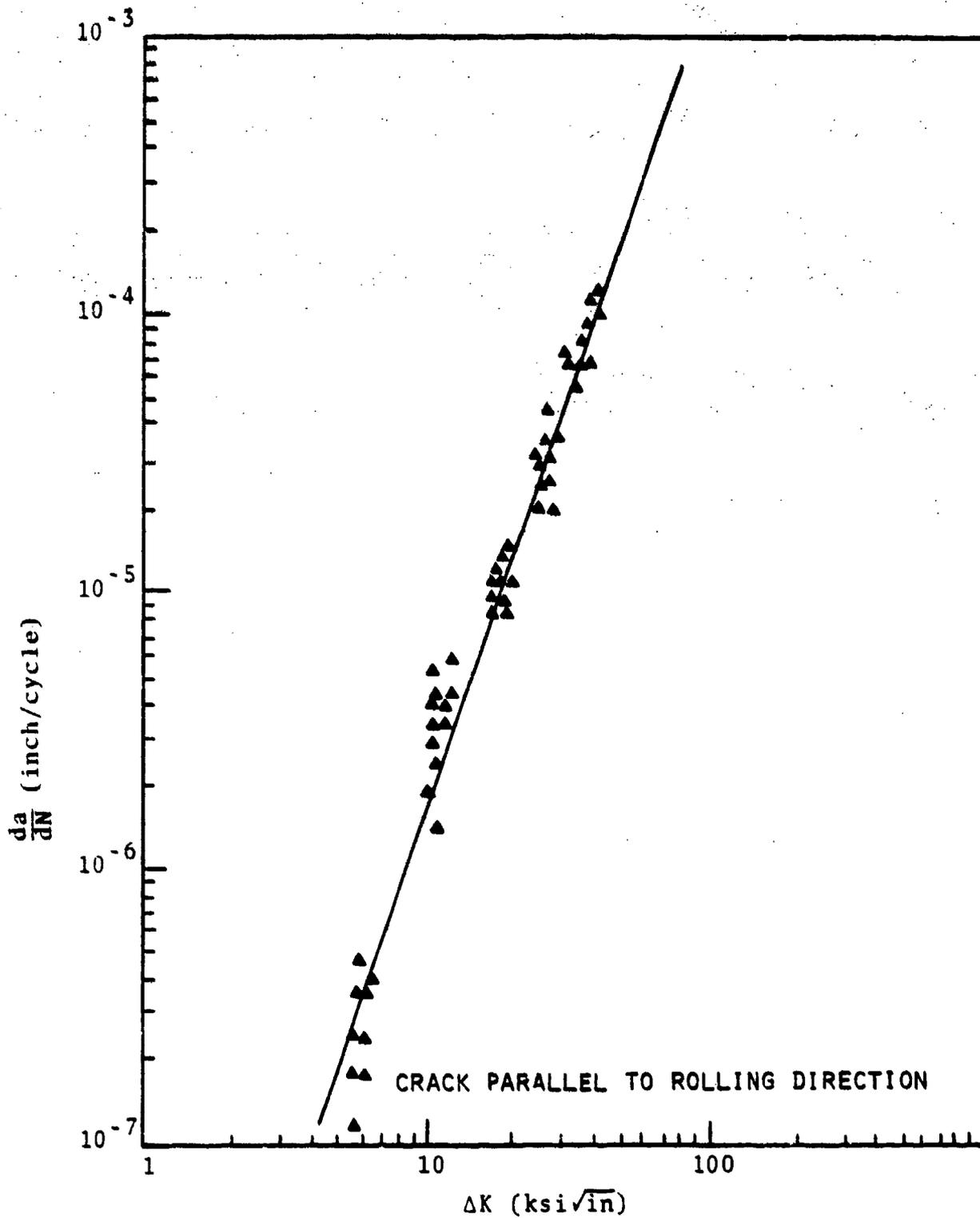
Fig. 66. Fatigue crack growth rate versus ΔK (logarithmic scale) for 2024-T3, k = 0.5.
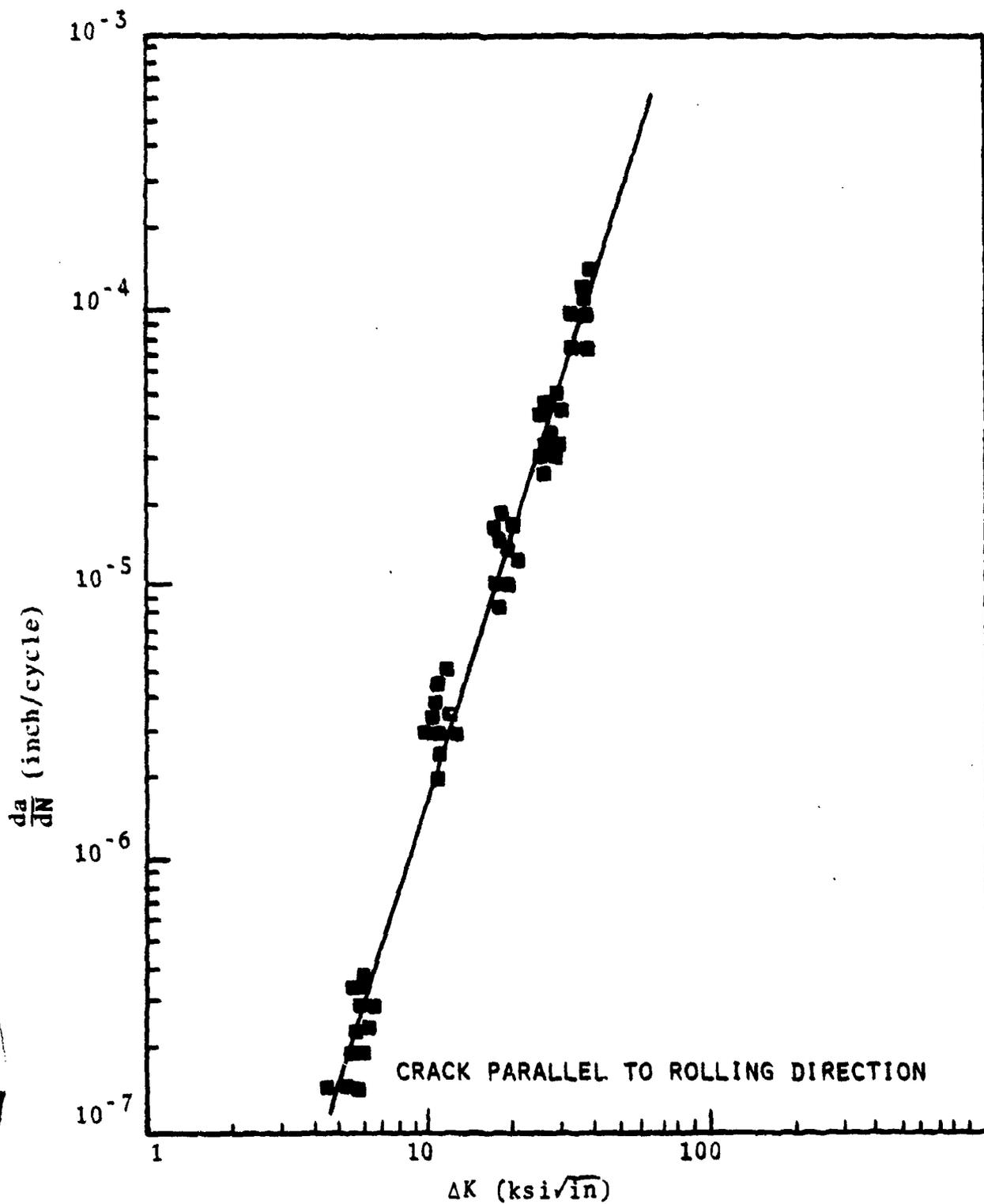
Fig. 67. Fatigue crack growth rate versus ΔK (logarithmic scale) for 2024-T3, k = 1.0.

THE GEORGE WASHINGTON UNIVERSITY
BENEATH THIS PLAQUE
IS BURIED
A VAULT FOR THE FUTURE
IN THE YEAR 2056

THE STORY OF ENGINEERING IN THIS YEAR OF THE PLACING OF THE VAULT AND
ENGINEERING HOPES FOR THE TOMORROWS AS WRITTEN IN THE RECORDS OF THE
FOLLOWING GOVERNMENTAL AND PROFESSIONAL ENGINEERING ORGANIZATIONS AND
THOSE OF THIS GEORGE WASHINGTON UNIVERSITY

BOARD OF COMMISSIONERS DISTRICT OF COLUMBIA
UNITED STATES ATOMIC ENERGY COMMISSION
DEPARTMENT OF THE ARMY UNITED STATES OF AMERICA
DEPARTMENT OF THE NAVY UNITED STATES OF AMERICA
DEPARTMENT OF THE AIR FORCE UNITED STATES OF AMERICA
NATIONAL ADVISORY COMMITTEE FOR AERONAUTICS
NATIONAL BUREAU OF STANDARDS U S DEPARTMENT OF COMMERCE
AMERICAN SOCIETY OF CIVIL ENGINEERS
AMERICAN INSTITUTE OF ELECTRICAL ENGINEERS
THE AMERICAN SOCIETY OF MECHANICAL ENGINEERS
THE SOCIETY OF AMERICAN MILITARY ENGINEERS
AMERICAN INSTITUTE OF MINING & METALLURGICAL ENGINEERS
DISTRICT OF COLUMBIA SOCIETY OF PROFESSIONAL ENGINEERS INC
THE INSTITUTE OF RADIO ENGINEERS INC
THE CHEMICAL ENGINEERS CLUB OF WASHINGTON
WASHINGTON SOCIETY OF ENGINEERS
FAULKNER KINGSBURY & STENHOUSE ARCHITECTS
CHARLES H TOMPKINS COMPANY BUILDERS
SOCIETY OF WOMEN ENGINEERS
NATIONAL ACADEMY OF SCIENCES NATIONAL RESEARCH COUNCIL

THE PURPOSE OF THIS VAULT IS INSPIRED BY AND IS DEDICATED TO
CHARLES HOOK TOMPKINS, DOCTOR OF ENGINEERING
BECAUSE OF HIS ENGINEERING CONTRIBUTIONS TO THIS UNIVERSITY TO HIS
COMMUNITY TO HIS NATION AND TO OTHER NATIONS

BY THE GEORGE WASHINGTON UNIVERSITY

ROBERT V FLEMING
CHAIRMAN OF THE BOARD OF TRUSTEES

CLOYD H MARVIN
PRESIDENT

To cope with the expanding technology, our society must
be assured of a continuing supply of rigorously trained
and educated engineers. The School of Engineering and
Applied Science is completely committed to this objective.